ALMA MATER STUDIORUM
UNIVERSITÀ DI BOLOGNA

DOTTORATO DI RICERCA IN

SCIENZE DELLA TERRA, DELLA VITA E DELL'AMBIENTE

Ciclo 37

Settore Concorsuale: 04/A2 - GEOLOGIA STRUTTURALE, GEOLOGIA STRATIGRAFICA, SEDIMENTOLOGIA E PALEONTOLOGIA

Settore Scientifico Disciplinare: GEO/01 - PALEONTOLOGIA E PALEOECOLOGIA

BIOSIGNATURES FROM EXTREME ENVIRONMENTS AS TARGETS FOR ASTROBIOLOGICAL EXPLORATION

Presentata da: Victor Amir Cardoso Dorneles

Coordinatore Dottorato

Barbara Cavalazzi

Supervisore

Barbara Cavalazzi

Co-supervisore

Keyron Hickman-Lewis

Esame finale anno 2025

Abstract

This PhD thesis focused on a comparative study of stromatolite occurrences in three highly alkaline, basalt-hosted lacustrine environments: Lake Ashenge (Ethiopia), Lake Abbe (Djibouti) and Carri Laufquen Lakes (Argentina). These ecosystems present occurrences of stromatolites observed to grow along the shorelines of (palaeo)lakes and around basaltic substrates, and may have formed in analogous environmental conditions to Jezero crater, a palaeolacustrine system on Mars. A multi-analytical approach was employed to characterise stromatolite formations. Although each site displays distinct macroscale morphologies, they exhibit comparable micromorphologies and microstructures on a microscale, suggesting shared formation process. We proposed two mechanisms of mineralisation: 1) primary precipitation via nanocrystal aggregation; and 2) early diagenetic replacement. Microscopy and spectroscopy analysis revealed biomineralised remnants of stromatolitic biomass, including microbial mats, filamentous cyanobacterial microfossils, and extracellular polymeric substances (EPS) preserved as Mg-bearing carbonates. EPS played a role in both mechanisms of mineralization. Raman and FTIR combined with ^{13}C-NMR demonstrated the preservation of aromatic and aliphatic organic material within filamentous microstructures, likely derived from primary microbial communities. Morphological and geochemical data suggest that photosynthetic organisms dominated these ecosystems, forming microbial mats and palisade structures, preserved in situ. Mineralogical characterisation indicates that Mg-Al-bearing silicates, including phyllosilicates, are associated with filamentous structures and play crucial role to their preservation. This study introduces a novel analytical approach as the first to apply ^{13}C-NMR to lacustrine stromatolites and, to our knowledge, providing the first detailed description of Lake Ashenge stromatolites. Key findings include insights into the organomineralization mechanisms within EPS biofilm, the relationship between sheaths preservation and Mg-Al-silicates, the influence of basaltic substrates on stromatolite formation, and the evaluation of the study areas as planetary field analogues. Studying terrestrial Martian palaeolake analogues is valuable for understanding microbial ecosystems and their fossilization models, as Martian carbonates are particularly promising for preserving ancient life evidence.

Contents

Chapter I – Introduction

1.1. Stromatolites: an ideal tool for paleobiology and astrobiology studies

Stromatolites are defined as organosedimentary structures formed as a result of interactions between communities of benthic microorganisms, that trap detrital sediments and/or precipitate chemical sediments, and their local environment (Fig. 1) (Burne & Moore, 1987; Riding, 1991; Bosak et al., 2013; Hickman-Lewis et al., 2019). The study of stromatolites as archives of microbial life has provided invaluable insights into the interactions between ancient microbial communities and their environment (Hofmann, 1973; Riding, 1991). Their fossil record extends to at least the Palaeoarchaean (e.g., Hickman-Lewis et al., 2023) and their architect microbes may have retained similar ecological functions and characteristics since that time (Bosak et al., 2013).

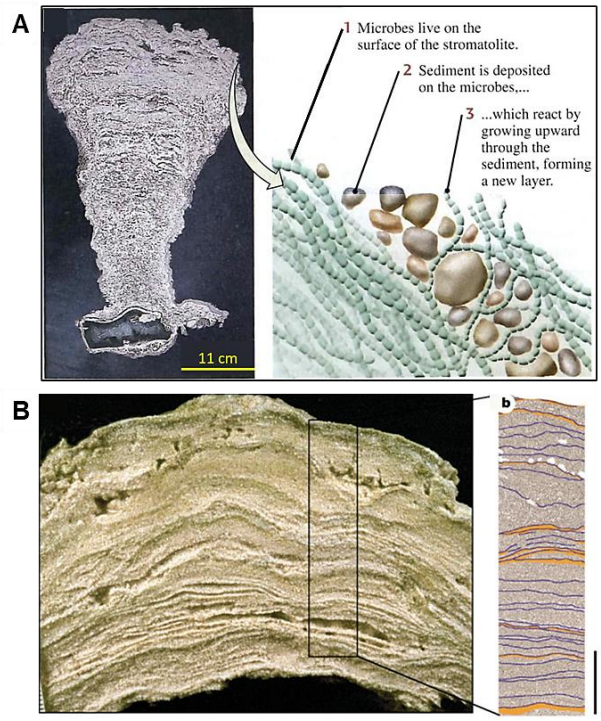

Fig. 1. Example of stromatolite. A) Representative columnar stromatolite from Shark Bay, Australia, and schematic image showing the interaction of the microbial community with the sediments during the stromatolite formation (Adapted from Grotzinger & Jordan, 2013). B) Characteristic laminated structure in stromatolites, generating high porosity.(Adapted from Reid et al., 2000).

Ancient stromatolites are among the oldest evidence of life on Earth. Examples in the Dresser Formation, Pilbara, Western Australia, are ~3.48 Ga in age (Walter et al., 1980; Van Kranendonk, 2006; Hickman-Lewis et al., 2022) and the Strelley Pool Chert stromatolites, Pilcara Craton, Australia, with 3,43 Ga (Allwood et al., 2006), have implications for understanding the origins of life on Earth and serve as fundamental record in the investigation

of environment–life interactions (Foster et al., 2020; Westall et al., 2021). The well-preserved and diverse stromatolitic outcrops in Strelley Pool offer unique insights into Earth's early biosphere and may represent some of its earliest fossils.

Although they were once widespread at Earth surface throughout the Archaean and Proterozoic, modern occurrences of stromatolites are mostly restricted to extreme environments, to which they are particularly resilient (Riding, 2011; Noffke & Awramik, 2013; Coman et al., 2015), such as hydrothermal settings (e.g., subaerial high altitude hot spring field, Buongiorno et al., 2019; Wilmeth et al., 2020), subtidal high-evaporative deposits (e.g., Jahnert & Collins, 2011), and hypersaline and hyperalkaline lakes (e.g., Valdespino-Castillo et al., 2014).

The best-known living stromatolites are perhaps from (shallow) marine environment, such as Hamelin Pool, Shark Bay, Western Australia (e.g., Papineau et al., 2005; Jahnert & Collins, 2012), and Highborne Cay, the Bahamas (e.g., Foster et al., 2009; Nutman et al., 2016). Extant stromatolites have also been reported in a multitude of lacustrine extreme environments including Lake Van, the world's largest alkaline lake, in eastern Turkey (Çağatay et al., 2024), the high-altitude volcanic Lake Socompa in the Argentinean Andes, South America (Farías et al., 2013), and the hydrothermally influenced Lake Bogoria (McCall, 2010) and Lake Turkana (Zăinescu et al., 2023) in the East African Rift System in Kenya.

The study of stromatolites may be done from different scales, from the largest structures to the most detailed components (Fig. 2) (Suosaari et al., 2019). Macrostructures refer to the overall shape, from columns to domes, ranging from decimeters to tens of meters. Mesostructures, or macrofabrics, are hand sample features such as lamination. Microstructures, or microfabrics, are microscopic, revealing the microorganisms and processes behind stromatolite formation. It is generally agreed that the macrostructures are largely controlled by environmental parameters such as current velocity or sediment accumulation rate, while the microstructures more faithfully record the ecology of the microbial ecosystem (Shapiro, 2007).

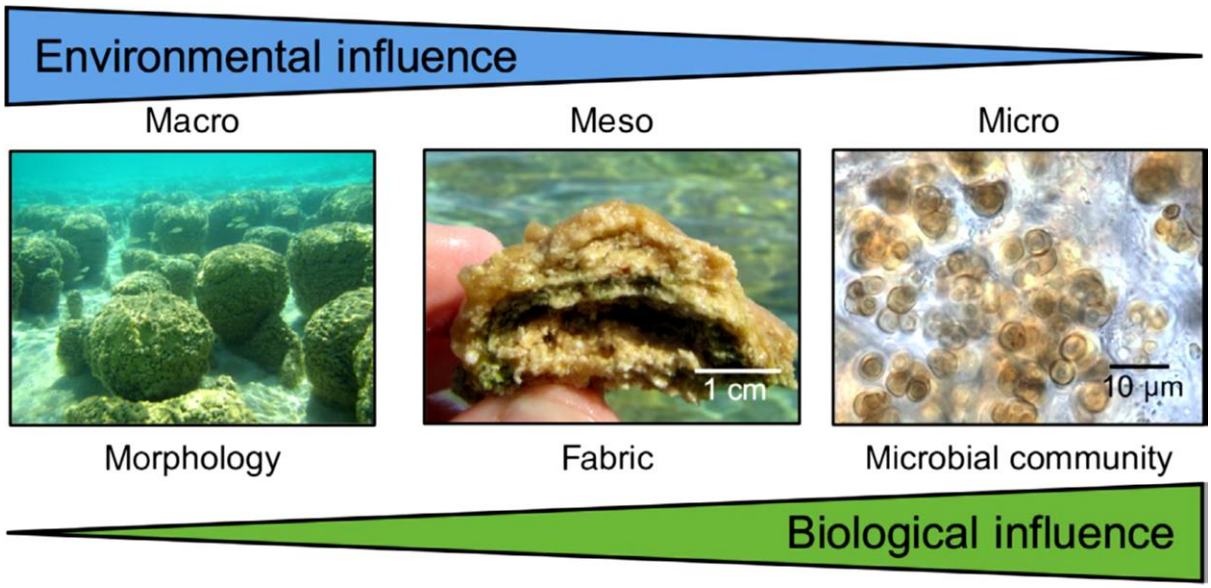

Fig. 2. Schematic image of the scales used for stromatolite descriptions: macro-, meso- and microscales (Suosaari et al., 2019).

The emergence and ecology of stromatolites, even before the initial rise of atmospheric oxygen at ~2.4 Ga, has changed over the time due to the evolution of eukaryotic algae and animals (Bosak et al., 2013). The paleoenvironmental reconstruction of the stromatolite fossil record indicating environmental conditions that prevailed in the past represents the geological relevance of stromatolites (Foster et al., 2020). In this way, they offer valuable clues about early microbial ecosystems on Earth and biogeochemical cycles, as well as improve our ability to recognize potential biosignatures (i.e. Hickman-Lewis et al., 2022).

Stromatolites are considered the main example of macrosctruture/texture biosignature, since they represent three-dimensional expression of microbial constructions (Westall et al., 2021; Hickman-Lewis et al., 2022). Biosignatures are the physical and chemical traces of past or present life, or biological processes (metabolic activities), such as morphological, chemical and isotopic signatures, preserved in minerals, rocks and sediments (Des Marais et al., 2008; Hays et al., 2017; Westall et al., 2021). They may be classified in six classes of biosignatures: organic molecules, minerals, macrostructures/textures, microstructures/textures, chemistry, and isotopes (Fig. 3).

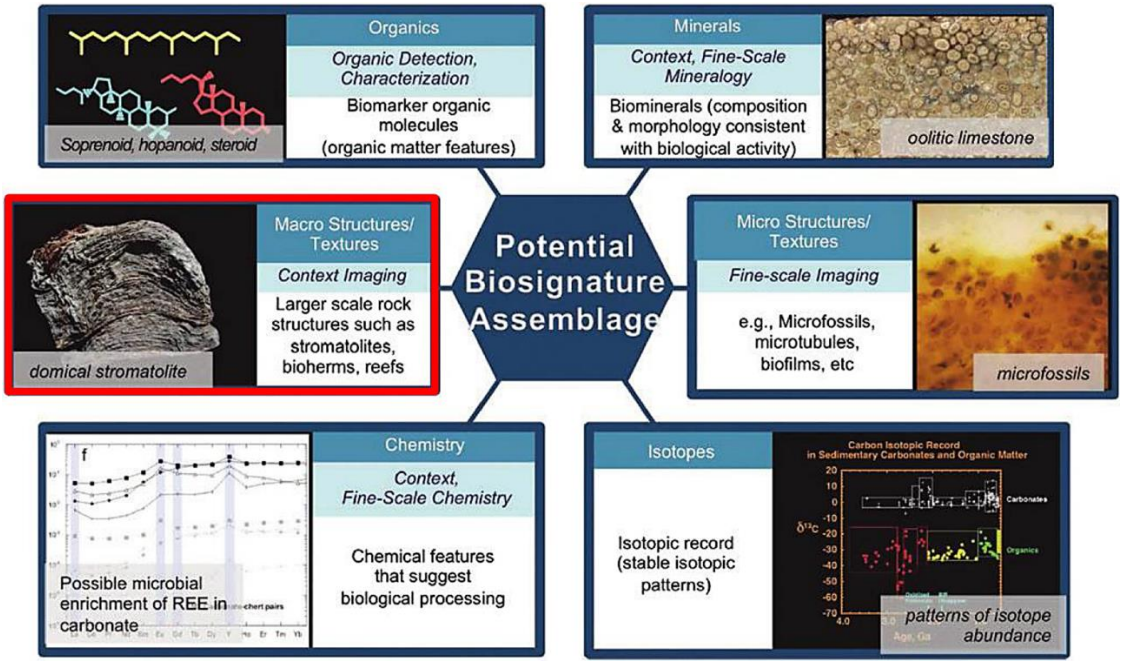

Fig. 3. Classes of potential biosignatures identified by the Mars 2020 Science Definition Team (Adapted from Hays et al., 2017).

1.1.1. The history behind the term stromatolites

The acceptance of stromatolites as an absolute terminology has been discussed over the time. Kalkowsky (1908) coined the term stromatolite, emphasizing the laminated structure and organic nature of stromatolites. For a long period of time, there were no works on the new term created in 1908; only in the 1960s new debates arose regarding the term stromatolite made the term become in fact accepted (Riding, 1999).

Logan (1964) proposed that stromatolite formation occurs normally in protected coastal or lake environments, shaped by physical and chemical factors such as drought, flooding, desiccation, storm waves, tidal runoff, sediment burial, and biotic activity. In this perspective that the environment shapes stromatolitic structures, Aitken (1967) firstly suggested classifications for stromatolite structures according to their external morphology in domal, columnar, digitate and polygonal stromatolites. The common point is that the proposed morphologies presented internal laminations.

Hofmann (1969) redefined stromatolites as rocks with layered structures formed by fine sediment accumulation on surfaces likely inhabited by microorganisms. The author also suggested that sediments accumulated through trapping, agglutination in the organic matrix, or precipitation from microbial metabolic activity. Later, Hofmann (1973) identified key requirements for stromatolite development: a growth substrate, open water system, metabolic compounds, an energy source like sunlight, a population of benthic microorganisms, fine

mineral matter for retention and binding, a periodic rhythm for discontinuous growth forming layers, and processes of lithification and burial for preservation.

Awramik & Margulis (1974) advanced the understanding of stromatolites by proposing that blue-green algae were the primary microorganisms involved. They also discarded lamination as a necessary feature, noting that some microbial deposits, e.i. Shark Bay, were either non-laminated or coarse-grained. The term stromatolite then became broadly applicable to any microbial organomineral structure, regardless of its internal structure, allowing Burne & Moore (1987) to coin the term microbialite that include stromatolites, thrombolites, dendrolites, microbial mats, oncoids and ooids.

Stromatolites can be distinguished from other microbialites based on their internal structure, commonly laminated, characterized by fine, more or less planar laminations (Riding, 1991). Riding (1999; 2000) updated the definition of microbialites to benthic sediments produced by the induction of microorganisms and included in this group all similar structures that occur as domes and columns in shallow water environments and are formed by the same process.

1.1.2. Formation processes of stromatolites

Stromatolites form in both marine and non-marine, but shallow, hypersaline carbonate environments are ideal due to their high calcium and bicarbonate levels, which facilitate calcium carbonate formation as a key material (Awramik, 1992). Living stromatolites thrive in areas with low faunal activity, absent macroalgae and plants, high salinity and alkalinity, low nutrients, high temperatures, periodic desiccation, and seasonal changes that promote mineral precipitation (McNamara & Awramik, 1992).

Stromatolites are mainly formed by cyanobacteria, however, communities of sulfate-reducing bacteria, methane-oxidizing bacteria, and small algae, thrive in environments with varying water chemistries (Riding, 2011), and may play a role in stromatolites formation. The microbiota that builds the stromatolite structure has the ability to migrate vertically to escape burial by sediments and recolonize the newly deposited surface and can reach several centimeters to decimeters in thickness (Gerdes et al., 1993).

The emergence of stromatolites is driven by the interplay between intrinsic factors, such as the radial growth of microbial mats, biofilms, and inorganic minerals, and extrinsic factors like environmental conditions, including light and sedimentation, which contribute to the diversity registered in the fossil record (Dupraz et al., 2006). Within stromatolite habitats,

bioinduced-carbonates form in waters with lower mineral saturation, while in settings that favour inorganic precipitation, bacterial activity contributes more to structural formation than sediment deposition (Riding, 2011).

Stromatolites exemplify how carbonate precipitation results from a combination of physicochemical processes and microbial mediation (Suosaari et al., 2016). Their structures are shaped by microbial trapping and binding, carbonate precipitation, organic content, sediment input, voids, skeletons, bioturbation, and macroporous orientation (Burns et al., 2004), with variations influenced by the deposition site and the distinct bacterial communities that produce different surface morphologies.

Microbes form stromatolites through two main processes: trapping and binding or mineral precipitation, which will be discussed deeply in the following chapter of this thesis. Both formation processes of stromatolites are greatly influenced by Extracellular Polymeric Substance (EPS) (Dupraz et al., 2009). However, abiotic carbonate precipitation has also an important contribution as microbes collectively form submillimetric layers within the EPS matrix, resulting in biofilms (Frantz et al., 2015).Various organisms such as cyanobacteria and bacteria are producers of EPS, which surround microbial cells for attachment, protection, and nutrient absorption, as well as may induce carbonate precipitation or serve as a substrate for crystal growth, and these factors can influence the morphology of carbonates (Dupraz et al., 2009; Pedley et al., 2009; Zhang et al., 2023).

Trapping and binding occur when sediments settle on microbial mats, are trapped by the sticky surface, and are bound by microbial growth, creating an agglutinated fabric. The process, enhanced by EPS production, is part of the radial growth cycle of microbial mats, biofilms, and minerals, contributing to stromatolite formation (Dupraz et al., 2006; Frantz et al., 2015).

In situ mineral precipitation mainly occurs within the EPS, where microbes actively promote carbonate formation through biologically-induced processes (Dupraz & Visscher, 2005). Cyanobacteria import bicarbonate (HCO_3^-) via CO_2-concentrating mechanisms, converting it into CO_2 for photosynthesis. This bicarbonate uptake raises the pH around the cells and within the EPS. When the saturation index for $CaCO_3$ minerals is sufficiently high, crystals can nucleate on or within the EPS (Dupraz & Visscher, 2005; Bissett et al., 2008; Dupraz et al., 2009).

1.2. Extreme terrestrial environments and planetary field analogues

Extreme environments are defined by a range of physical and chemical stressors, such as ionizing and UV radiation, pressure, pH, salinity, dryness, and toxic metals, where life has nonetheless been discovered (Fig. 4) (Cockell et al., 2016). The exact limits for many of these stressors remain unclear, and how organisms adapt to multiple extreme conditions is still not well understood. Geothermal areas, including active marine hydrothermal vents and subaerial volcanic settings, are examples of multiple extreme conditions where yet are inhabited by a wide variety of metabolically diverse microorganisms (Cavalazzi et al., 2019).

To enhance the chances of detecting life on other planets, it's crucial to first understand the conditions that support life on Earth and use that knowledge to identify similar habitats elsewhere (Arrigo, 2022). The most promising analogue environments are located near the poles, where thick ice sheets, isolated saline lakes, and seasonal sea ice create extreme habitats for microbial communities, or in the deep sea, where tectonic activity generates energy-rich hydrothermal plumes that sustain a chemosynthetic food web (Michalski et al., 2017).

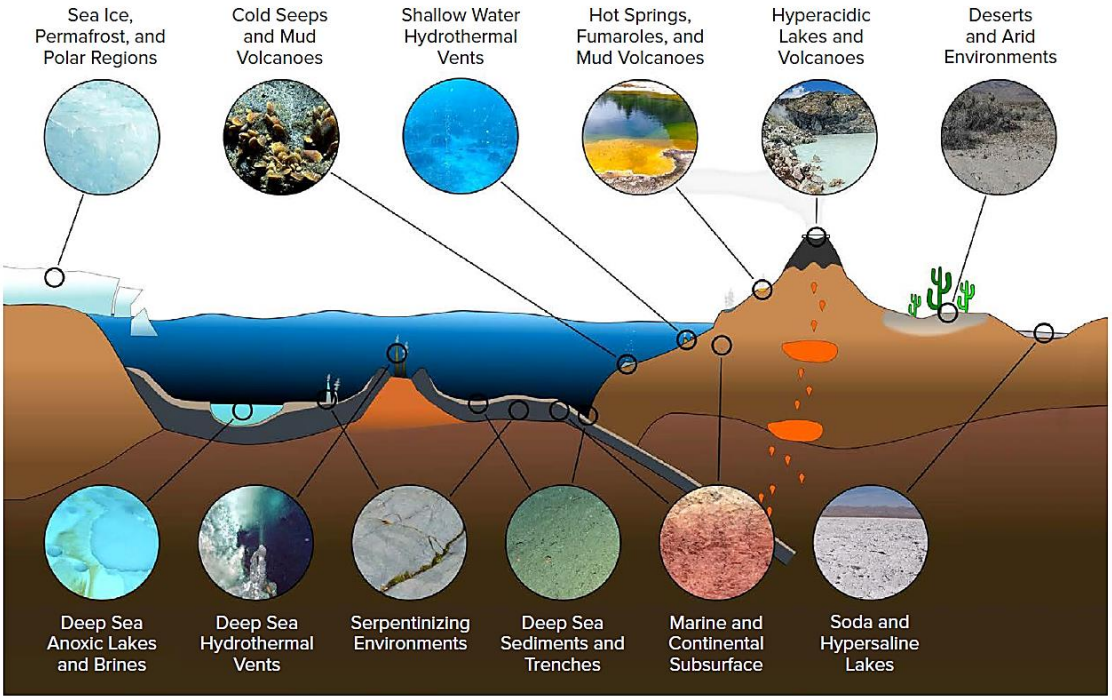

Fig. 4. Representative idealized cross section of Earth's crust showing the diversity of extreme environments where microbes have been found and their approximate location (Arrigo, 2022).

Farias et al. (2013) reported actively forming stromatolites occurrence in volcanic lake Socompa, an extreme environment in the Argentinean Andes, where the extremophile microbes

thrive conditions of high UV radiation, alkalinity, concentrations of arsenic and dissolved salts, and reduced atmospheric O_2 partial pressure.

Extremophiles are organisms that flourish in physically or chemically extreme conditions that are typically harmful to most life on Earth (Rampelotto, 2013). By thriving in environments with temperatures ranging from -15 to 121°C, pH levels from 0 to 14, high pressure, low water availability, high salt concentrations, and exposure to radiation, extremophiles push the boundaries of what we understand about life's limits (Martínez-Espinosa, 2020).

Studying extremophiles offers valuable insights into the origins of life and the potential for life beyond Earth, as these organisms can survive in conditions similar to those found on other planets and moons. Additionally, studying extreme environments on Earth, such as the Dallol Hot Springs (e.g., Cavalazzi et al., 2019), allows researchers to understand microbial adaptation to conditions similar to those on Mars, such as high temperature, high salinity, and low pH.

Extremophiles are classified based on the conditions they thrive in (Fig. 5): thermophiles and hyperthermophiles grow at high and very high temperatures, respectively; psychrophiles are best suited for low temperatures; acidophiles and alkaliphiles are adapted to acidic and basic pH levels, respectively; barophiles thrive under high pressure; and halophiles require high concentrations of NaCl to grow (Gupta et al., 2014; Martínez-Espinosa, 2020).

Many extremophiles are polyextremophiles, meaning they are adapted to survive in environments where multiple physicochemical factors are at extreme levels (Gupta et al., 2014). For example, many hot springs are both acidic or alkaline and rich in metals; the deep ocean is typically cold, nutrient-poor, and under high pressure; and some hypersaline lakes are also highly alkaline (Cavalazzi et al., 2019).

Archaea is the most common extremophiles group and have unique genomes combining bacterial and eukaryotic traits (Eme et al., 2017). Among bacteria, cyanobacteria are the most adaptable to extreme environments (Rampelotto, 2013), forming microbial mats from Antarctic ice to hot springs. They can also thrive in hypersaline and alkaline lakes, tolerate high metal levels, and survive low water availability, even in desert rocks. Among eukaryotes, fungi are the most versatile (Rampelotto, 2013).

Term	Factor	Limits
Acidophile	pH	≥3
Alkaliphile	pH	≥9
Halophile	High salt concentration	1–4 M
Hyperthermophile and Thermophile	High temperatures	Hyperthermophile: above 80 °C (176 °F) Thermophile: between 45–122 °C (113–252 °F)
Piezophile (also called Barophile)	High pressures	~1100 bar
Psycrophile (also called Cryophile)	Low temperatures	≤−15 °C (5 °F)
Radiophile (also called Radioresistant)	UV radiation, cosmic rays, X-rays	1500 to 6000 Gy
Xerophile	Desiccating conditions	≤50% relative humidity

Fig. 5 - General classification of extremophilic microorganisms according to each extreme environment condition (Martínez-Espinosa, 2020).

Investigating planetary field analogue environments is fundamental for identifying the physical and chemical limits that allow life to thrive on Earth and beyond (Martins et al., 2017; Cavalazzi et al., 2019). This type of research is crucial for defining and evaluating habitability criteria on other celestial bodies, including the potential for preserving biosignatures and conducting in situ tests of technologies aimed at detecting life (Cavalazzi et al., 2019; Foucher et al., 2021).

Planetary field analogues serve as natural laboratories for testing field techniques and collecting samples of both biological and non-biological materials (Martins et al., 2017). These samples are then analysed in the laboratory to investigate the relationship between biosignatures and their geological context. Foucher et al. (2021) documented different types of planetary analogue sites, according to their general analogy in their relevance, use and limitations. In the case of astrobiological interest, planetary analogue sites are essential for developing biosignature detection techniques. In addition, studying the metabolism of extremophiles in these environments helps us understand the limits of life and the potential biosignatures they might produce.

Past studies on Mars have focused on detecting signs of ancient water bodies, uncovering a significant number of locations with water-related features (Fig. 6) (Hays et al., 2017). The existence of sedimentary rocks on Mars, dating back approximately 3.7 billion years, along with their potential for habitability, indicates that planets can maintain liquid water and habitable surface conditions over billions of years without plate tectonics (Grotzinger et

al., 2014). One could envision a scenario where Mars or a similar planet experiences hotspot volcanism and an active hydrological cycle, facilitating the movement of C-H-N-O-P-S elements and other ions through rock weathering and chemical imbalances, thereby sustaining local habitable conditions (Cockell et al., 2012).

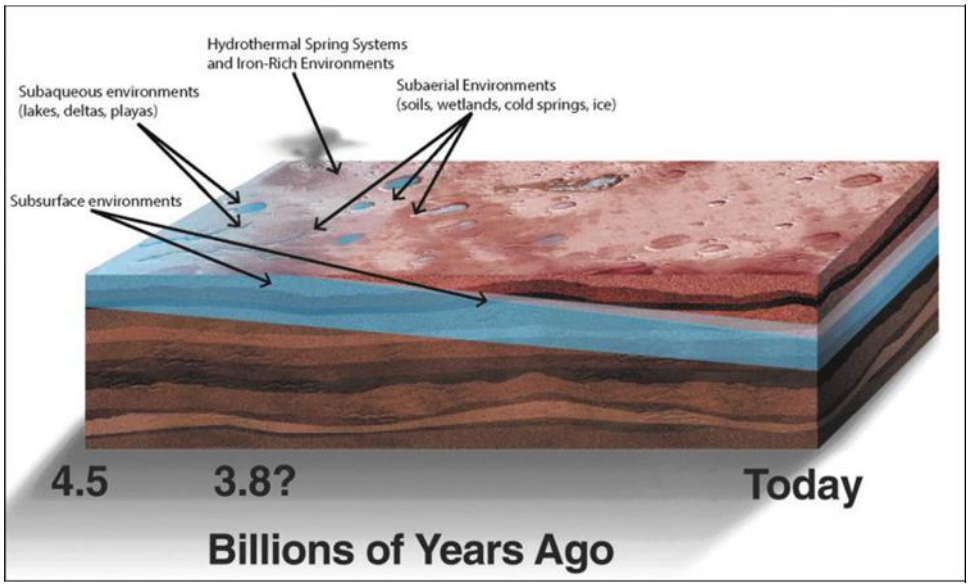

Fig. 6. Ancient Martian environments that should be considered when selecting terrestrial analogue sites (Hays et al., 2017).

Terrestrial analogs for Mars are locations on Earth with geological and biological features that may resemble those on Mars (Marshall, 2006). Potential sites for past or present life on Mars include areas where water was present for extended periods (such as paleolakes and water-eroded channels), hypersaline brines, evaporite deposits indicating salt mineral formation, permafrost, hydrothermal regions, impact craters (which may also be hydrothermal sources), and lakes formed by catastrophic outflows.

Hypersaline systems may thus well be considered a primary hydrological target for studies of Martian habitability (e.g., Barbieri, 2013), due to the abundance of salts on the Martian surface and shallow subsurface, salt tolerance should be considered an important requirement for (present or past) survival on the red planet.

Terrestrial fields may serve as Mars analogues by examining geological and geomorphological structures, as well as mineral precipitation and alteration features that may preserve biosignatures (Marshall, 2006). These analogues offer insights into potential spring deposits on Mars and aid in developing remote sensing techniques to identify them, which is essential for astrobiological research.

1.3. Overview of own research

This PhD research represents a rigorous investigation into the morphological, structural, and geochemical characteristics of continental stromatolites from extreme alkaline lacustrine environments, specifically chosen for their potential as analogues to Martian paleohabitats. Conducted over the last three years, this study aimed to deepen our understanding of stromatolite formations by integrating theoretical insights and innovative analytical techniques. The work was organised in three primary stages: a theoretical literature review, extensive laboratory analysis and fieldwork, and final data integration and interpretation, culminating in the presentation of findings through this thesis and associated scientific papers.

The first stage of the research focused on a detailed literature review, presented in the first chapter of this thesis, examining prior studies on stromatolites, especially those related to alkaline lake systems. This phase provided a comprehensive view of stromatolite characteristics, such as their morphology, textures, geochemical conditions, and associated biological components. Additionally, this theoretical investigation explored the implications of stromatolites for astrobiology, highlighting their significance as sources of biosignatures and their relevance to potential Martian analogues. By examining existing research, we identified key questions and research gaps that guided the subsequent stages of the investigation.

The second phase of the research involved field sampling conducted in the chosen study areas: Lake Ashenge and Lake Abhe in the East African Rift system; and Carri Laufquen Lakes in Argentinean Patagonia. The posterior detailed laboratory stage of the research, represented by the selection and description of the samples, preparation of thin sections, petrographic descriptions, geochemical sampling and performance of laboratory analyses.

The final phase involved synthesising and interpreting the collected data, evaluating the preservation of biosignatures, the influence of organic components on mineral precipitation, and the formation processes of these stromatolitic deposits. This comparative study across different geological sites examined the morphogenetic factors and microstructures of stromatolites, offering new perspectives on their astrobiological relevance. By presenting this thesis and accompanying scientific articles, this research seeks to contribute significantly to the understanding of alkaline lake systems and their potential as planetary analogues.

The material and methods, results, and discussions are detailed in the subsequent chapters of this thesis. Each study area is addressed individually, with Lake Ashenge covered in Chapter 2, Lake Abhe in Chapter 3, and the Carri Laufquen Lakes in Chapter 4. Finally,

Chapter 5 presents a comparative analysis of the three sites and examines their potential as planetary field analogues.

1.3.1. Aims and Rationality of the study

The primary objective of this research was to characterize stromatolites from extreme alkaline lacustrine environments, investigating their formation processes, biotic influence on mineral precipitation, and the preservation of biosignatures. A comparative analysis across three geological sites was conducted to assess the development of micromorphologies, microstructures, and biosignature preservation, evaluating the potential of these environments as astrobiological field analogues for Martian lake palaeoenvironments.

Lacustrine alkaline environments, characterized by high pH levels, offer a distinct setting for the preservation of stromatolites and their associated biosignatures due to a complex interplay of environmental factors, microbial activities, and geological processes (Kempe et al., 1991). Investigating stromatolite formation and preservation within such settings may provide insights into the development of such ecosystems in deep time. Understanding these dynamics is crucial for interpreting the biological and environmental information encoded in stromatolites (Schopf, 2006; Riding, 2006).

Furthermore, lake environments often experience rapid changes in water chemistry and sedimentation rates, influencing the preservation potential of stromatolites. The role of microbial communities in adapting to these changes and contributing to the formation of distinct stromatolitic structures was previously studied (e.g., Mono Lake, USA, Brasier et al., 2018; Las Eras, Central Spain, Sanz-Montero et al., 2019; Lake Salda, Turkey, Balci et al., 2020). Previous research has emphasized the role of microbialites and their mineralization processes in preserving geobiological signatures.

Specific objectives included: 1) define the microfacies of the East African Rift and Patagonian systems, analysing the primary texture, morphology, geomicrobiological components, and mineralogical composition of stromatolites; 2) characterise the biosignatures within stromatolites across three extreme environments, assessing the influence of biofilms, exopolymeric substances and microorganisms on precipitation processes; and 3) investigate morphogenetic and preservation processes as indicators for astrobiological exploration.

The chosen areas have received limited scientific attention, despite the unique characteristics of the alkaline lakes in Africa and Patagonia. To our knowledge, this is the first work presenting a detailed description of Lake Ashenge stromatolites. By examining

stromatolites from alkaline lake systems, we can gain valuable insights into the interplay between biological and geochemical processes that shape these microbial structures. Furthermore, the innovative application of advanced analytical techniques to the study of these stromatolites, for example using ^{13}C Nuclear Magnetic Resonance, will advance our methodological capabilities and deepen our understanding of the complex interactions between microorganisms and minerals in extreme environments.

Lake Ashenge, Lake Abhe and Carri Laufquen Lakes provide a rare opportunity to study biosignature preservation within these settings and to assess their potential as analogues for ancient Martian lake habitats. The three regions, shaped by distinct geological contexts, share critical features that make them suitable for investigating life persistence in harsh conditions, thus serving as invaluable sites for astrobiological exploration.

1.4. Analytical techniques

This PhD research involved multi-analytical techniques, which contributed to specific insights into the morphology, mineral composition, and microstructures of the stromatolites. These techniques included:

- Optical microscopy;
- Raman microspectroscopy;
- Scanning electron microscopy with energy-dispersive X-ray spectroscopy (SEM-EDX);
- Carbon-13 nuclear magnetic resonance spectroscopy (NMR);
- X-ray diffraction/micro-X-ray diffraction (XRD/μXRD);
- TESCAN Integrated Mineral Analyzer (TIMA);
- Fourier-Transform Infrared Microspectroscopy (FTIR).

The samples from the three study areas were equally examined using optical microscopy, SEM-EDX, Raman, and NMR. However, the XRD/μXRD, TIMA, and FTIR analyses were only performed on samples from Lake Ashenge and Carri Laufquen Lakes. The optical microscopy, Raman, XRD, and SEM-EDS analyses on fresh sample fragments, were performed at Università di Bologna. While the FTIR, TIMA, μXRD and SEM-EDS investigations on thin sections, were conducted at the Natural History Museum London. Finally, the NMR analysis was carried out at the Slovenian NMR Center.

Petrographic studies were performed under transmitted and reflected light using a ZEISS Axiophot optical microscope, focal distance of 35 mm (objectives used: 2.5×/0.075, 10×/0.30, 20×/0.50, 40×/0.85), equipped with a Nikon DS-Fi2 digital camera. These observations were complemented by Raman microspectroscopy performed using an Oxford WITec Alpha300 R microscope equipped with a 532 nm green laser. Raman spectra were collected using a 100× Nikon objective and a frequency doubled Nd:YAG (532 nm) Ar-ion 20 mW monochromatic laser source. Beam centring and spectral calibration were performed before spectral acquisition using a Si standard (111) with a characteristic Si Raman peak at 520.4 cm–1, whereas the optimum power for the analyses of different mineral phases was determined experimentally. Raman analyses were visualised and interpreted using WITec Project Management and Image Project Plus software suite and compared with reference spectra from the RRUFF database (Laetsch & Downs, 2006), Frezzotti et al. (2011) and Cavalazzi et al. (2012).

Gold-coated thin sections were studied using a JEOL JSM-IT500 scanning electron microscope equipped with an Oxford Instruments X-Max energy-dispersive X-ray spectrometry, operating at 15 kV. Freshly fractured pieces of samples were gold-coated for observation using a JEOL JSM-5400 SEM-EDS, equipped with an iXRF Si-drift detector with ultra-thin window, operating at 15 kV.

Samples for NMR were powdered with the aid of a Dremel micro-drill instrument (1.6 mm diameter), in order to collect separate layers, avoiding mixing the microfabrics. NMR samples were treated with HCl (10%) for 48 hours to dissolve the inorganic carbonate, thereby concentrating the organic matter, and analyzed using a Bruker Avance Neo 400 MHz NMR spectrometer equipped with 4 mm CP-MAS probe. All samples were spun at a magic angle with 10 kHz at 28 °C. The 1H-13C CP-MAS NMR experiments consisted of excitation of protons with a 90° pulse (P1) of 3.5 us, contact time of 2 ms, and signal acquisition with high-power proton decoupling. A total of 7168 or 8192 scans were accumulated with a repetition delay of 5 s. The chemical shifts were referenced externally using adamantine.

XRD bulk samples were prepared using an agate mortar and pestle to produce a < 10 μm powder and analysed using a Philips PW 3710/00 X-ray powder diffractometer with a Cu K-beta filter (40 kV, 30 mA) over an angular range of 3–70° 2θ. Mineral phases were identified with the QUALX2.0 software, using the POW_COD database.

Non-destructive μXRD measurements were conducted employing a Rigaku D-max Rapid2 Micro-XRD with a curved 2D imaging plate detector. Specimens were examined using Cu radiation at 40 kV and 36 mA. The X-ray beam was adjusted to a dimension of 300 x 100

μm. The specimens were repositioned during the measurements along two axes (omega and phi-rotation) with microscope to load and align flat sample. Measurement at fixed omega angle of 20 º2theta with data collection durations of 15 minutes. 2D data were converted to 1D XRD patterns using the 2DP software (Rigaku). Phase identification was executed using HighscorePlus (Panalytical) in conjunction with the PDF-4 database from ICDD. The Mg content in calcite was derived from the position of the d104 reflection of calcite. The μXRD patterns underwent background subtraction before to phase identification.

Automated mineralogy analysis using the TIMA has been performed with a Tescan TIMA Scanning Electron Microscope. The field emission instrument is equipped with four EDAX Element 30 Energy Dispersive X-ray Spectroscopy (EDX) detectors and was operated at 25 kV accelerating voltage, 13–14 nA probe current and a working distance of 15mm. Analysis of polished thin sections acquired over 21 million EDX points over a duration of 8 hours per sample. Mineralogy was determined by collecting Back Scattered Electron Maps (BSE) combined with EDX analysis at 7 μm pixel resolution with a total of 1000 X-ray counts per pixel.

FTIR spectral maps were obtained using a Nicolet iN10 mx FTIR microscope (ThermoFisher Scientific). The aperture was set to 50 μm × 50 μm. Maps covered the areas of interest with a grid spacing of 30 μm in both axes. Spectra were collected in transmission over a wavenumber range of 4000–675 cm−1 with a spectral resolution of 4 cm−1 using a liquid nitrogen-cooled MCT/A detector and a KBr beamsplitter. For hyperspectral maps, each spectrum was collected for 19.73 seconds (64 scans). A background spectrum with the same parameters was collected through air every 20 minutes. Single spectra were acquired for 78.92 s (256 scans) with the aperture set to 50 μm × 50 μm. A background spectrum with the same parameters was collected through air prior to each single spectrum acquisition. Data were acquired and processed using OmnicPicta software (ThermoFisher Scientific).

Chapter II – Stromatolites from Lake Ashenge, Ethiopia: Controls on Preservation in Extreme Alkaline Environments

The data presented in this chapter correspond to the following manuscript:

Dorneles, V.A.C., Hickman-Lewis, K., Haileselassie, T.H., Hagos, M., Šket, P., Balotti, L. & Cavalazzi, B. Stromatolites from Lake Ashenge, Ethiopia: Controls on Preservation in Extreme Alkaline Environments. Submitted for *Astrobiology*.

2.1. Introduction

Lake Ashenge (also spelled Lake Hashange or Lake Hashengi, Marcus, 1975), is a highly alkaline closed-basin lake located in the southern part of the Tigray region in NE Ethiopia (Fig.1). The lake presents an altitude of ~2440 m, with pH ~8.8 and conductivity ~1600 µS cm^{-1}. The surface area of Lake Ashenge is approximately 15.4 km^2 and its maximum depth is 23 m, ephemeral inflows drain from the north, but there is no current surface runoff, and the lake level is controlled by evaporation and underground infiltration (Marshall et al., 2009).

In this chapter, we report and describe stromatolites from Lake Ashenge, which were first reported by Marshall et al. (2009) and simply described as Holocene microbialite crusts on basaltic boulders and bedrock. We present for the first time a detailed study from outcrop to submicron scale of the microfacies, microbial components and geochemical signatures of subfossil stromatolites from Lake Ashenge, aiming to understand their morphogenetic and preservational processes, thereby providing novel information about the development of stromatolites in extreme alkaline environments.

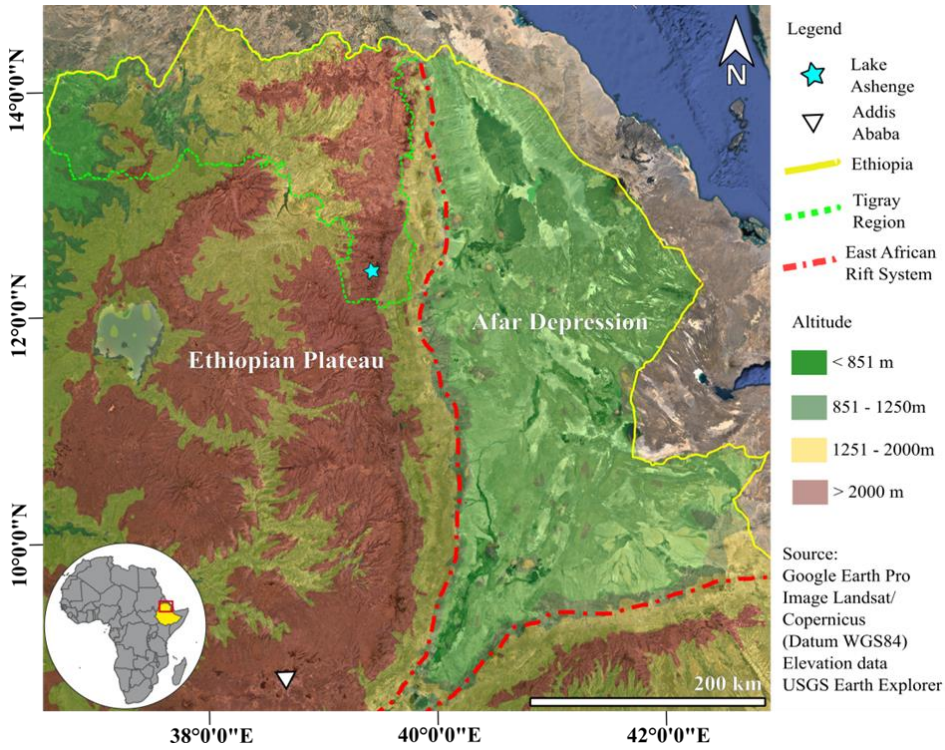

Fig 1. Location and geological context of Lake Ashenge (pale blue star) area, settled on the Ethiopian Plateau, Tigray Region, northern Ethiopia, within the East African Rift System.

2.2. Geological Context

Lake Ashenge is located in the Ethiopian Plateau (Fig. 1) or Highland, in which the highest peaks standing well above 3500 m above sea level, at the western bord of the Afar Depression (or Afar Triangle) of the East African Rift System (EARS) (Cavalazzi et al., 2019). The Afar Depression is an active continental rift system consisting of an NNE–SSW trending fault structure cutting the eastern part of the African continent from the Red Sea to the lower Zambezi Valley (Ebinger, 1989; Corti, 2009; Cavalazzi et al., 2019), including prominent marginal grabens, such as Ashenge graben (Marshall et al., 2009).

The Ashenge graben included in the larger Raya graben is situated along the Red Sea branch of the EARS typified by moderate volcanic activity if compared to its western branch (Tiercelin, 1991). The different lake physiography of the EARS (Casanova, 1994) seems to reflect the different tectono-volcanic dynamics of the area: the western lakes are larger and deeper such as the Tanganyika Lake (1470 m; Verburg & Hecky, 2009), whereas lakes are smaller and shallower on the east side such as Turkana Lake (114 m; Zainescu et al., 2023). The graben bottom which hosts the lake is a mid-Tertiary volcanic formation corresponding to flood basalt pile of the Ashangi Group (Marshall et al., 2009; Lanckriet et al., 2015; Shishaye & Asfaw, 2020). The volcanic basement rocks of Lake Ashenge likely contributed to its alkalinity (Casanova, 1994; Cerling, 1994; Marshall et al., 2009) and play a major role in its water geochemistry dominated by Na^+, CO_3^{2-} and HCO_3^- with lower concentrations of K^+, Ca^{2+}, Mg^{2+}, Cl^- and SO_4^{2-} (Marshall et al., 2009).

Moreover, different (living and non-living) stromatolites are reported from extreme lacustrine environments of the EARS (Casanova, 1994; Marshall et al. 2009; Ghinassi et al., 2012; Deocampo & Renaut, 2016; Renaut et al., 2017; Mologni et al., 2021). These lacustrine high alkaline (pH=10) and saline (salinity <300 mg/L) lakes, and hydrothermal (T=35-100ºC) environments, have been colonized by microbial communities and stromatolite-forming consortia over the past ten million years (Lower–Middle Miocene) (Casanova, 1994). The oldest recorded occurrence of stromatolites is in the Ch'orora Formation, in the northern part of the Rift in Ethiopia, dated to 10.5 Ma (Late Miocene) (Tiercelin et al., 1979). EAR lacustrine stromatolites have been used as indicators of paleolake levels, and better understand relationship between their morphology with the geological and hydroclimatic settings, examples are Lake Abiyata (Legesse et al., 2002), Lake Tana (Marshall et al., 2011), Lake Hayk (Lamb et al., 2007), Lake Abaya-Chamo (Foerster et al., 2012) and Lake Turkana (Bloszies & Forman, 2015).

2.3. Material and Methods

Lake Ashenge stromatolites were sampled in a field campaign conducted in December 2019. Sample preparation took place at the Università di Bologna, Italy, followed by investigation using routine and advanced analytical techniques. Nineteen samples were embedded in epoxy resin to produce 26 uncovered petrographic thin sections (~30 µm thickness and 60x90 mm dimension).

Microfacies and microbial textures were described under optical microscope. Elemental, mineralogical am biomolecular composition of selected regions of interests were analyzed using Scanning Electron Microscopy and Energy Dispersive X-ray Spectroscopy (SEM-EDX), Raman microspectroscopy, Micro X-ray Driffraction (µXRD) and Fourier-Transform Infrared microspectroscopy (FTIR). X-Ray Diffraction (XRD) and solid state ^{13}C Nuclear Magnetic Resonance (NMR) spectroscopy were performed in order to investigate the mineralogical composition and molecular organic components of the bulk samples.

Six thin sections were used for the SEM-EDX analyses, in addition to freshly fractured pieces of five samples from the same thin section group. Four thin sections were studied using Raman and FTIR spectroscopy. For µXRD, eight thin sections were analysed. In the case of XRD and NMR, bulk samples were used: three for XRD and four for NMR.

2.4. Results

2.4.1. Lake Ashenge outcrops and stromatolites

Stromatolites at Lake Ashenge occur as macroscale subspherical to domed bioherms with diameters and height varying from centimetre- to metre-scale. Stromatolites samples were collected along distinct terraces on the shores of Lake Ashenge (Fig. 2A) represented by different topographic levels 1 to ~30 m above present lake level, which correspond to exposed higher palaeolevels of the lakeshore (Fig. 2B-C). The lowest palaeolevel corresponds to stromatolites developed along the current waterline at an altitude of 2433 m (Fig. 2D), and the paleolevels above reach an altitude of 2452 m.

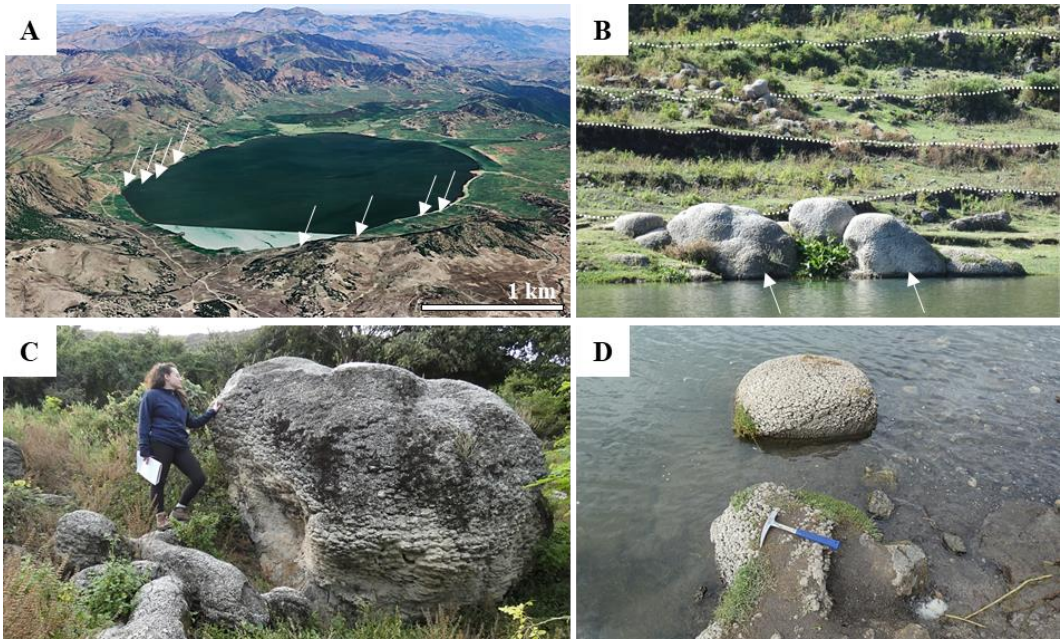

Fig 2. Lake Ashenge overview and outcrops images. A) 3D image of Lake Ashenge and all the spots where the samples were collected represented by the yellow arrows on the shores of the lake (Source: Google Earth). B) Palaeoshorelines of Lake Ashenge are delimited by yellow dashed lines and occurrences of domal stromatolites on the current shore domal stromatolites (yellow arrows). C-D) Outcrop view showing decimetre to metre-scale domal stromatolites on the northwestern shore of Lake Ashenge.

Stromatolitic outcrops present macroscopic isolated columnar and isolated and coalescing domal morphologies up to 3.5 m in diameter. Interior fabrics, where exposed in the field, exhibit a layered structure comprising diverse flat-laminated and mesocolumnar structures (Fig. 3A), which present a sharp contact between layers (Fig. 3B). The stromatolites, initially coating the boulder with a millimeter-scale carbonate crust (Fig. 3C), continue their growing with bulbous and columnar microstructures form a laterally continuous layer reaching up to several centimeters in thickness. Lake Ashenge stromatolites are also observed to grow over (directly in contact) the volcanic bedrock and around basalt boulders (Fig. 3D).

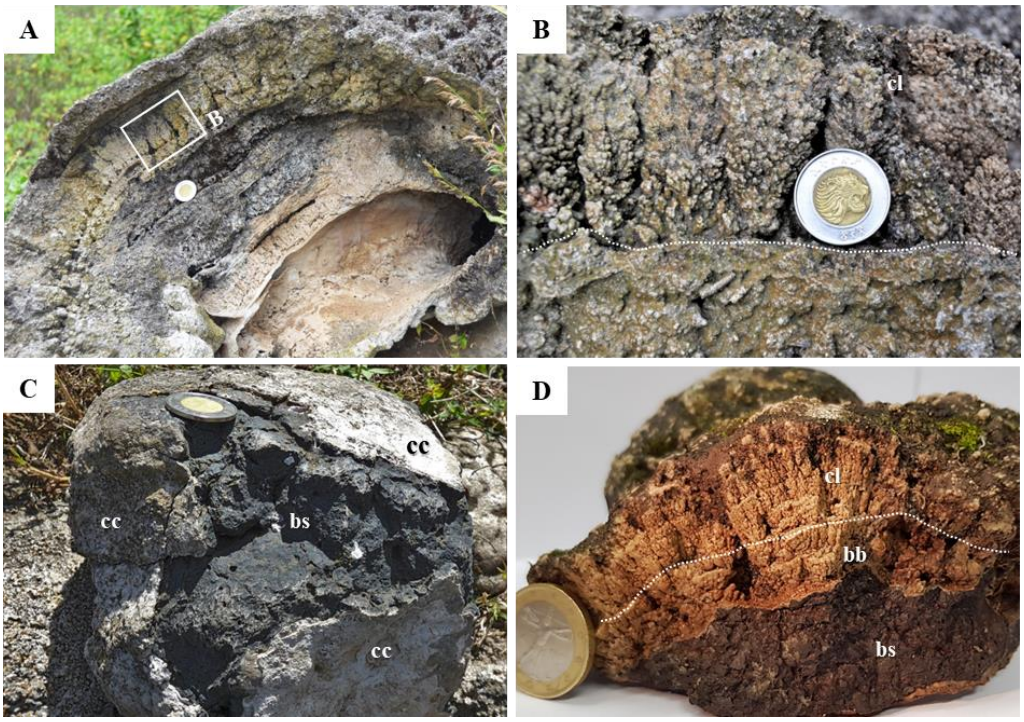

Fig 3. Stromatolite field photographs and samples. A) Domal stromatolite showing an internally layered structure comprising a columnar fabric (B square) interleaved with carbonate crust layers. B) Close-up of the columnar fabric, showing the very-well developed columns (cl) forming a stromatolite layer. C) Basaltic boulder (bs) surrounded by millimetre-scale carbonate crust (cc), representing the initial stage of carbonate precipitation. B) Hand sample showing well-developed columnar and bulbous (bb) stromatolite growth over a basaltic substrate and the gradual contact between the microfacies (white dashed line). A, B and C, one birr coin for scale; D, one euro coin for scale.

We present our microscopic results in two sections: the first corresponding to the different microfacies, morphologies and mineral composition; and the second section will deal with the microbial components and biomolecules associated with the stromatolites studied.

2.4.2. Morphology, petrography, mineralogy and chemical composition of stromatolites

Lake Ashenge stromatolites are composed of diverse microstructures that configure two distinct microfacies: a) columnar stromatolites (e.g., Hofman, 1973), the major element constituting the stromatolite domes; and b) bulbous stromatolites (e.g., Jones et al., 2000a), occurring most commonly at the bottom of the dome in contact with the volcanic rock of the lake basement and palaeoshorelines. Columnar and bulbous stromatolites may occur either in association or independently, often showing a gradual change of microfacies from bulbous to columnar or the opposite (Fig. 4A). In some cases, the basal stromatolitic microstructures develop as bulbous forms that grade into columns within the same layer.

Columnar stromatolites are formed of straight to branching columns that are either isolated or close-linked (Fig. 4B). Individual columns are approximately 1.6 to 6.0 mm in height and 0.3 to 1.3 mm in width. Columns develop different branching styles during growth, such as 1) anastomosed, with coalescence of columns initially growing parallel to each other, then migrating to a close-linked growth, forming interconnected layers that again grade into single parallel columns; 2) multifurcate, when columns grow in different directions from within the same initial layer; and 3) lateral branching, when a new column grows from the side of a pre-existing column.

Bulbous stromatolites are instead formed of non-branching cumulate structures, as convex vertically stacked hemispheroids, which can occur isolated or closely linked, forming clusters or layers (Fig. 4C). They range from 0.7 to 1.7 mm in length with a maximum width of 0.6 to 1.4 mm and present a regular growth such that several bulbous structures of similar size and with flattened tops grow in a closely linked arrangement to form a layer that serves as a substrate on which new bulbous or even columnar stromatolites can develop.

A yellow-brown mineral phase was also observed with two modes of occurrence: around the microstructures and partially filling voids (Fig. 4D). Both microfacies feature micrometre-scale slightly laminated microfabrics consisting of hemispherical moderately to parabolic convex upward laminae within columnar and bulbous microstructures. Stromatolitic laminae are laterally continuous and composed of thinner layers of brown micrite, characterized by a cryptocrystalline texture (grains < 4 μm), intercalated with thicker layers of non-isopachous gray microsparite, characterized by a fine-grained calcite matrix (grains 5 to 30 μm).

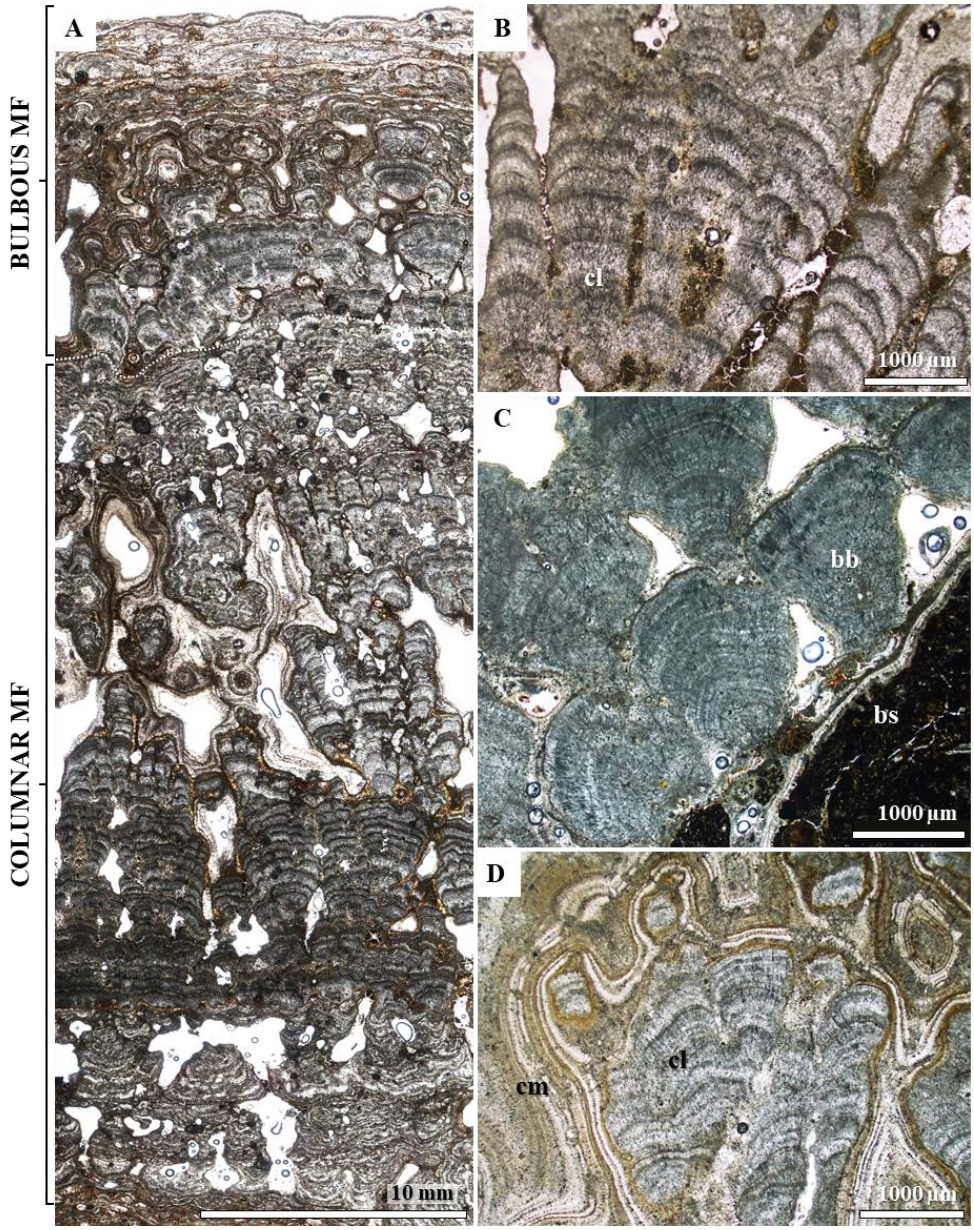

Fig 4. Overview of the representative examples of the Lake Ashenge stromatolites main components under optical microscope. A) Thin section scan showing the microstratigraphy of a representative laminated structure of a domal stromatolite, presenting a layered structure with a prevailing internal microcolumnar microfacies (MF) in the bottom part of the sample and a bulbous microfacies at the top. The yellow dashed line shows the contact between the microfacies. B) Columnar microfacies featuring internally layered columns (cl) that grow convex-upward showing closely linked branching columns and straight single columns. C) Bulbous microfacies composed of regular bulbous structures (bb) growing convex-upward directly on the underlying basaltic rock (bs) and forming the basal layer of the stromatolite. D) Microspar cement (cm) filling intercolumnar voids, showing different layers of precipitation, in association with a yellow-brown material.

XRD powder diffraction analyses showed that both microfacies are composed of Mg-calcite (6% mole $MgCO_3$), as also indicated by SEM-EDX and Raman. SEM-EDX analyses showed an elemental composition typified by Ca, Mg, O and C for both columnar (Fig. 5) and bulbous (Fig. 6) stromatolitic microfacies and the surrounding microsparitic cement. The

yellow-brown material described under optical microscopy was identified as possibly stevensite ($Ca_{0.2}\,Mg_{2.9}\,Si_4O_{10}\,(OH)_2\,4H_2O$) using µXRD.

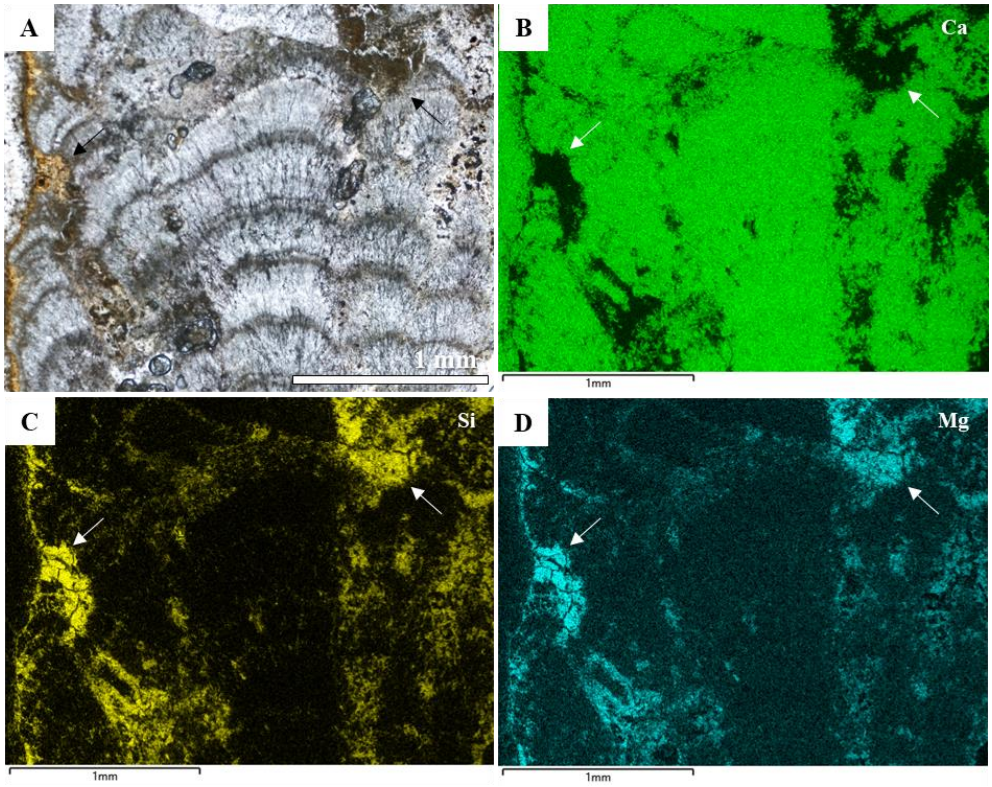

Fig 5. Optical photomicrograph and EDS compositional maps of columnar stromatolites. A) Optical photomicrograph showing an overview of columns surrounded by a void-filling yellow-brown material (white arrows). B-C-D) EDS elemental maps showing the respective distribution of calcium (Ca), silicon (Si) and magnesium (Mg). Mg is correlated with Si in the void-filling phase surrounding the columns, while the columns are represented as a Ca-rich phase.

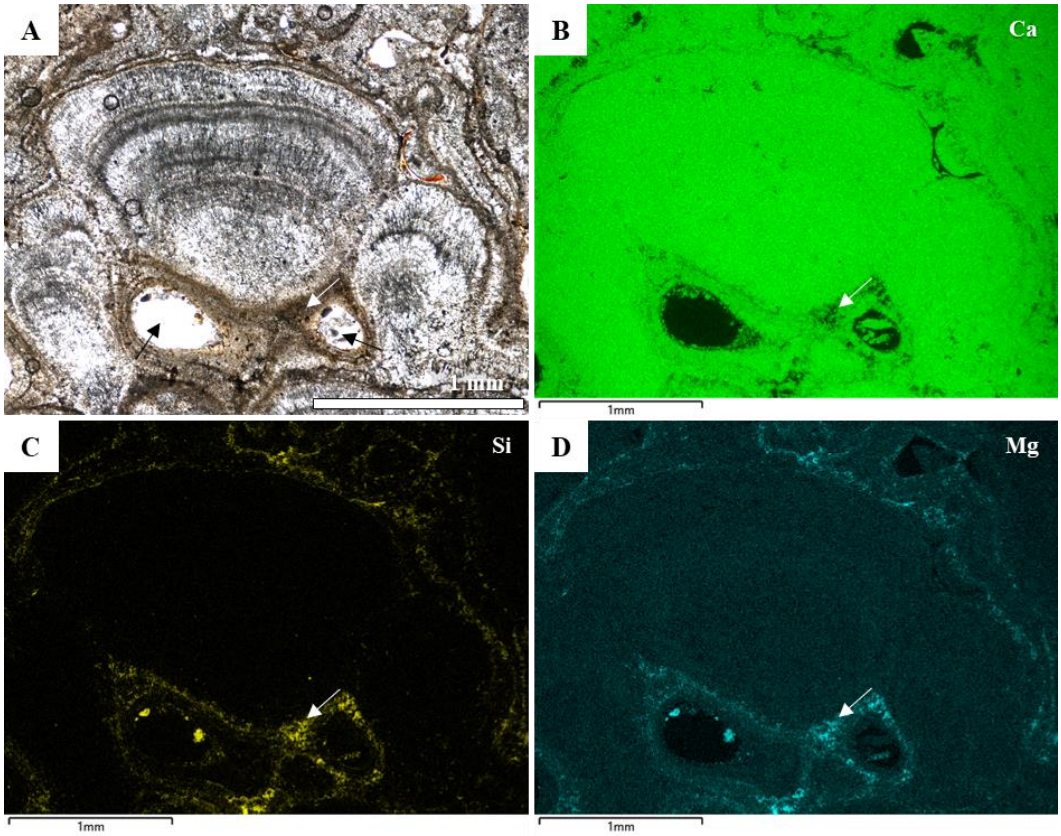

Fig 6. Optical photomicrograph and EDS compositional maps of bulbous stromatolites. A) Optical photomicrograph showing a bulbous microstructure surrounded by a void-filling yellow-brown material (white arrow); red arrows indicate holes in the section filled by resin. B-C-D) EDS elemental maps showing the respective distribution of calcium (Ca), silicon (Si) and magnesium (Mg). Mg occurs correlated with Si surrounding the bulbous microstructure, which is represented as a Ca-rich phase.

Raman microspectroscopic mapping and spectral analysis confirms a Mg-calcite composition for the matrix (bands at 157, 284, 714 and 1088 cm^{-1}) and also identifies filamentous structures containing carbonaceous materials, characterized by the D (1336 cm^{-1}; disordered carbon) and G (1593 cm^{-1}; graphite) bands (Fig. 7).

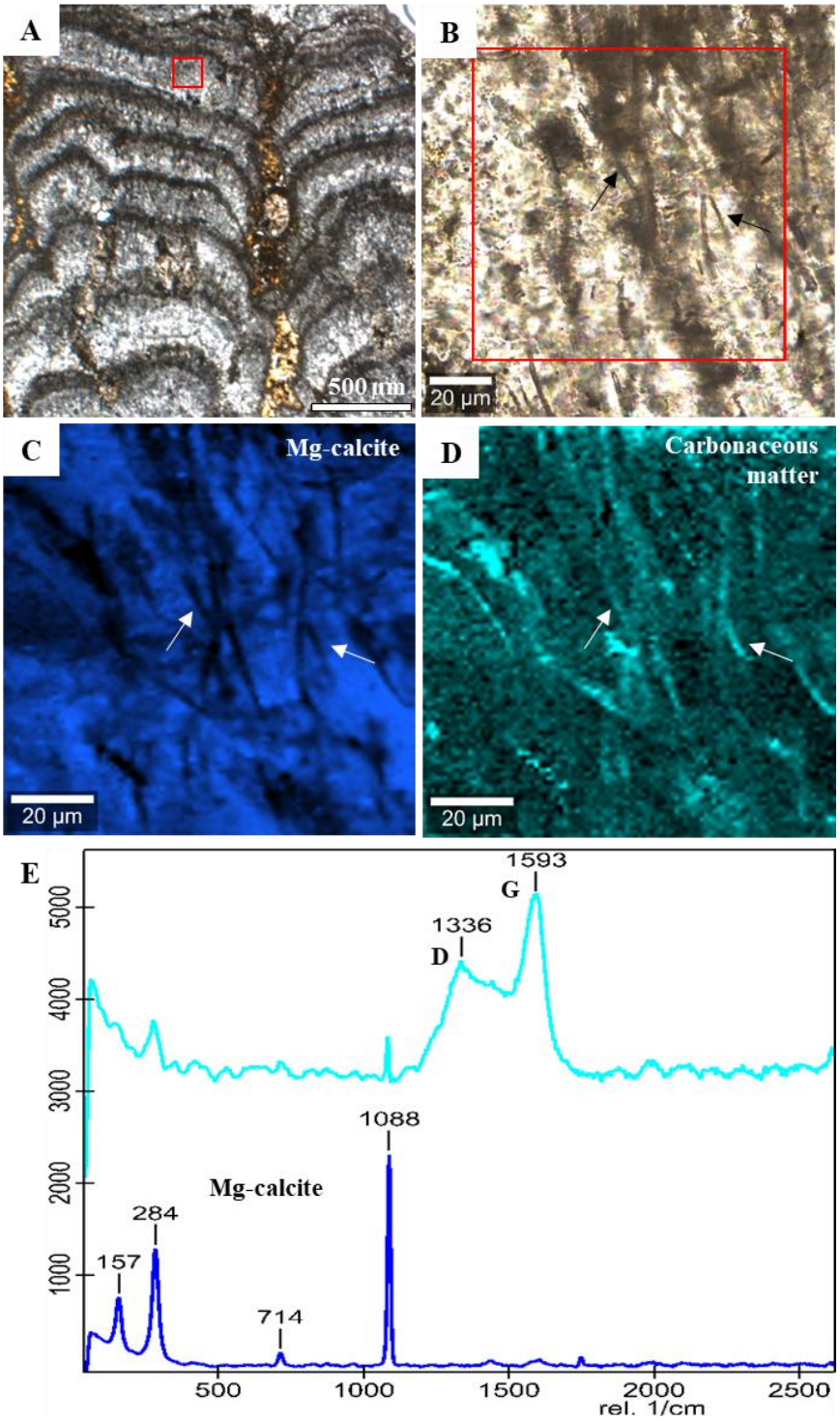

Fig 7. Optical photomicrograph and Raman microspectroscopic maps of filamentous structures. A) Optical photomicrograph showing an oveverview of the columns and the selected area for mapping the filamentous structures (red square). B) Close-up of the region of interest with the filamentous structures (arrowed). C) Raman microspectroscopic map showing the matrix composed of Mg-calcite (blue area). D) Raman map showing the distribution of carbonaceous matter-rich filaments highlighted in pale blue. E) Raman spectra representing in dark blue the Mg-calcite (157, 284, 714 and 1088 cm-1) as the main phase; and in pale blue the filamentous structure observed under optical microscope previously, filled up with carbonaceous matter represented by the D and G bands (1336 cm-1 and 1593 cm-1, respectively).

Lake Ashenge stromatolites collected on both sides of the lake also show the participation of other intraclasts as components in their formation, such as bioclasts and detrital. Basal layers of the domal stromatolites and rarely the tops of columns feature trapped sediments consisting of distended or entire ostracod valves in life position, which were also recognized in voids between microcolumnar and bulbous microstructures. Trapped gastropod shells were also observed as isolated clasts between the microstructures, ranging in size from 1.2 to 4.0 mm and partially filled with sparry calcite cements. To a lesser extent, detrital siliciclastic grains composed of pyroxene, olivine and opaque minerals were also identified trapped within the intercolumnar void spaces. The siliciclastic grains are angular with low sphericity, vary in size <1 mm, and do not show features suggesting long transport distances. No significant diagenetic features, such as micritization, dissolution or recrystallisation were identified in the studied microfacies.

2.4.3. Microbial components of stromatolites

Lake Ashenge stromatolites are dominated by exceptionally well-preserved filamentous structures within both the micritic and microsparitic laminae. The filamentous structures are straight to slightly curved, non-septate and unbranched, and occur either isolated or in clusters. They are oriented vertically and perpendicular to the stromatolite laminar growth, displaying distinct palisade-like spatial arrangements (e.g., Campbell et al., 2015) (Fig. 8A). In columnar stromatolites, filaments occur mostly in parallel or interlaced vertical arrangements, commonly delimited by layers; in bulbous stromatolites, filaments form shrub-like clusters (e.g., Chavetz & Guidry, 1999) throughout their entire volume (Fig. 8B), as well as at the base of the structure, grading to a vertical parallel arrangement at the top.

Across both microfacies, the diameters of the filaments are constant from 3.5 to 5.5 µm and reach up to ~250 µm in length. Filamentous structures appear best preserved in microsparitic laminae, where they form densely aggregated colonies laterally distributed within the layer; in micritic laminae, which are characterized by an aphanitic texture, relatively few spaced filamentous structures or concentrated clusters are present. Filaments occur as empty thicker molds or filled with a brown translucent phase, as well as thinner filamentous structures (Fig. 8C). They may occur as isolated empty filamentous structure in a micritic matrix (Fig. 8D).

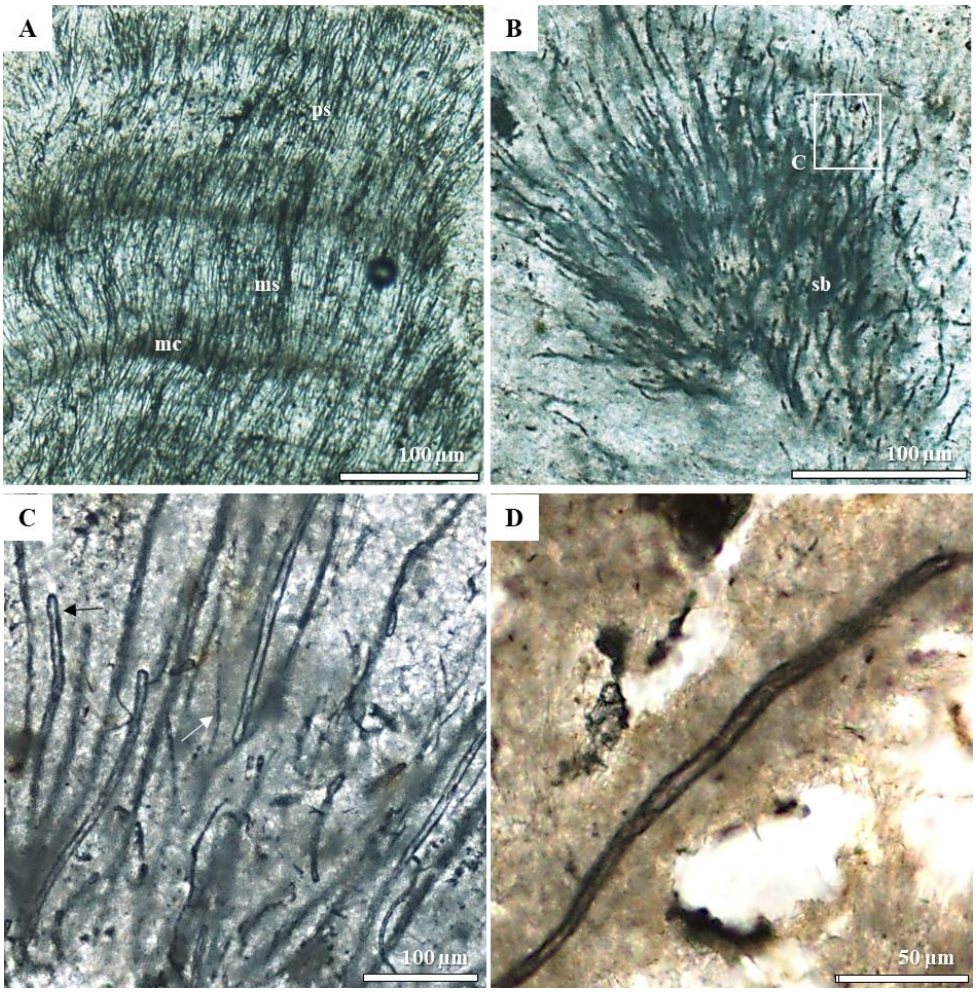

Fig 8. Photomicrographs of filamentous structures in Lake Ashenge stromatolites. A) Typical stromatolitic fabric showing filamentous structures preserved within columnar stromatolite as palisade-like (ps) textures in a variation of laminae composed of micrite (mc) and microsparite (ms). B) Bulbous stromatolites show filamentous structures forming a shrub-like (sb) textures. C) Close-up of B showing the cluster of filamentous structures preserved either as empty filamentous sheath molds (black arrow) or thinner filamentous structure (white arrow). D) Close-up of a single empty filamentous preserved isolated in the mineral matrix.

SEM observations of both microfacies confirm that filamentous structures are the main components of the stromatolites. SEM imaging shows variation in the preservation of structures associated with distinct micrite and microsparite laminae (Fig. 9A). In microsparite laminae, filamentous structures are preserved as densely parallel vertically oriented semi-open remains forming a palisade-like texture (Fig. 9B). In contrast, in micritic laminae, only the molds of the filamentous structures were preserved, with multiple orientations (Fig. 9C).

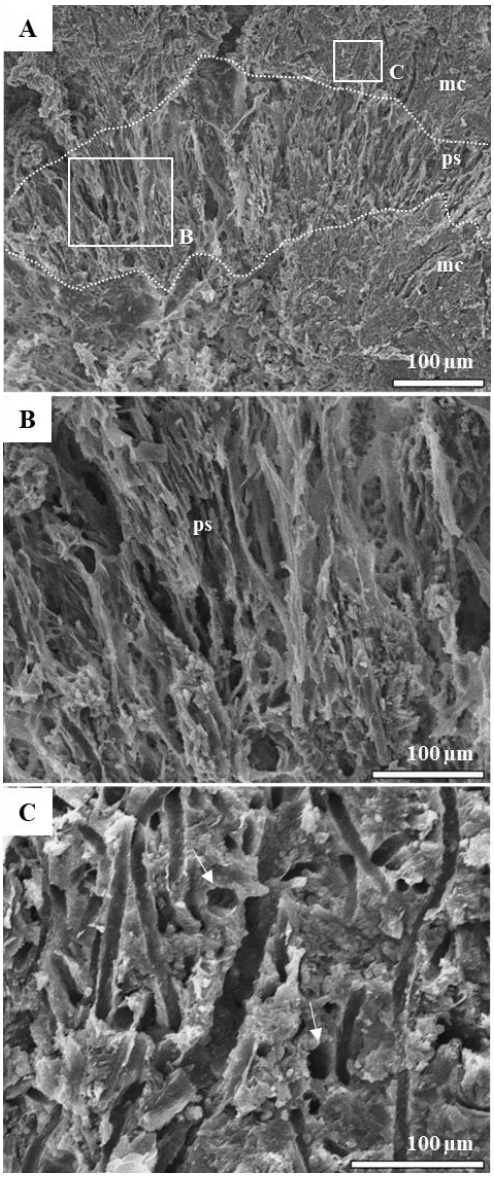

Fig 9. SEM micrographs showing the different layers forming Lake Ashenge stromatolites. A) Layered fabric composed of massive micrite (mc) and microsparite containing densely vertical filamentous structures cluster that forms a palisade-like (ps) texture. B) High-magnification image showing densely packed filamentous structures with a vertical parallel growth pattern forming the palisade-like texture in A. Filamentous structures were preserved in this layer mainly as a cluster of semi-open and empty tubes. C) High-magnification image of the micrite layer in A showing molds of filamentous structures in a massive aphanitic micrite matrix. Filamentous mold structures present no preferential orientation of preservation in these layers; molds were recognized in both vertical and horizontal orientations (white arrows).

SEM imaging also revealed a matrix composed of carbon-rich amorphous structures with an alveolar network (Fig. 10A), in which microscopic components, such as pennate diatoms, are trapped (Fig. 10B), occasionally showing fractures and dissolution of the valves (Fig. 10C). Elongated crystals of Mg-calcite formed of micrometer-scale anhedral polyhedrons are intrinsically associated with carbon-rich amorphous structures in the matrix (Fig. 10D); and they occur as products of the coalescence of triangular nanocrystals (Fig. 10E). On the walls

of the open molds of the filamentous structures, we also recognized the initial developmental stages of Mg-calcite nanocrystals (Fig. 10F).

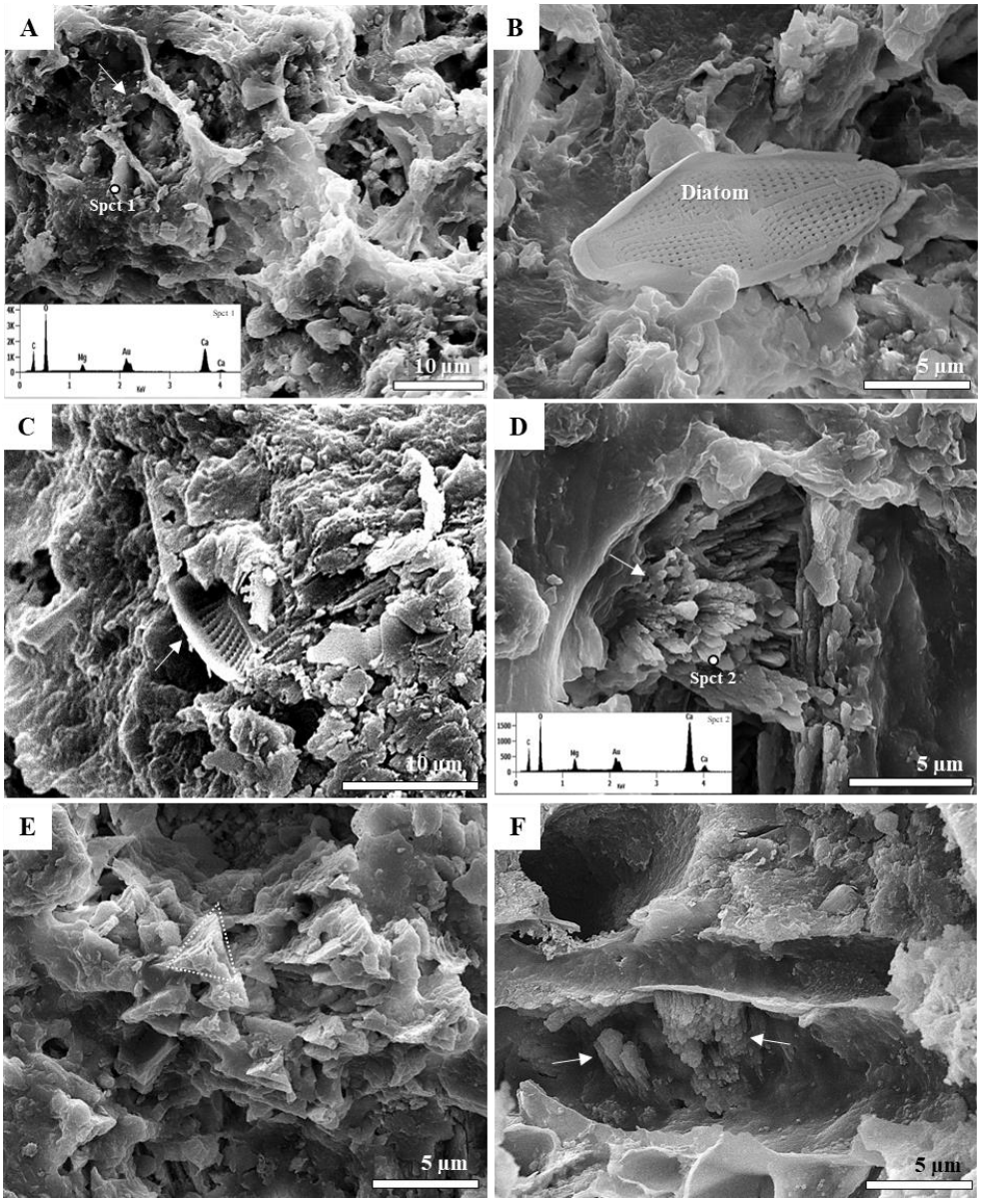

Fig 10. SEM micrographs showing the nano- to micrometre-scale components of the Lake Ashenge stromatolites. A) Carbon-rich amorphous structure in the matrix, showing an alveolar network (white arrow); inset shows EDX elemental spectrum indicating a high carbon content. B) Representative example of preserved pennate diatom valve in association with amorphous-like structure. C) Occurrence of fractured and partially dissolved diatom frustule (yellow arrow) in association with amorphous carbon-rich material. D) High-magnification image showing amorphous structure in association with anhedral nanocrystalline precipitates of Mg-calcite in the matrix; inset shows EDX elemental spectrum indicating elevated magnesium content. E) Nanocrystalline precipitates occur also as tetrahedrons (red dashed line) formed by the coalescence of previous polyhedrons associated with the organic matrix. F) Opened filamentous mold structures showing nanocrystalline precipitates developed around the walls of the molds. EDX spectra were obtained with voltage 6.8 kV. Au peak corresponds to the gold used for coating the samples.

SEM-EDX observations allow distinct processes involved in the preservation of filamentous structures within Lake Ashenge stromatolites to be recognized. An amorphous material rich in Mg and Si partially or completely filled the molds, suggesting the presence of Mg-silicate phases forming the counterpart of filamentous structures (Fig. 11A). The fossilized filled filamentous structures correspond to the yellow-brown translucent phase described previously in thin section. Empty molds of filamentous structures were also preserved; in these cases, we observed the presence of carbon-rich amorphous structures covering the mold walls as sheaths (Fig. 11B).

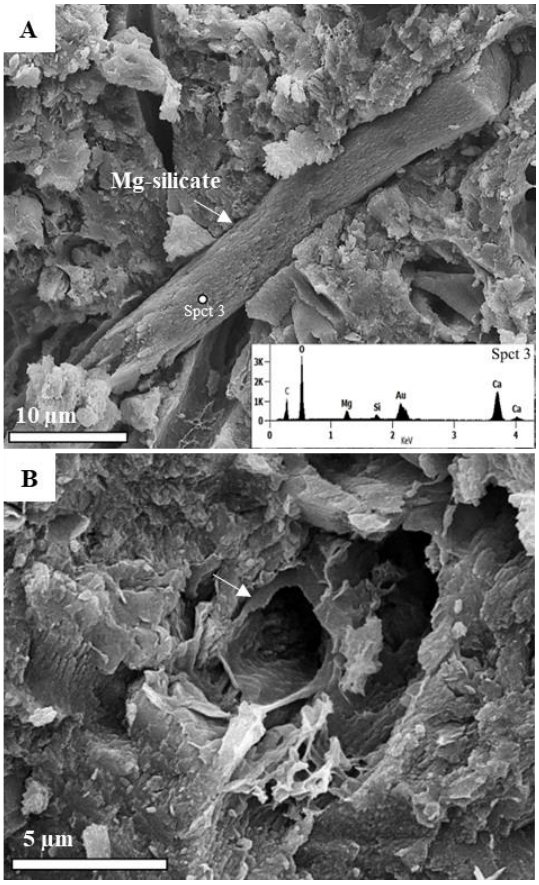

Fig 11. SEM micrographs of filamentous structures preserved in the Lake Ashenge stromatolites. A) Filamentous structure preserved as molds filled with amorphous material rich in Mg and Si, suggesting the presence of Mg-silicate phases (see inset EDX spectra). B) Close-up of a filamentous structure preserved as an empty mold in association with carbon-rich amorphous structures in the matrix, and amorphous structure remains preserved in the walls of the mold (white arrow). EDX spectra were obtained with voltage 6.8 kV. Au peak corresponds to the gold used for coating the samples.

Higher magnification EDS maps show that the filamentous structures are composed of Si and Mg, preserved in a Ca-rich matrix (Fig. 12). The elemental maps indicate an inverse relationship between the Ca and Si+Mg content. Detrital silicate grains were also observed trapped in the matrix. As previously shown, Raman microspectroscopic mapping (Fig. 7) also

indicates the presence of carbonaceous materials, characterized by the D and G bands within the filamentous structures.

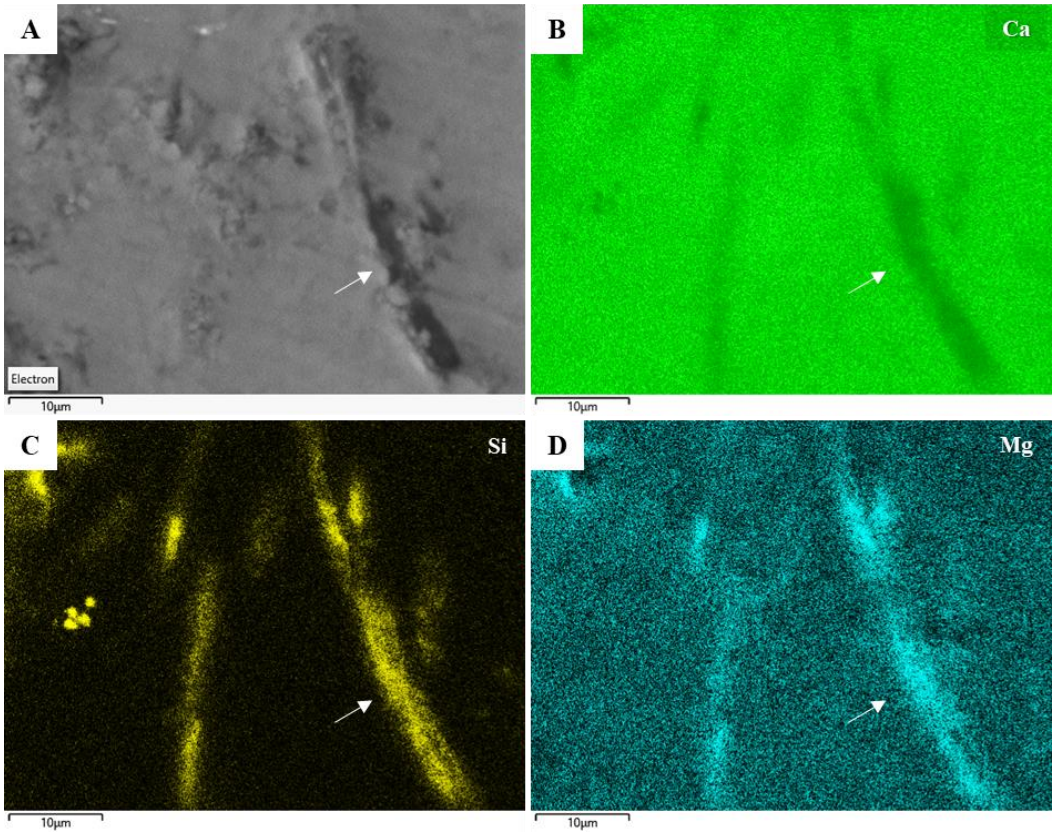

Fig 12. SEM-EDX image and compositional maps of filamentous structures. A) SEM micrograph showing filamentous mold structures (arrowed). B-C-D) EDX elemental maps showing the distribution of calcium (Ca), silicon (Si) and magnesium (Mg). Si is correlated with Mg within the filamentous structures, which are embedded in a Ca-rich matrix; O (not shown here) is ubiquitously distributed throughout the sample.

We used 13C NMR and FTIR to investigate in detail the composition of the carbonaceous material identified using Raman microspectroscopy. The solid state ^{13}C NMR spectrum shown in Figure 13 corresponds to a representative sample of Lake Ashenge stromatolites in comparison with previous works (for more NMR data, see Supplementary Material 1). Strong signals identified in the NMR spectrum, ranging from 10 to 180 ppm, represent different organic bands. Lake Ashenge NMR spectrum is dominated by broad peaks of aliphatic carbon (C_{aliph}) centered at 32 ppm (most intense signal), carbon-oxygenated (C–O) functionalities at 69 ppm, unsaturated carbon (C=C) at 128 ppm, and carboxylic acid (COO^-) at 168 ppm and 157 ppm.

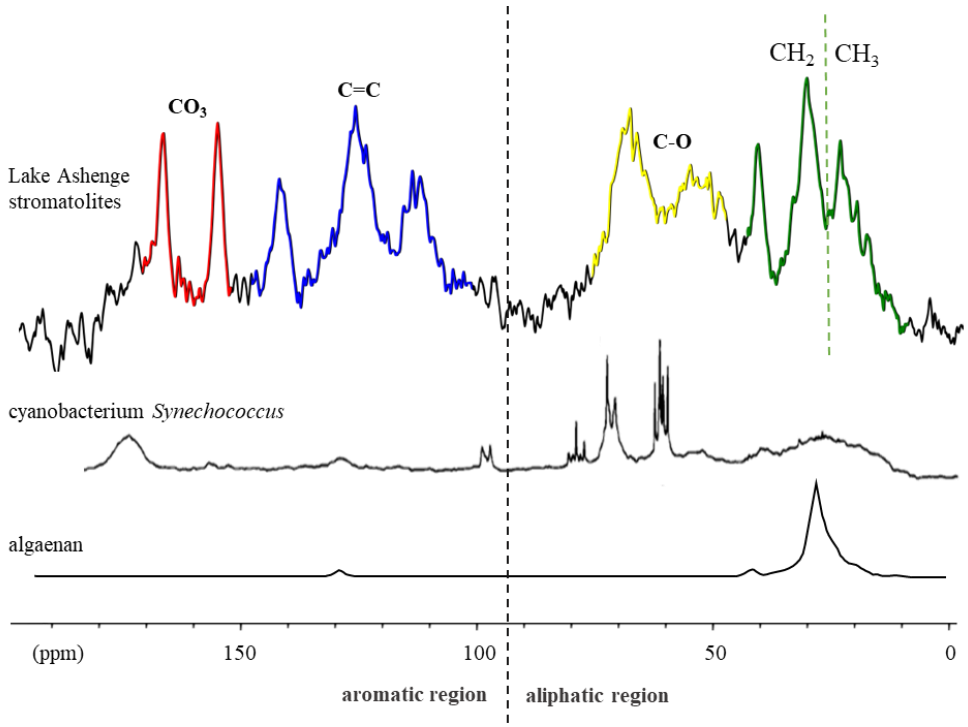

Fig 13. Solid state 13C NMR spectra of Lake Ashenge stromatolites. 13C NMR spectrum represents the ranges of biomolecule bands recognized according to the 13C NMR intensity, in which the highlight colors correspond to aliphatic carbon (Cali, green), carbon-oxygen (C-O, yellow), unsaturated carbon (C=C, blue) and carboxylic acid (CO3, red) moieties. For comparison proposal, the spectrum of cyanobacterium Synechococcus (adapted from Mackay and Norton, 1987) showing a correlation in the C-O bands with Lake Ashenge data; and the algaenan spectrum (adapted from Nguyen et al., 2003), strongly correlated regarding the Cali signals from Lake Ashenge spectra.

Multiple laminated and filament-rich regions of interest in four stromatolite samples were studied using FTIR microspectroscopy. Hyperspectral FTIR mapping indicates that dark laminations rich in organic materials and filament-rich regions of the samples exhibit more intense signals relative to the surrounding matrix in the aliphatic C–H stretching region (3000–2800 cm–1) (Figs. 14 and 15). The absorption characteristics of this region show features consistent with the presence of CH2 (the symmetrical stretch at ~2850 cm–1 and the asymmetrical stretch at ~2920 cm–1) and CH3 (the symmetrical stretch at ~2870 cm–1 and the asymmetrical stretch at ~2960 cm–1). The relative enrichment of CH2 over CH3 suggests that the aliphatic hydrocarbon fraction is dominated by long, unbranched fatty acids with a CH3/CH2 ratio less than 0.4 (cf. Igisu et al., 2012). Signal intensity and signal-to-noise ratio is generally higher in filament-rich regions (Fig. 15) than in bulk laminations (Fig. 14). The FTIR spectra obtained confirm the detections of aliphatic carbon made by NMR.

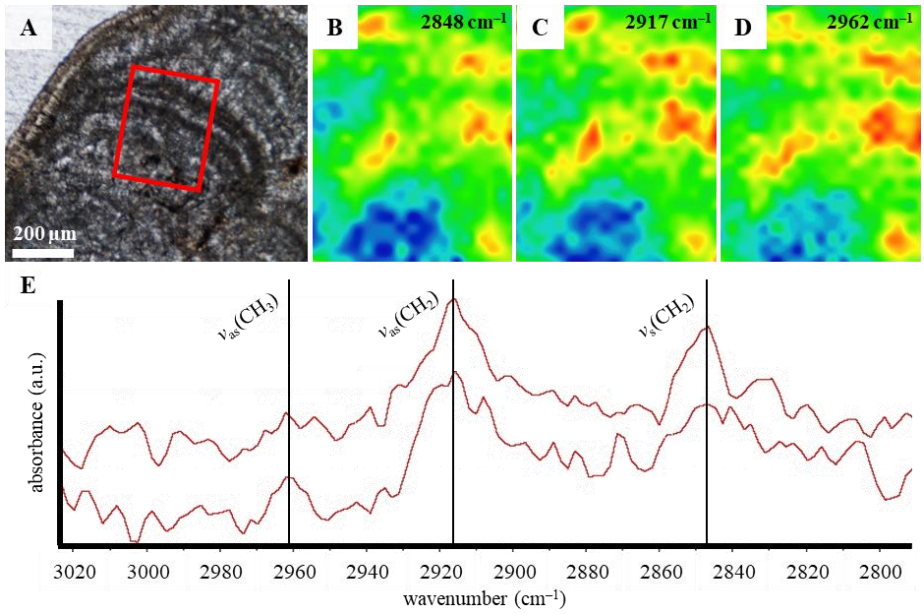

Fig 14. FTIR characterization of organic-rich laminations. Red box indicates the region analyzed in B–D. B–D) FTIR intensity mapping of aliphatic C–H moieties (see text for details). E) Representative FTIR spectra showing aliphatic C–H complexity in organic-rich laminations.

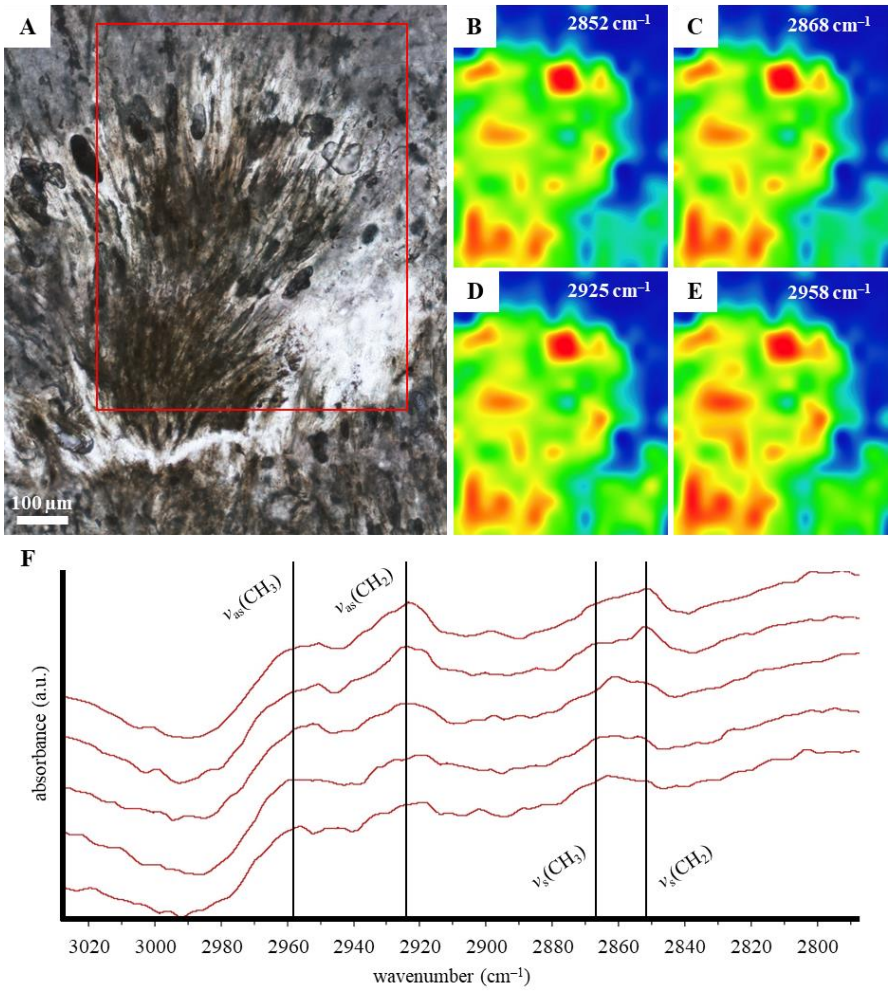

Fig, 15. FTIR characterization of organic-rich filamentous structures. Red box indicates the region analyzed in B–E. B–D) FTIR intensity mapping of aliphatic C–H moieties (see text for details). F) Representative FTIR spectra showing aliphatic C–H complexity in organic-rich filamentous structures.

2.5. Discussion

Lake Ashenge stromatolites exhibit textural and micromorphological characteristics denoting their formational processes; they exhibit microcolumnar and bulbous microfacies with well-defined internal lamination composed of intercalated of micrite and microsparite laminae (Fig. 4). Very well-preserved filamentous structures within correspond to typical fabrics of modern and fossil stromatolites (e.g., Grotzinger and Knoll, 1999; Riding, 2000; Reid et al., 2000; Dupraz et al., 2006; Hickman-Lewis et al., 2019).

Numerous lakes of the EARS show modern occurrences of structures described as stromatolites, similar to those of Lake Ashenge, e.g., Lakes Natron and Magadi (Hillaire-Marcel et al., 1986), Lake Manyara (Casanova & Hillaire-Marcel, 1992), Lake Tanganyika (Cohen et al., 1997), Lake Abbe (DeMott et al., 2021; Dorneles et al., 2024) and Lake Turkana (Zainescu et al., 2023). Lake Ashenge stromatolites are particularly similar to those in the deposits of Lake Hayk, another lake in the EARS, located approximately 141 km to the south. Ghinassi et al. (2012) described Lake Hayk stromatolites as well-laminated biostromes initially coating basalt gravels and later forming domes and tabular structures containing internal layers with millimeter-scale columns. Both Lake Ashenge and Lake Hayk present similar environmental parameters, such as high alkalinity, and both are closed-basin lakes more than 2000 m above sea level on the eastern margin of the Ethiopian highlands (Fig. 1).

The high alkalinity of the Lake Ashenge makes it inhospitable to most aquatic life, however, certain types of microorganisms, such as cyanobacteria and algae, can survive and thrive in these extreme conditions, forming stromatolites. Indeed, lacustrine microbial carbonates develop within a wide range of environments of varying salinity, from fresh to hypersaline, unlike their marine counterparts (Wright, 2012). Similar morphological features to those described in Lake Ashenge stromatolites (Figs. 3 and 4) have also been reported in other lacustrine carbonates from the Eocene Green River Formation (Sarg et al., 2013; Ingalls et al., 2022), specifically domical structures composed of microcolumns (Fig. 3D), and shrub textures (Fig. 9B) preserved within a micritic matrix (Ingalls et al., 2022).

Morphological observations using optical microscope suggested two distinct modes of growth in Lake Ashenge stromatolites represented by microstructures accumulating from a locus and influenced by the simultaneous growth of mats and mineral precipitation: columnar stromatolites reflect slower rates of growth of the upper surface and continuous accumulation of layers, forming microcolumns or pillars (Fig. 4B), whereas bulbous stromatolites denote fast and concentrated growth with accumulation of sediments in a localized area, forming larger and flatter cumulate structures (Fig. 4C). Dupraz et al. (2006) proposed that slower flows tend to favour the development of columnar and branch stromatolites, whereas stronger currents tend to develop knobs structures, comparable to bulbous stromatolites. The variation of microfacies present in the Lake Ashenge samples demonstrates the water circulation dynamics of this environment, however, distinctive morphologies may not indicate stromatolite diversity, since different sets of intrinsic and extrinsic parameters can produce similar morphologies (Dupraz et al., 2006).

Stromatolite morphology can be influenced by several factors in addition to water circulation, such as the contribution of siliciclastic sediments, presence of microorganism communities, and geochemical conditions of the environment (Hofmann, 1973; Batchelor et al., 2003; Dupraz et al., 2006; Bosak et al., 2013; Hickman-Lewis et al., 2019). Although these factors are always interrelated, Castro-Contreras et al. (2014) demonstrated, based on stromatolites samples from Laguna Bacalar (Mexico), that the growth rate of the cyanobacterial communities present in the stromatolites is one of the main variables that determines the final morphology. Factors like recycling of nutrients may also affect the formation of laminae lithification in stromatolites, as discussed by Dupraz et al. (2006), such that the concentration of nutrients in a water body varies according to the energy of water circulation, which may influence the growth of microorganisms, and this process favours the formation of thicker laminae of microsparite instead of thinner laminae of micrite. In the Lake Ashenge stromatolites, we observed that micrite laminae are less thick and denser, therefore less porous (Fig. 9A and 10). In contrast, the microsparite laminae are up to five times thicker and typically enhance the preservation of cyanobacterial sheaths (Fig. 10A-B).

Microbial mat composition and the energy acquisition methods employed by microbial communities influence the overall morphogenesis of stromatolites. Nevertheless, a study conducted by Dupraz et al. (2006) utilized a numerical model to demonstrate that morphology may not serve as a reliable indicator of stromatolite diversity. This is attributed to the observation that distinct combinations of intrinsic and extrinsic parameters can generate comparable morphologies. Similar findings were noted in stromatolites from Lake Ashenge,

where both columnar and bulbous microfacies exhibited analogous organic and mineralogical compositions (Figs. 5 and 6), as well as comparable preservational processes.

2.5.1. The role of microbes in the formation of Lake Ashenge stromatolites

Cyanobacteria are considered the major group of microorganisms responsible for the formation of modern stromatolites (Riding, 2000; Willmer & Rasser, 2022; Boussagol et al., 2024); therefore, the exceptional preservation of cyanobacteria suggests a strong biogenic component in the formation of stromatolites in Lake Ashenge. Cyanobacteria sheaths consist of carbohydrate fibrils arranged in a helical pattern, forming a rigid and highly ordered structure that makes direct contact with the cell surface (Hoiczyk, 1998; Schopf, 2012). In contrast, the filaments are surrounded by a mucilaginous sheath, comprising extracellular polysaccharide (Briones-Nagata, 2007).

Moreover, microfossil structures are preserved mostly vertically in relation to the laminated fabric of the columnar and bulbous microfacies (Fig. 9 and 10), indicating that the microbes were preserved in life position (Castro-Contreras et al., 2014; Willmer & Rasser, 2022). This life position arrangement is most consistent with photosynthetic microorganism growth, where the colonies of microbes forming the laminae require sunlight (Noffke & Awramik, 2013; Hickman-Lewis et al., 2019).

Filamentous structures representing single filaments of cyanobacteria were recognized rarely only in thin sections (Fig. 9C) and are therefore likely less readily preserved than cyanobacterial sheaths (Fig. 9D) which presents more resilience (Newman et al., 2016) and being observed on optical microscopy, SEM-EDS and Raman datasets. Filaments and sheaths of cyanobacteria described in Lake Ashenge stromatolites may be correlated with those identified in previous work (e.g., Schopf et al., 2007; Cavalazzi et al., 2011; Kremer et al., 2012; Schopf, 2012; Willmer & Rasser, 2022; Dorneles et al., 2024). The regular succession of laminae observed in all stromatolites samples studied suggests cycles of development of cyanobacterial communities that promote the organomineralization of carbonate (Castro-Contreras et al., 2014; Shiraishi et al., 2022; Willmer & Rasser, 2022); this most clearly observed in laminae within the columnar stromatolites, where the vertical occurrence of cyanobacterial filaments is restricted to the base and top of each lamina (Fig. 9A).

The EPS observed using SEM (Fig. 11A, 11D and 12B) are efficiently excreted by cyanobacteria (Dupraz & Visscher, 2005; Dupraz et al., 2009; Burnie et al., 2023), and consist of polysaccharides, proteins, small amounts of extracellular DNA, exoenzymes, trace metals

and minerals (Boussagol et al., 2024). EPS in Lake Ashenge samples is always associated with cyanobacterial filaments, whether within or surrounding sheaths. SEM-EDS, Raman and NMR data showed a composition of high content of organic matter represented by high signal of carbon (Fig. 11A and 11D), D and G bands and carotenoids in Raman (Fig. 7 and 8) and by the preservation of biomolecules in NMR spectrum (Fig. 13).

Permineralization process within stromatolites occur due to the encrustation of cyanobacterial filaments and micritization associated with the decomposition of the extracellular organic matrix, represented by the EPS (Dupraz et al., 2009; Shiraishi et al., 2022), since EPS macromolecules contain hydroxyl and carboxyl groups that tend to bind tightly with Ca^{2+} and Mg^{2+} cations to form $(Ca,Mg)CO_3$ crystals (Dupraz & Visscher, 2005; Shiraishi et al., 2017). Biologically-induced mineralization by the degradation of EPS is the major process for fine-grained carbonate mud production in lacustrine environments (Boussagol et al., 2024).

Mg-calcite nanocrystals associated with EPS were identified in the matrix of Lake Ashenge stromatolites (Fig. 11D-E), as well as in the walls of cyanobacterial sheaths (Fig. 11F), suggesting that both EPS and cyanobacterial sheaths served as an organic matrix for the nucleation and growth of these nanocrystals. Dupraz et al. (2009) corroborates that stromatolite mineral precipitates are commonly bioinduced, i.e. intrinsic to microbial metabolism, and that nucleation occurs within EPS. Due to the microbially mediated decomposition of EPS, the liberation of HCO^{3-} and Ca^{2+} creates nucleation points at which the saturation index (SI) and precipitation rates tend to increase (Dupraz & Visscher, 2005; Shiraishi et al., 2010).

The growth of carbonate crystals may be regulated by the inclusion of organic materials that encourage specific growth forms (Rogerson et al., 2021). Pedley et al. (2009) demonstrated experimentally that the presence of specific functional anionic groups in EPS molecules, such as CO_3^{2+}, aid in calcite precipitation through chelation with Ca^{2+} ions during the initial stage of mineralization in non-marine environments. This experiment implied that the presence of EPS increases the calcite saturation index and precipitation rates to a greater extent than environment parameters such as salinity and temperature. Among the metabolic processes that lead to precipitation, photosynthesis plays a crucial role in lacustrine environments: through the absorption of CO_2 molecules, this metabolism promotes an increase in both the pH of the system and its carbonate anion (CO_3^{2+}) concentration, resulting in increased alkalinity (Dupraz et al., 2009; Petrash et al., 2012; Castro-Contreras et al., 2014).

Noffke et al. (1997) and Dupraz et al. (2009) elucidates that the two of the main suites of processes involved in the formation of laminated microbialite structures are trapping and binding and in situ precipitation. In the trapping and binding mechanism, detrital grains are

trapped by the mat adhesive surface and become permanently incorporated as microbes grow over and bind them. In the other hand, in situ precipitation occurs whereby metabolic activities induce the mineralization of the organic matrix that subsequently influence crystal morphology and composition (Mercedes-Martín et al., 2021). Ingalls et al. (2022) described a pervasive occurrence of trapped and bound sand grains within the microstructures forming or interrupting the microlaminations of the Green River Formation stromatolites; however, the very low detrital grain content in the columnar and bulbous layers of Lake Ashenge stromatolites suggests that autochthonous mineral growth from in situ precipitation is more significant than trapping and binding. Wright (2012) corroborates that the absence of tides and reduction of wave energy in closed-basin lakes promote a decrease of sediment transportation rate, thereby generating an environment dominated by in situ sediment accumulation. A very small amount of siliciclastic detrital grains was identified, such as quartz and ferromagnesian minerals, identified in the voids of the columns and bulbous, likely originated from the weathering of volcanic rocks (basalts of the Ashangi Group) surrounding Lake Ashenge.

2.5.2. Preservation of morphological biosignatures in Lake Ashenge stromatolites

The preservation of cyanobacterial filaments in Lake Ashenge stromatolites occurred in three different ways: 1) the filaments themselves are not preserved, but their molds are preserved as empty tubes in the micritic matrix (Fig. 10C); 2) the walls of the filaments are partially or completely preserved, leaving a hollow tube with remnants of preserved organic material and in which nanocrystals tend to grow (Fig. 11F and 12B); 3) the molds of the filaments are completely filled with a poorly crystalline Mg-silicate phase, identified as stevensite clay mineral (Fig. 12A). Preservational phenomena 1 and 3 are most commonly identified in samples; phenomenon 2 is comparably rare.

The presence of Mg-silicates associated with the preservation of stromatolite fabrics has been discussed in several previous works. Bontognali et al. (2010) demonstrated, studying modern microbial mats from Abu Dhabi, that EPS has the ability to preferentially bind Mg and Si over Ca, acting as a kinematic catalyst for the formation of Mg-silicates. The presence of Mg-silicates in microbialites has also been reported by Souza-Egipsy et al. (2005) in Mono Lake (USA), an example of an alkaline lacustrine system hosted in a volcanic bedrock. A biological influence was suggested for the Mg-silicate based on the spatial correlation of biofilms, areas of Mg^{2+} adsorption, and Mg-silica complexation. Souza-Egipsy et al. (2005) also demonstrated that conditions of pH = 9 facilitate the generation of silica ions, which then

interact with the decomposing cyanobacteria, incorporating Mg2+ onto their surfaces. The adsorption of Mg2+ is associated with the decay and post-mortem stages of the cyanobacteria cell walls (Souza-Egipsy et al., 2005). A comparable phenomenon is anticipated within the EPS surrounding deteriorating biofilms or, in the case of Lake Ashenge, associated to the cyanobacteria sheaths, promoting the filing composed of Mg-silicate phases (Fig. 12A).

Kremer et al. (2012) evaluated the role of different mineral phases in the formation of lacustrine stromatolites from volcanic calderas with similar alkaline conditions to those in Lake Ashenge, proposing that carbonate may damage cyanobacterial original structures due to the transition of nucleated nanoparticles into larger crystals, while silica permineralization fully saturates organic material and preserves soft organic components like cells. This hypothesis of degradation of organic fabrics during carbonate permineralization may justify the common preservation of empty cyanobacterial sheaths as molds in a matrix composed of Mg-calcite as observed in the stromatolites of Lake Ashenge (Fig. 10C), in addition to the localized growth of nanocrystals in the sheath walls, obstructing the original structure (Fig. 11F).

Arp et al. (2003) discussed a possible variation in pH to explain the mineralization of non-identifiable Mg-silicate amorphous phases in microbialites of the Satonda crater Lake, Indonesia. According to the authors within the entombed biofilms, diatoms and spicules were dissolved at high pH (8.5-9.0), in turn, the following aerobic heterotrophic decay of exopolymers caused a dissolution of Mg-calcite and reprecipitation of silica at lower pH to form an amorphous Mg–silicates. Similar processes may explain the passive mineralization of Mg-silicate phases, as autogenic stevensite, in Lake Ashenge stromatolites. We observed no evidence for the replacement of organic matter by Mg-silicate, as proposed by Kremer et al. (2012), but instead we suggest the passive percolation of this material into the empty molds of the cyanobacterial sheaths, since the same Mg-rich silicate material was also recognized around the microstructures and within voids in the stromatolitic microstructure (see EDS maps; Figs. 5–6). In Lake Ashenge, the precipitation of Mg-calcite on the sheath walls (Fig. 11F), therefore, occurs in the post-mortem of the cyanobacteria within the sheaths embedded in EPS (Fig. 12B). The subsequent degradation of the EPS will then generate a local decrease of pH followed by the dissolution of the former carbonate and the potential percolation of the siliceous fluid will precipitate as Mg-silicate phase and fill the sheath mold (Fig. 12A), similar to what have been demonstrated by Arp et al. (2003).

Burnie et al. (2023) described microbe-like structures, diatom frustules and EPS as examples of entombed biomass mineralized and preserved in aragonite-rich samples from basin-closed alkaline environments similar to Lake Ashenge, such as Lake Alchichica

(Mexico), Atlin Mg-carbonate playas (British Columbia, Canada) and Clinton Creek open pit pond (Canada). However, at Lake Ashenge, diatoms were found in small number and always trapped within the voids (Fig. 11B); this indicates that they did not play an efficient role in the production of EPS and growth of those stromatolites but may be still considered as a silica source in this system, once dissolved valvas were recognized under SEM (Fig. 11C). Diatoms, as highlighted by McNair (2018), play a significant role in silica production within lacustrine environments, with this silica constituting a crucial component of diatom frustules preserved in lake sediments.

Burnie et al. (2023) demonstrated that entombed biomass, enclosed within Mg-carbonate minerals, leads to microfossil preservation and the retention of biomolecules and morphological biosignatures as a result of the rapid precipitation rate and inherent stability of these minerals, particularly aragonite, which tends to form in subaqueous environments favorable for microbial activity. We interpret that a similar phenomenon, based on Mg-calcite, played a role in the preservation of microfossils and other cellular materials in the Lake Ashenge stromatolites.

Previous studies have shown that lakes fed by rivers that drain basic volcanic terrains promote conditions of high CO2 input and carbonate alkalinity, in addition to high concentrations of dissolved silica, Mg, Ca, and even Na and Fe, especially if these environments are coupled with thermal and spring inflow (Wright, 2012). Cerling (1994) demonstrated that the East African Rift lakes, where volcanic terrains are predominantly poor in sulfates and chlorides, so their resulting evaporite deposits are limited in primary minerals, such as calcite, trioctahedral smectite, analcite, and sodium bicarbonate-carbonate phases.

2.5.3. Organic Preservation in Lake Ashenge Stromatolites

Where filamentous structures are very well preserved in Lake Ashenge stromatolites, biomolecular signatures may also be retained. NMR and FTIR spectra obtained from organic materials show bands of unsaturated carbon, aliphatic carbon, and oxygenated carbon (Fig. 14), which strictly correlates to the spectrum of kerogen (Mackay & Norton, 1987; Nguyen et al., 2003; Marshall et al., 2007; Delarue et al., 2016). Cyanobacteria material is a significant precursor of kerogen because they contain a lipid membrane structure (bilayers of fatty acid lipid esters linked to glycerol-3-phosphate) with kerogen-forming potential (Summons et al., 2022). They also possess algaenan in their cell walls; this is an aliphatic-rich biomacromolecule

that resists diagenetic degradation, aiding its sediment preservation for kerogen formation (Biller et al., 2015; Vandenbroucke and Largeau, 2007).

Lake Ashenge NMR spectrum was correlated with the spectrum of the cyanobacteria Synechococcus, from Mackay and Norton (1987), regarding the C-O bands (Fig. 14); and strongly correlated with the algaenan spectrum from Nguyen et al. (2003) for the CH group, that correspond to aliphatic carbon bands (Fig. 14). The strong signal of aliphatic carbon in the NMR, centered at 32 ppm for Lake Ashenge samples, was also reported by Vandenbroucke & Largeau, (2007) reflecting the contribution of preserved algaenan, as this biomacromolecule breaks down to form kerogen during early diagenesis (Wang et al., 2023). The presence of algaenan and their resistance in degradation may explain the localized preservation of cyanobacterial content in Lake Ashenge stromatolites, especially in the second form where the walls of the sheaths remained preserved (Fig. 12B). The peaks at 69 and 128 ppm probably reflect the survival of some carbohydrates and a substantial signal is observed at 168 ppm for carboxylic groups, as demonstrated previously by Vandenbroucke & Largeau (2007). The stability of kerogen is evident when it is protected within a mineral matrix which may occur through adsorption on mineral grains, within nanopores or through alternation of organic and clay nanolayers (Vandenbroucke & Largeau, 2007). In the Lake Ashenge stromatolites, the preservation of entombed organic matter appears to be efficient both in the adsorption processes on mineral grains through the formation of Mg-calcite organomineral aggregates as well as in the formation of a coating of clay mineral in the cyanobacteria sheaths remains by nucleation with adsorbed ions in the stevensite phase.

FTIR hyperspectral measurements indicating aliphatic C–H complexity further demonstrate an exceptional level of organic preservation in Lake Ashenge stromatolites (Figs. 15 and 16). The presence of all four symmetric and asymmetric absorption bands of CH2 and CH3 moieties indicates minimal diagenetic influence on original biochemistry and the CH3/CH2 ratio is estimated at less than 0.4, consistent with a fatty acid-dominated biomolecular ecological composition, and thus a bacteria-dominated primary stromatolite-building community (Igisu et al., 2012; Hickman-Lewis et al., 2020), corroborating the NMR data.

2.6. Conclusions

This chapter described for the first time the stromatolites from Lake Ashenge and their distinctive textural and micromorphological features, showcasing microdigitate columnar and bulbous microfacies. They contain a remarkable preservation of cyanobacterial structures, particularly filaments and sheaths. The life position arrangement, observed through various analytical tools, suggests photosynthetic microorganism growth, with cycles of cyanobacterial community development promoting organomineralization of carbonate.

Contrary to prior proposals suggesting the replacement of organic matter by Mg-silicate, our findings indicate a passive precipitation of stevensite filling empty molds of cyanobacterial sheaths due to a slight decrease of pH, caused by decomposition of EPS. The Mg-rich silicate material was identified around microstructures and within voids in the stromatolitic microstructure. The resilience of algaenan, degrading to form kerogen during early diagenesis, may explain the exceptional well-preservation of cyanobacterial remains in Lake Ashenge stromatolites.

Chapter III – Microbe–mineral interactions in the microstromatolitic crusts of the lacustrine chimneys and volcanic bedrock of Lake Abhe, Republic of Djibouti

The data presented in this chapter correspond to the published paper:

Dorneles, V.A.C., Hickman-Lewis, K., Barbieri, R., Caminiti, A.M. & Cavalazzi, B. (2024) Microbe-mineral interaction in the microstromatolitic crusts of lacustrine chimneys and volcanic bedrocks from the eastern cost of the Lake Abhe, Republic of Djibouti. *Bollettino della Società Paleontologica Italiana, 63*(3), 229-244. Doi: 10.4435/BSPI.2024.17

3.1. Introduction

Lake Abhe (11°11'50.66"N / 41°46'50.91"E), also spelled Abbe or Abbé, is located on the southern-western edge of the Republic of Djibouti across its border with Ethiopia (Fig. 1). Lake Abhe is part of the eastern branch of the East African Rift system and is well-known for its large carbonate chimneys (Fontes & Pouchan, 1975; Caminiti, 2000; Dekov et al., 2014, 2021; Le Gall et al., 2018; DeMott et al., 2021). These chimneys formed on the floor of the hypersaline, hyperalkaline, hydrothermally influenced lake and are now exposed near the south-eastern coast of the lake (Figs 1-2); together with basaltic rocks outcropping in the area, these chimneys exhibit peculiar microstromatolitic crusts (Dekov et al., 2014, 2021; Le Gall et al., 2018; DeMott et al., 2021).

In this chapter, we present a detailed study of the carbonate fabrics of peculiar microstromatolitic encrustations from lacustrine chimneys and volcanic bedrocks of Lake Abhe. We used a multi-analytical approach, seeking to understand the relationship between microorganisms and encrustations, and the preservation potential of microfossils in this hyperalkaline and hypersaline polyextreme lake.

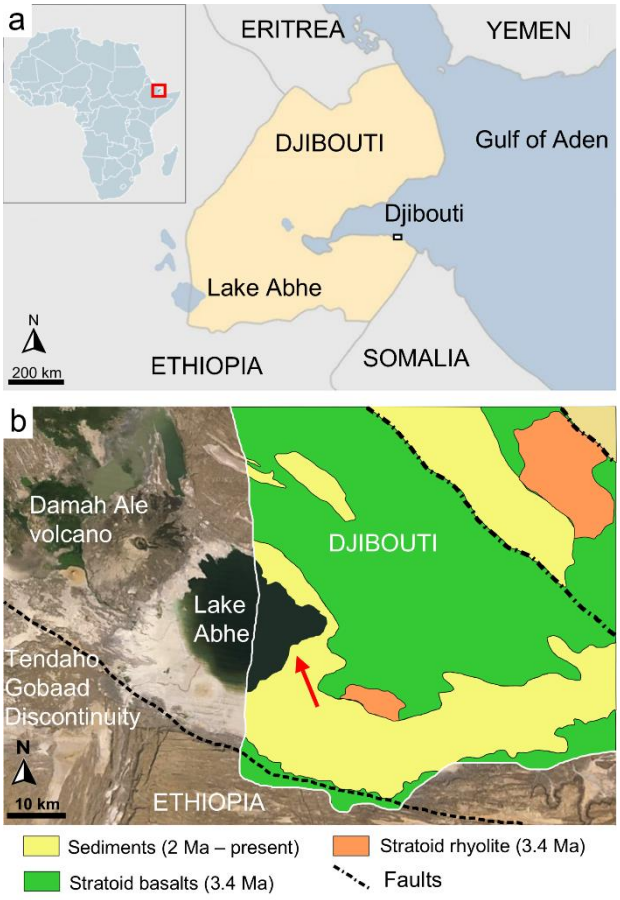

Fig. 1. Location of the study area. a) Simplified map showing the location of Lake Abhe. b) Simplified geological map of Lake Abhe and its surrounding (adapted from Boschetti et al., 2018), showing the location of chimneys (arrowed) on the south-eastern margin of the lake (geology of Djibouti shown). Data source: Google Earth (2024 imagery: CNES/Airbus-Landsat; 2034 imagery: DigitalGlobe).

Fig. 2. Relict hydrothermal carbonate chimneys at the south-eastern shore (see Fig. 1) of Lake Abhe, Republic of Djibouti. a) Isolated chimneys. b) Chain of coalescing chimneys.

3.2. Geological setting

Lake Abhe is located within the Afar Rift, a depression formed by the intersection of the Main Ethiopian Rift with the oceanic Gulf of Aden and Red Sea Rifts (e.g., Tesfaye et al., 2003; Corti, 2009; Varet, 2018). The Afar Depression and the East African Rift system, characterised by zones of thinned continental lithosphere related to asthenospheric intrusions from the upper mantle, graben valleys and basins, major faults, seismicity and volcanism (e.g., Corti, 2009; Cavalazzi et al., 2019), features a large number of hydrothermally influenced pools and lakes, hot and warm springs which host a large variety of polyextreme environments and relatively poorly studied stromatolite-forming microbial consortia (e.g., Casanova, 1994; McCall, 2010).

Lake Abhe is located in the western section of the Gobaad tectonic basin, an E–W-striking system linked to the larger Tendaho Rift system, which developed during the Pleistocene–Holocene on a volcanic basement mainly composed of basalts and subordinate acid rocks (Fig. 1b) (Abbate et al., 1995; Tesfaye et al., 2003; Varet, 2018). The oldest exposed sedimentary rocks in the Gobaad basin are the Early Pleistocene lacustrine shales interstratified within

Stratoid Series basaltic lava flows, diatomites, gypsum and ash flows (Gasse & Street, 1978), followed by Lower and Middle Holocene carbonate-dominated deposits of lakes including stromatolitic crusts, littoral deposits with ripple marks and shell accumulations (e.g., Gasse & Street, 1978).

3.2.1. Lake Abhe and carbonate chimneys

Lake Abhe (Fig. 1), located ESE of the Damah Ale volcano, is an hyperalkaline (pH = 9.9–10) and hypersaline (TDS >90,000 mg) lake at 240 m above sea level, with an area larger than 350 km^2 and an average depth of 12–15 m (Valette, 1975; Caminiti, 2000; Dekov et al., 2014, 2021; Awaleh et al., 2015). Lake Abhe is fed by the Awash River, a major river of the Ethiopian Plateau. A wide, flat area (up to 5 km^2) surrounding the eastern shoreline of the Lake Abhe is typified by lacustrine deposits and isolated and/or coalescent carbonate chimneys, reaching heights of up to 35 m (Fontes & Pouchan, 1975; Dekov et al., 2014; Le Gall et al., 2018; DeMott et al., 2021; Walter et al., 2023; Fig. 2).

The Lake Abhe chimneys formed due to carbonate precipitation from the mixing of sulphide-calcium hydrothermal fluids and carbonate-soda lake waters (Caminiti, 2000; Dekov et al., 2014, 2021), consistent with the high pH and salinity increases caused by changes in the course of the Awash River and the arid climate of Afar (DeMott et al., 2021; Awaleh et al., 2015). Hot springs at the bottom of the chimneys discharge effluent with pH 7–9 and temperatures of 90–100°C (Caminiti, 2000). Isotopic data of ^{13}C and ^{18}O ($\delta^{18}O = –2.25$ ‰ and $\delta^{13}C = +0.67$ ‰, Fontes & Pouchan, 1975) in the Afar Rift, indicate a dominant influence from highland runoff with a minor contribution from evaporation (Gasse & Street, 1978; Gasse & Fontes, 1989). Awaleh et al. (2015) suggested that the Lake Abhe geothermal reservoir is recharged by meteoric water infiltrating the regional aquifer and descending through volcanic fractures, mixing with fluids undergoing deep regional circulation, which causes the water to heat, ascend and discharge through hot springs.

The formation of carbonate chimneys is also associated with fluctuations in the level of Lake Abhe as recorded in its lacustrine carbonate deposits (e.g., Fontes & Pouchan, 1975; Gasse & Street, 1978; Gasse, 2000; Gutherz et al., 2015), characterised by major episodes of aridity during the Late Pleistocene, followed by transgressive events throughout the Holocene (between 8000 and 6000 years before present), when the lake experienced high-water levels, then a decrease in lake level (between 6300 to 2700 years before present), corresponding to alternating dry and wet climatic phases.

3.3. Materials and methods

The microstromatolitic crusts studied herein were collected in 2018 during a field campaign at Lake Abhe. Sample preparation and analyses were performed at the Dipartimento di Scienze Biologiche, Geologiche e Ambientali, Università di Bologna, Italy. Eight samples were embedded in epoxy resin to produce 23 standard petrographic thin sections (~40 µm thick). Petrographic and microfabric descriptions were performed using optical microscopy Complementary, Raman microspectroscopy was performed in five thin sections for mineral and organic content characterization. Scanning electron microscopy and energy dispersive X-ray spectroscopy analyses were performed on gold-coated, freshly fractured fragments of seven samples, for the characterization of microbial compounds.

3.4. Results

The sampled outcrops are located on the south-eastern shores of Lake Abhe (see Fig. 1) and include microstromatolites encrusting carbonate chimneys and basaltic bedrock (Fig. 3). Microstromatolitic crusts reach thicknesses of up to 25 cm, exhibit distinct internal layering and external patterns, and occur in direct contact with the underlying carbonate and volcanic substrate (Figs 3-4).

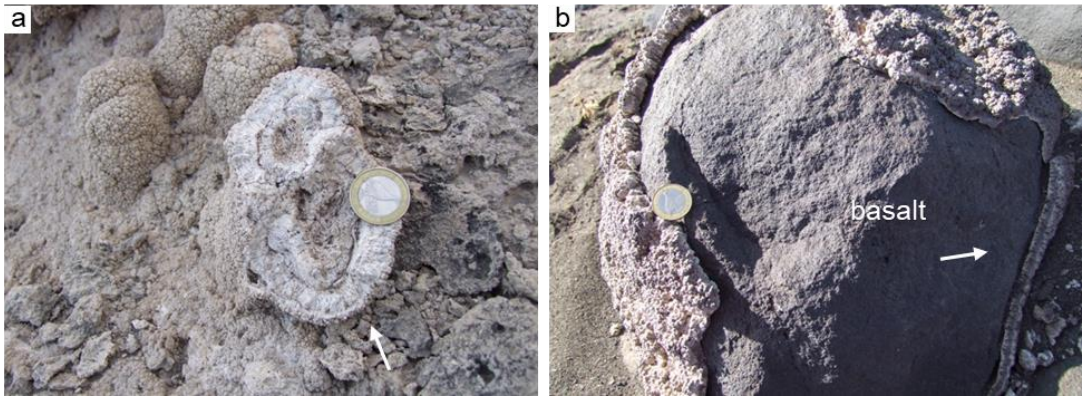

Fig. 3. Outcrop photographs of microstromatolitic crusts (arrows) growing on different bedrock types from the south-eastern shores of Lake Abhe. a) Representative stromatolitic crust formed on the exterior of a carbonate chimney. b) Representative stromatolitic crust developed directly on basaltic bedrock. Coin (29 mm in diameter) for scale.

Microstromatolitic crusts occur as centimetre-scale domical and tabular structures with layered internal fabrics and a popcorn-like (*sensu* DeMott et al., 2021) external textures (Fig. 4a-c).

Stromatolitic domical crusts are composed of several centimetre-scale layers enveloping a friable and porous (sugary texture *sensu* DeMott et al., 2021) calcitic core (Fig. 4a, d). The internal domical crusts show layers with distinct fabrics: microcolumnar, crystalline and coated grains (Fig. 4). The most common is the microcolumnar fabric, which often occurs immediately surrounding the calcitic core (Fig. 4a). This is followed by the crystalline fabric, which generates the external popcorn-like texture (Fig. 4c). Rarely, the calcitic core is directly covered by crystalline and/or rounded carbonate-coated grains, up to 2 mm in diameter (Fig. 4d).

Tabular microstromatolitic crusts are also characterised by microcolumnar, crystalline and coated grain fabrics (Fig. 4b) which mostly occur as a flat to slightly wavy laminated structure dominated by microcolumnar fabrics growing directly on the basaltic bedrock and overlain by a layer of crystalline fabric.

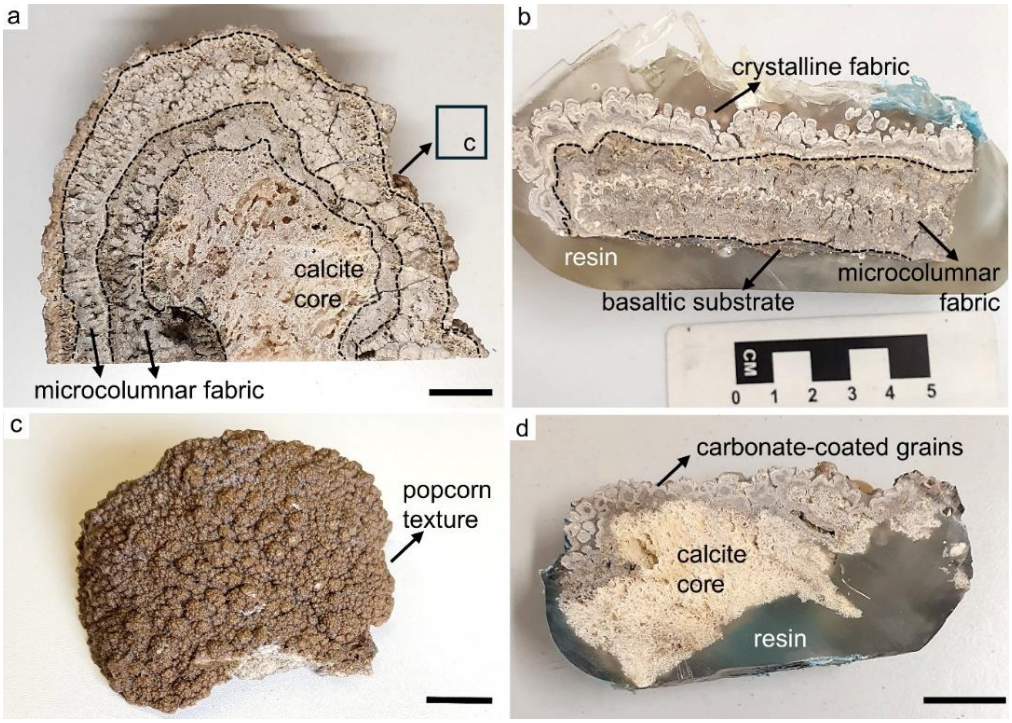

Fig. 4. Hand samples of microstromatolitic crusts; all samples are oriented as collected. a) Stromatolitic dome formed of a calcite core enveloped by layers of microcolumnar fabric. b) Fine laminations within the tabular stromatolite are formed of microcolumnar fabric at the bottom, and crystalline fabric at the top. Note the contact with basalt (bottom). c) Top view of the external crust of the domical sample (in (a)) exhibiting an external popcorn-like texture. d) Crust of coated grains covering a layer of crystalline fabric enveloping a calcite core. Scale bars equal 2 cm.

The transition between the different fabrics of the microstromatolitic crusts was also observed using optical microscopy. At the micro-scale, the transition is commonly marked by an erosional and/or sharp contact (Fig. 5), with no preference observed for the growth of one fabric over another.

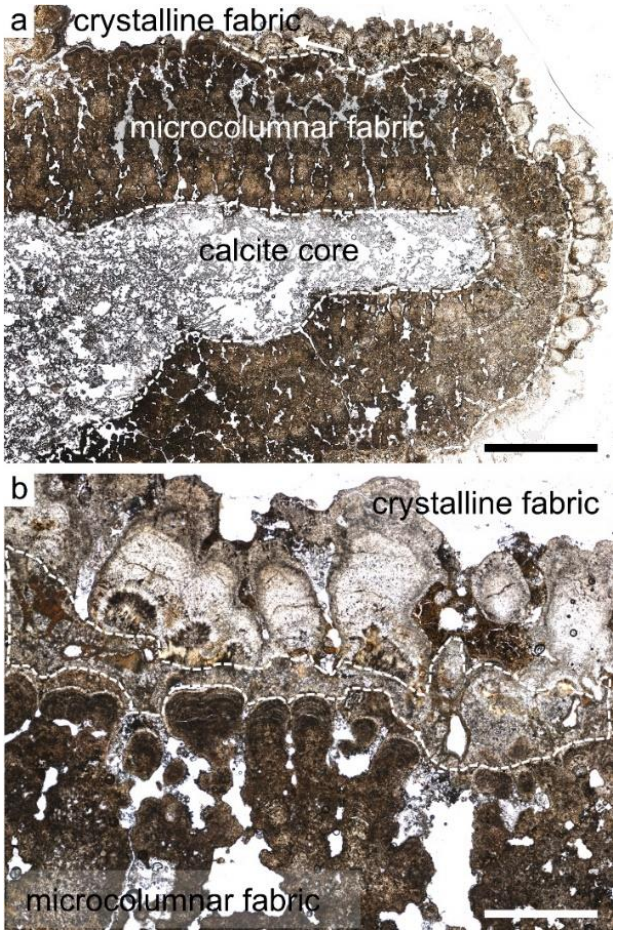

Fig. 5. Optical photomicrographs showing transitions between the different fabrics of the microstromatolitic crusts. a) Microcolumnar fabric growing on top of the calcite core (note the sharp contact), also showing the overlying crystalline fabric. Scale bar equals 5 mm. b) Transition from microcolumnar to crystalline fabric showing erosional contacts (white dashed lines). Scale bar equals 1 mm.

Optical microscopy imaging shows that the domical and tabular microstromatolitic crusts are composed of microcolumnar, crystalline and coated grain fabrics, each of which exhibits distinctive characteristics. The microcolumns occur as closely packed, straight to slightly branched structures growing directly on the calcitic core (Fig. 6a). Less than 1 mm high and 0.1 to 0.6 mm wide, microcolumns consist of moderately to parabolic hemispherical convex ascending laminae. These laminae are laterally continuous and composed of thinner interlayers of brown micrite, characterised by a cryptocrystalline texture (grains < 4 μm), interspersed with thicker laminae composed of non-isopachous grey microsparite, characterised by a fine-

grained calcite matrix (5–30 μm grains) (Fig. 6a). Locally, laterally linked microcolumnar layers with a maximum size of 0.7 mm in height are formed (Fig. 6b). The calcitic core, on top of which microcolumn growth occurs, consists of highly porous (subhedral to euhedral) rhombohedral calcite crystals arranged in a translucent dendritic structure (Fig. 6c). The core is entirely composed of crystalline sparite calcite, featuring an internal flat lamination (Fig. 6d). The popcorn-like texture corresponds to the outermost part of the microstructures. Locally, rounded coated-carbonate grains (Fig. 6e) composed of autochthonous spherical fragments of crystalline calcite and coated by concentric sparite form sub-spherical to spherical pisoid-like structures (Fig. 6f).

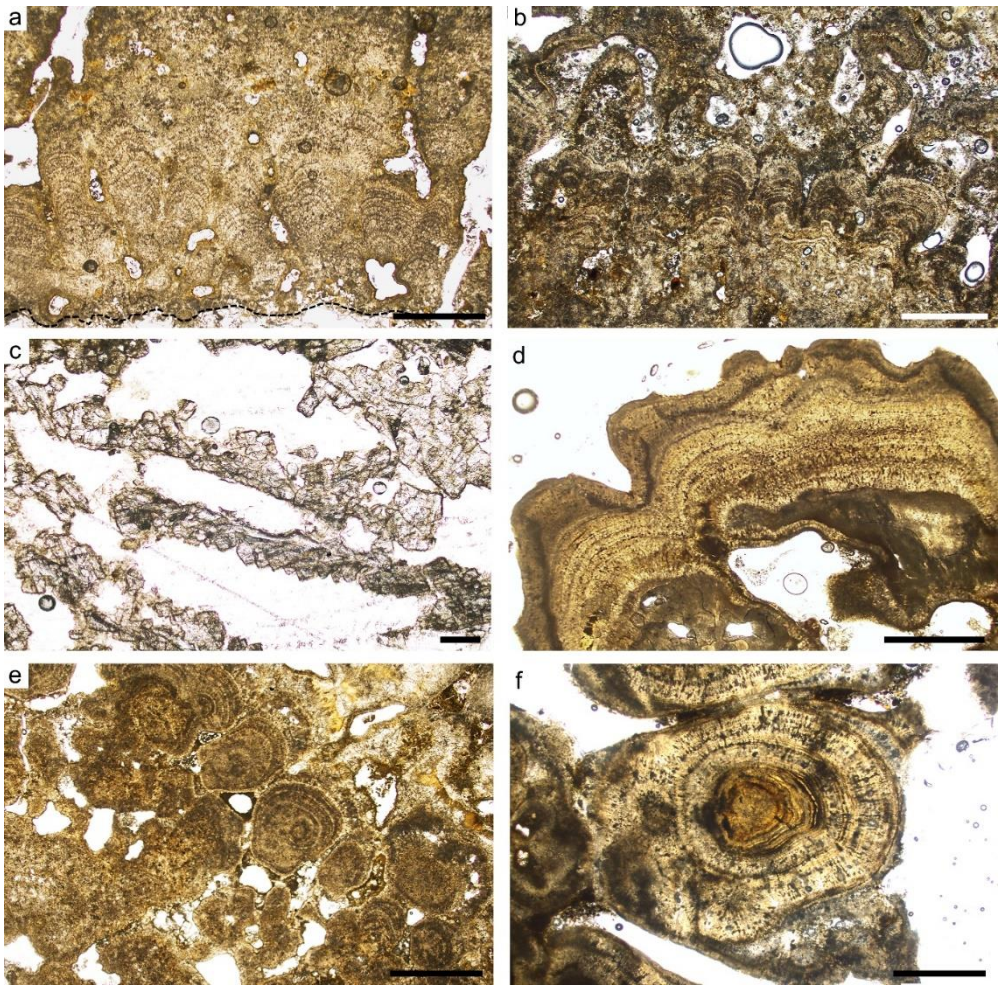

Fig. 6. Optical photomicrographs showing representative fabrics of microstromatolitic crusts. a) Closely packed microcolumnar fabric. Scale bar equals 1 mm. b) Layered fabric composed of laterally linked microcolumns. Scale bar equals 1 mm. c) Calcitic core comprised of thin branches of translucent euhedral calcites. Scale bar equals 0.1 mm. d) Crystalline fabric showing internal lamination. Scale bars equal 1 mm. e) Packed carbonate-coated grains. Scale bars equal 1 mm. f) Representative spherical carbonate-coated grain with a core and concentric laminae resembling a pisoid-like structure. Scale bar equals 0.5 mm.

Microsparite and micrite laminae forming the microcolumns host slightly curved, non-septate filamentous structures (Fig. 7) that occur as isolated filaments, commonly preserved in contact with wavy micritic laminae containing high concentrations of carbonaceous materials (CM; Fig. 7a-b). Some filamentous structures form clusters perpendicularly oriented relative to laminae growth, within both the micrite (Fig. 7d) and microsparite laminae (Fig. 7e); or as densely packed clusters exhibiting a palisade-like texture (Fig. 7f).

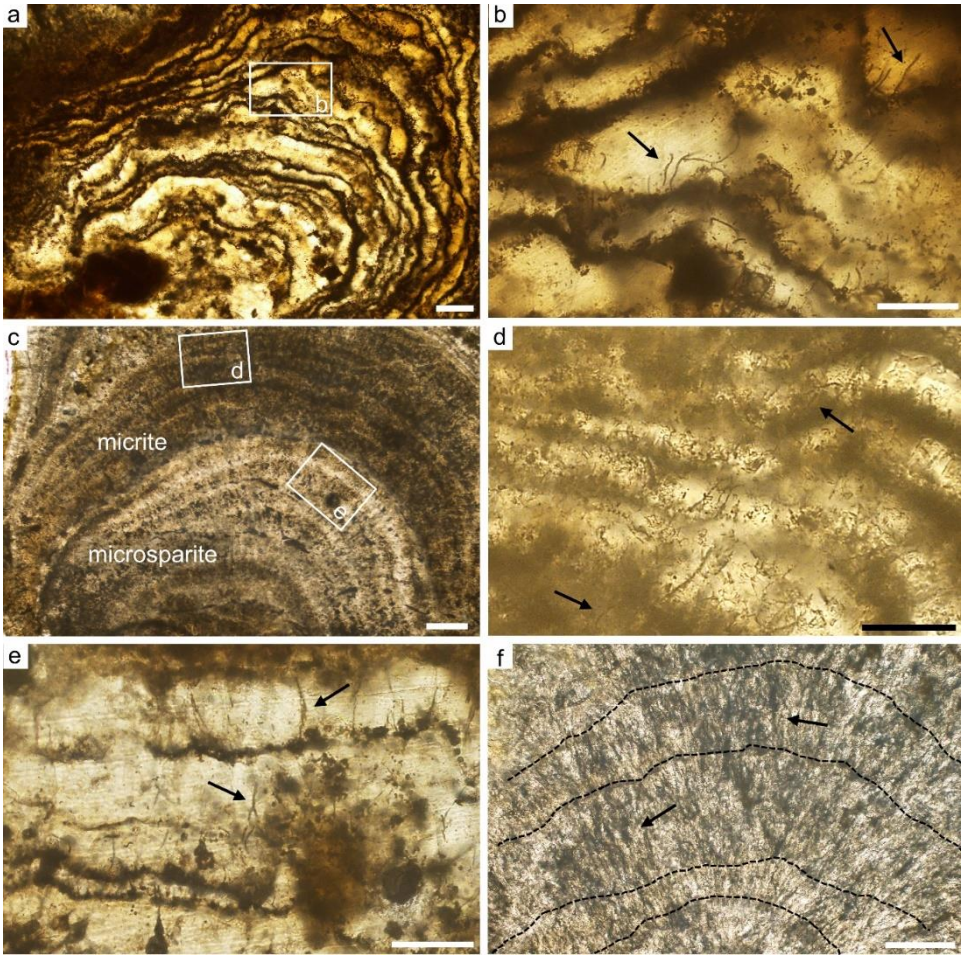

Fig. 7. Optical photomicrographs showing laminae and filamentous structures in microcolumns. a) Wavy laminae composed of CM-reach micrite alternating with microsparite. Boxed area detailed in (b). Scale bar equals 100 µm. b) Close-up of the boxed area in (a), showing isolated filamentous structures (arrows) preserved in the microsparitic laminae. Scale bar equals 50 µm. c) Representative view of micritic and microsparite laminae preserving filamentous structures. Boxed areas detailed in (d, e). Scale bar equals 100 µm. d) Close-up of the boxed area in (c), showing isolated and clusters of filamentous structures within the micrite laminae. Scale bar equals 50 µm. e) Close-up of the boxed area in (c), showing rare and isolated filamentous structures within the microsparite laminae. Scale bar equals 50 µm. f) Filamentous aggregates forming palisade-like textures within the laminae (dashed lines). Scale bar equals 50 µm.

Using Raman microspectroscopy (Figs 8-9), filamentous structures are shown to be spatially associated with concentrations of CM and are embedded within a magnesian calcite

matrix (identified by Raman bands at 155, 281, 713 and 1086 cm^{-1}; Fig. 8c, e). The CM in filamentous structures is characterised by bands of the first- (disordered carbon, D, at 1341 cm^{-1} and graphite, G, at 1596 cm^{-1}) and second-order (between 2500 and 3200 cm^{-1}) regions of the spectrum (Fig. 8d, f).

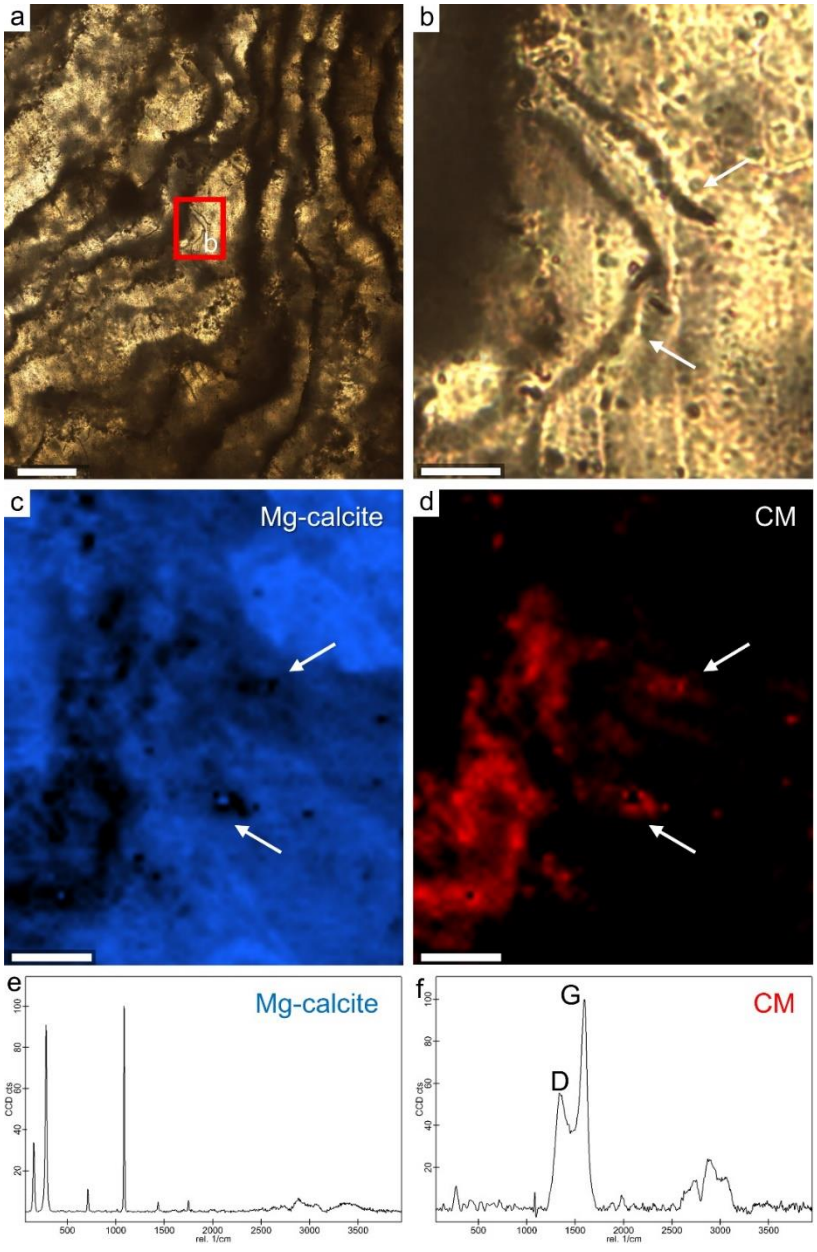

Fig. 8. Optical photomicrographs and 2D Raman spectral maps of wavy laminae and associated filamentous structures in the microcolumnar facies. a) Optical photomicrograph showing wavy laminae (part of a microcolumn) including filamentous structures. Boxed area detailed in (b). Scale bar equals 100 µm. b) High-magnification image of the boxed area in (a) showing details of filamentous structures (arrowed). Scale bar equals 8 µm. c-f) Raman characterisation of the area imaged in (b): (c, e) show the distribution and spectral signature of Mg-calcite; (d, f) show the distribution and spectral signature of CM (arrowed). c-d) Scale bars equal 8 µm.

Crystalline fabrics show flat laminations in which molds of filamentous structures are poorly preserved (Fig. 9a-c). Raman microspectroscopy enabled the recognition of two main components in thin section (Fig. 9d-h): Mg-calcite in the matrix identified by major bands at 155, 281, 713 and 1087 cm^{-1} (Fig. 9e, g) and CM, characterised by the first-order D (1336 cm^{-1}) and G (1583 cm^{-1}) bands, and second-order bands (Fig. 9f, h).

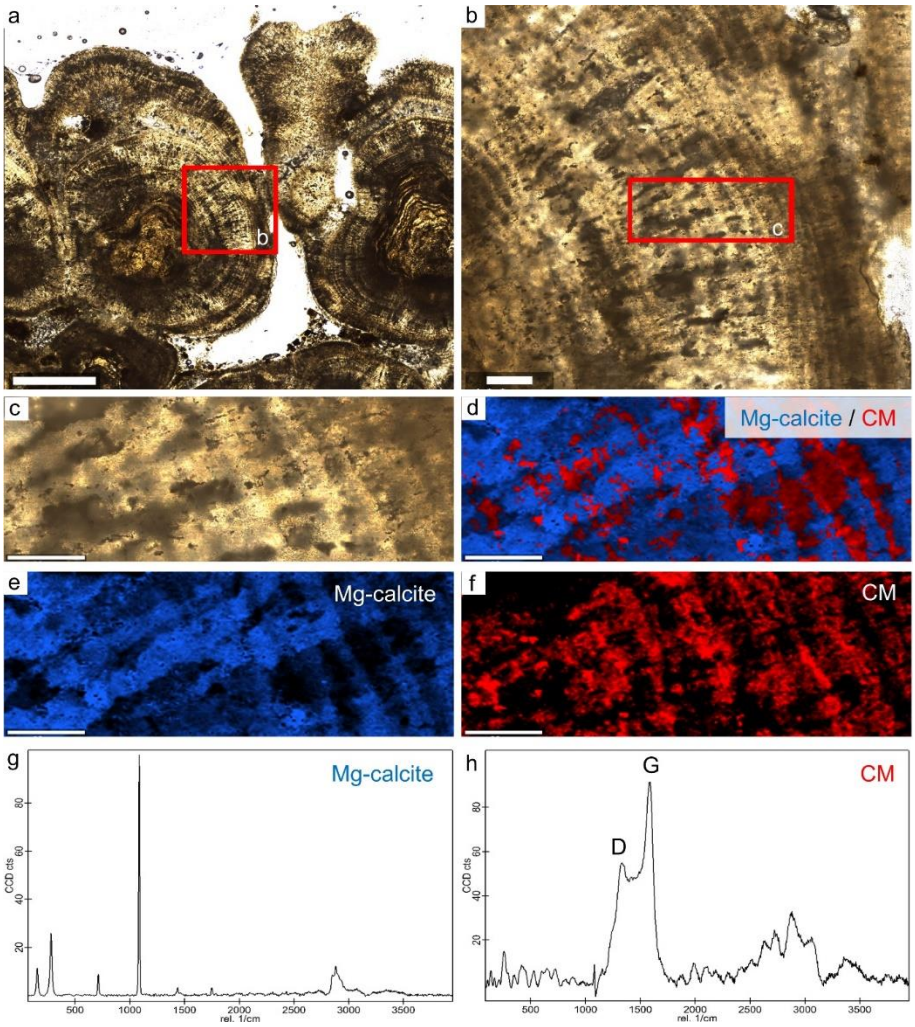

Fig. 9. Optical photomicrographs and Raman characterisation of laminae in the crystalline fabric. a) Optical photomicrograph showing an overview of the fabrics and their association with carbonate-coated grains. Red box indicates region of (b). Scale bar equals 900 µm. b) Detail of the red box in (a), showing the flat crystalline laminae. Red box indicates the region of interest for Raman mapping. Scale bar equals 150 µm. c) Selected region of interest for Raman mapping across several laminae. d) Multiphase map showing the contrast between Mg-calcite (blue) and CM (red) in alternating layers. e, g) Raman map and spectral signature of Mg-calcite. f, h) Raman map and spectral signature of CM. c-f) Scale bars equal 60 µm.

SEM observations showed well-defined laminations (Fig. 10a) confirming that microcolumns are generated by alternating micrite layers of microgranular micrite and densely packed microsparite layers, both made of a Mg-calcite mineral phase (Fig. 10a). The calcite

forming the cores of the microstromatolitic crusts shows large well developed rhombohedral crystals of Mg-calcite (Fig. 10b).

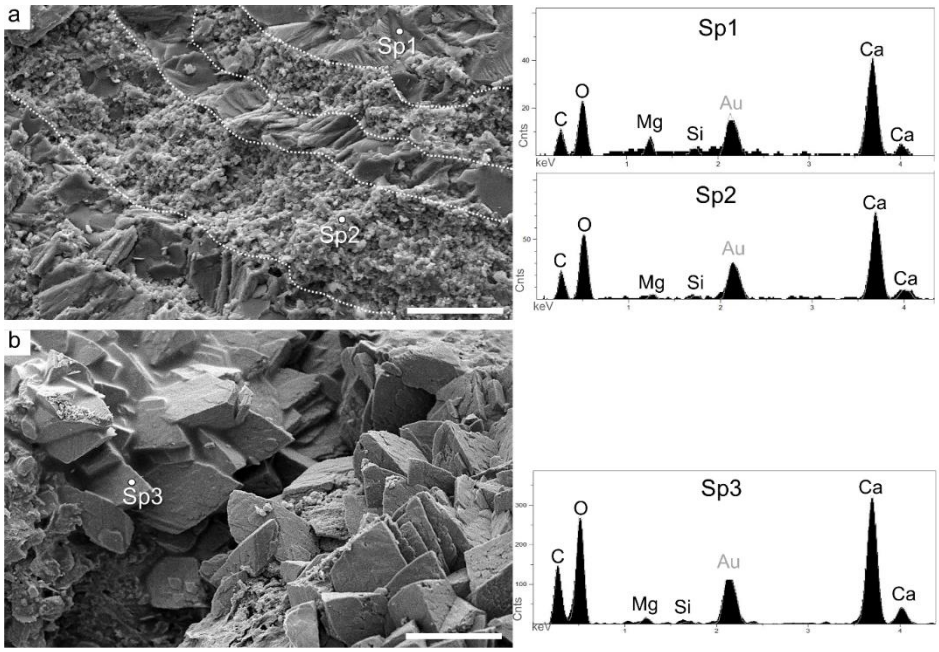

Fig. 10. SEM and EDX characterisation of microfabrics of the microstromatolitic crusts. a) Micrograph showing laminae composed of granular micrite and microsparite calcite; EDX spectra show similar elemental compositions of predominantly Mg-calcite, with a slight variation in MgO%, and very low Si content. Scale bar equals 20 µm. b) Micrograph showing rhombohedral calcite crystals from the calcite core; EDX spectrum again indicates Mg-calcite. Scale bar equals 100 µm. In all spectra, the Au peak corresponds to the gold used for coating the samples.

SEM imaging also revealed the presence of microbial components within the laminated structures. Carbon-rich amorphous structures associated with filamentous structures were locally observed, showing different modes of occurrences:

1) A mucus-like texture distributed throughout the matrix, in which trace Na, Si and Cl were identified in EDX spectra (Fig. 11a), suggesting the presence of NaCl;

2) Amorphous structures occurring in association with a microgranular texture, composed of an aggregate of nano- to micrometric spherical particles (Fig. 11b). EDX data for this microgranular texture exhibit a variety of elements in trace quantities, including Na, Al, Si, Cl and K. The combined signals of Al-K with Si-O suggests the presence of aluminous phyllosilicates.

3) Porous alveolar networks with empty cavities (Fig. 11c) containing possible Mg-bearing silicate phases and a very low Ca content.

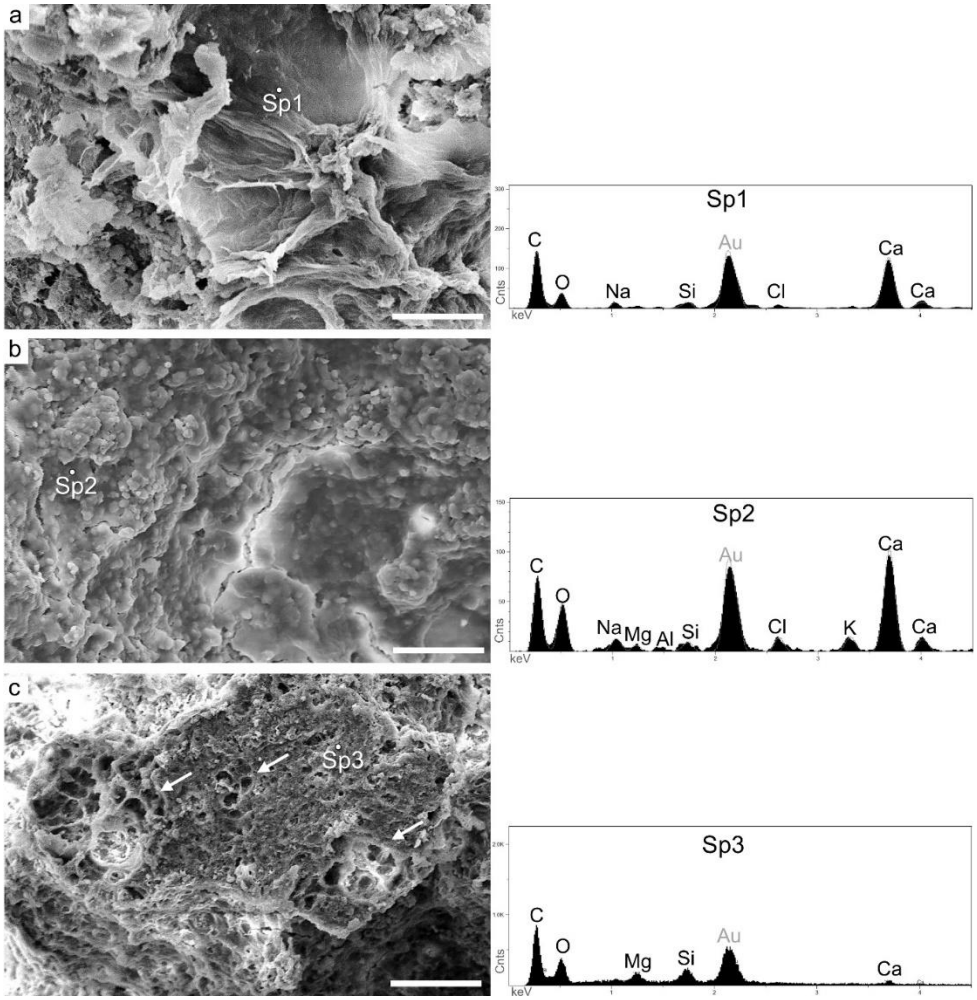

Fig. 11. SEM micrographs and EDX spectra showing diverse carbon-rich amorphous structures derived from microbial communities in Lake Abhe microstromatolitic crusts. a) Mucus-like carbon-rich material in the matrix. Scale bar equals 10 µm. b) Carbon-rich amorphous structures associated with microgranular texture. Scale bar equals 20 µm. c) Carbon-rich amorphous structure exhibiting an alveolar network (white arrows). Scale bar equals 50 µm. In all spectra, the Au peak corresponds to the gold used for coating the samples.

SEM observations of microstromatolitic crusts enables detailed characterisation of the filamentous structures and their two modes of preservation (Fig. 12): a) empty molds of filamentous structures with no preferential orientation (Fig. 12a), which are the most common type of preservation; and b) filamentous molds completely or partially filled with amorphous materials (Fig. 12b) that, although less common, preserve densely arrangements of parallel vertically oriented filaments forming a palisade-like texture, as previously observed using optical microscopy (Fig. 7c-f). EDX analyses demonstrated that the amorphous material filling the filamentous mold structures is composed of Si, O and Mg, suggesting the presence of Mg-silicate phases forming the counterpart of filamentous structures (Fig. 12c).

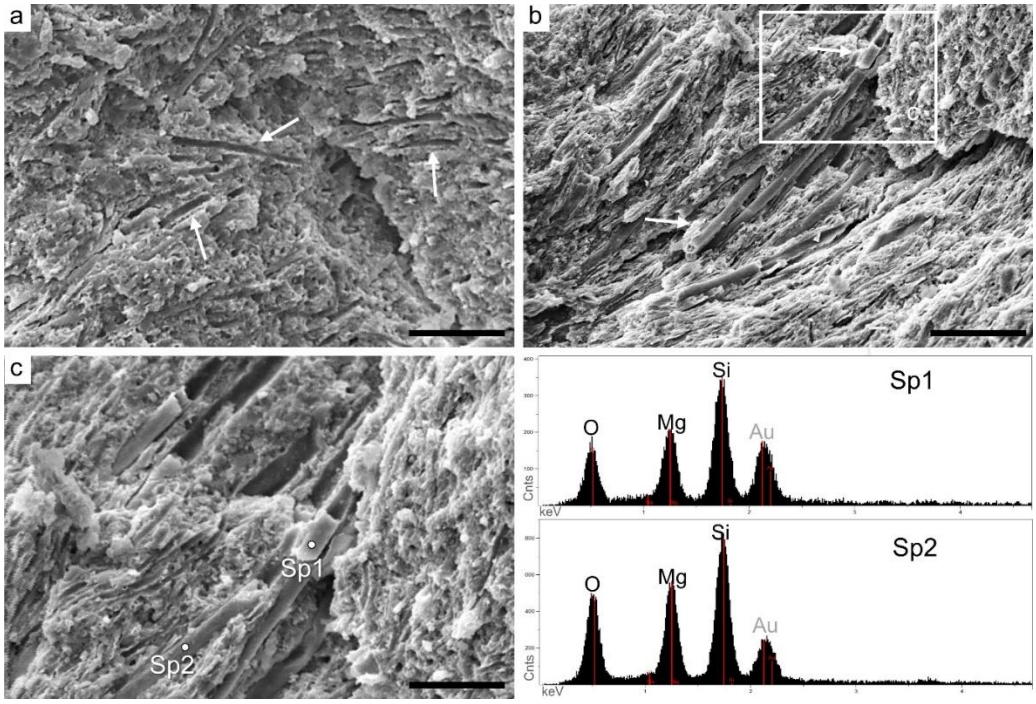

Fig. 12. SEM micrographs showing filamentous structures. a) Filamentous empty molds (arrows) preserved in a micrite matrix. Scale bar equals 20 µm. b) Cluster of closely packed filamentous structures forming a palisade-like texture. Boxed area detailed in (c). Scale bar equals 50 µm. c) Higher magnification micrograph and EDX spectra showing molds of filaments filled with an Mg-silicate phase. Scale bar equals 20 µm. In all spectra, the Au peak corresponds to the gold used for coating the samples.

3.5. Discussion

3.5.1. Formation of Lake Abhe microstromatolitic crusts

The formation of microstromatolitic crusts at Lake Abhe has previously been linked to rapid carbonate precipitation due to interactions between hydrothermal fluids and lake waters (Dekov et al., 2014); however, the role of microbial communities in the formation of these crusts remains poorly constrained.

The microcolumns forming the crusts have a laminated structure of dark micritic and light sparite calcite laminae, resembling stromatolites found throughout the geological record (Grotzinger & Knoll, 1999; Riding, 2011). Cyanobacteria are considered the primary microorganisms responsible for the formation of modern stromatolites (e.g., Schopf, 2012; Nguyen et al., 2022), the internal lamination of which generally results from the rhythmic stratification of cyanobacteria-rich laminae (containing fossilised filaments and sheaths) and more porous laminae with lower concentrations of microbial components (Grotzinger & Knoll,

1999). Due to continuous calcite precipitation, cyanobacteria must migrate upward to maintain access to sufficient sunlight for photosynthesis. As a result, the older biomass dies and is entombed beneath subsequent layers of living cyanobacteria.

The formation of the microstromatolitic crusts occurred underwater and reflects the reaction between Ca-rich hydrothermal waters, and the surficial lake waters sourced from the Awash River, that caused a precipitation of $CaCO_3$ (Demange et al., 1971; Fontes & Pouchan, 1975; Dekov et al., 2014; 2021; DeMott et al., 2021). The chimneys present an alignment suggesting that they formed along active faults oriented WNW–ESE, which likely served as conduits for the percolation of fluids. Isotopic analyses (^{44}Ca, ^{13}C and ^{18}O) have revealed that the inner microstromatolitic crusts of the chimneys were formed by out-of-equilibrium calcite precipitation from a predominantly hydrothermal Ca source (Fontes & Pouchan, 1975; Dekov et al., 2014). The outer layer of low-Mg calcite received Ca contributions from both hydrothermal fluids and lake waters, with a C source consisting of atmospheric CO_2 in equilibrium with alkaline lake water (Dekov et al., 2014).

The microstromatolitic crusts exhibit a combination of abiogenic and biogenic characteristics (Figs 3-12), which also seem to mirror the mixing and fluctuation of fluids. Thicker, more densely laminated layers may indicate a stronger microbial influence on precipitation, whereas thinner, isopachous acicular laminae may have formed under limited microbial influence (DeMott et al., 2021; Bisse et al., 2022). A similar configuration has been described in microdigitate lacustrine stromatolites from the Green River Formation in the USA, which formed in a similar closed-basin lacustrine system (Frantz et al., 2014). In the Green River Formation, two distinct mechanisms of carbonate formation have been identified: a fan calcitic sparite microfabric, composed of low Mg-calcite, resulting from abiogenic precipitation from lake water, and a micrite microfabric, composed of dolomite and/or calcite, resulting from microbially mediated precipitation, grain trapping and binding. Figure 10 shows a similarly striking difference between the laminae of micrite and microsparite that make up the microcolumns of the Lake Abhe microstromatolitic crusts. EDS spectra, however, detect a slight increase in Mg content in the microsparite relative to the micrite. In the Green River Formation, Frantz et al. (2014) established a direct relationship between changes in the characteristics of laminations and variations in lake level, temperature and salinity, which in turn can influence microbial development and the ability of the ecosystem to generate laminae with different fabrics. A similarly direct relationship between climate change and lake level was also detected in the lacustrine carbonate deposits of Lake Van, Turkey (Yeşilova et al., 2019).

The textural and morphological variations observed in microstromatolitic crusts at Lake Abhe can be attributed to several growth mechanisms. Internal lamination is the result of calcite precipitation mediated by cyanobacteria, whereas calcite accretion occurs through the trapping and binding of particles, resulting in inorganic accumulation (Castro-Contreras et al., 2014). Carbonate precipitation mechanisms also seem to depend on lake currents. Micrite lamination is favoured by calm water conditions in which no sediment is deposited on the surface of the microstromatolitic crusts. Thus, calcite may precipitate from supersaturated waters, producing laminations as bacteria periodically migrate upward (Castro-Contreras et al., 2014). In hotter and drier climates, or under high evaporation conditions, alkalinity increases and the microbial community proliferates, inducing greater precipitation of laminated carbonate with preservation of filaments (Muller et al., 2022).

A further mechanism, detected in microbialites from the hydrothermal systems La Salsa, Bolivia (Bougeault et al., (2019), may also have occurred at Lake Abhe, whereby carbonate mineralisation may occur within the capillary waters of microbial mats at the microbial mat–air interface, where evaporation induces CO_2 degassing. CO_2 degassing through evaporation reduces the concentration of dissolved inorganic carbon within microbial mats sufficiently for the photosynthetic activity of cyanobacteria to induce a significant increase in calcite supersaturation and precipitation (Muller et al., 2022).

The fabrics of Lake Abhe microstromatolitic crusts (Figs 4-6), such as the microcolumns and the porous calcite with a sugary texture, are comparable with those observed in microbialitic crusts from the alkaline crater lake Alchichica, Mexico (e.g., Kazmierczak et al., 2011). In Lake Alchichica, the porous cores are composed of hydromagnesite precipitated due to the rapid diagenetic replacement of primary aragonite in the living cyanobacterial biofilm. In contrast, the calcitic cores observed at Lake Abhe (Figs 4, 6c) showed no evidence of CM (Figs 5a, 6c). The euhedral and translucent Mg-calcite crystals of the core (Fig. 6c) suggest abiogenic calcite precipitation (Dupraz et al. al., 2009). Dekov et al. (2021), based on a comparative study of microstromatolitic crusts from Lake Abhe with similar structures from Lake Asal (Ethiopia), proposed that the calcite core (Fig. 3a) corresponds to the hot spring vents at the bases of the chimneys and fumaroles of Lake Abhe. Dendritic calcites similar to those observed in Lake Abhe seem to typify spring-associated carbonates in both subaerial and sub-lacustrine environments (Jones, 2017). Sub-lacustrine formation suggests that the inactive vents formed during periods of higher lake levels than today, and that different layers of Lake Abhe microstromatolitic crusts correspond to lake level fluctuations and regional temperature

changes recorded since the Late Pleistocene and throughout of the Holocene in this region (Gasse & Street, 1978; Dekov et al., 2014; DeMott et al., 2021).

3.5.2. Microbe–sediment interactions

The Lake Abhe microstromatolitic crusts are dominated by authigenic carbonate with rare detrital minerals trapped within their microstructures. EDX spectra reveal trace elements, such as Mg, Al, Si, Cl, Na and K (Fig. 11) associated with fossilised carbon-rich amorphous structures, probably originating from dissolved salts and authigenic phyllosilicates, which are common in such environments (Casanova, 1994) and are not related to detrital minerals. The rarity of detrital grains suggests that microstromatolite growth occurred solely through calcite precipitation. Several factors can influence the precipitation of authigenic calcite in lake systems.

Photosynthetic absorption of CO_2 can locally increase pH and carbonate anion (CO_3^{2-}) concentration, increasing alkalinity and the activity of the Mg^{2+} and CO_3^{2-} ions, which co-precipitate with dissolved Ca^{2+} to form Mg-enriched calcite phases, mainly as microcrystalline cements (Dupraz et al., 2009; Petrash et al., 2012). As primary producers migrate up and away from the lithified substrate, the composition of water in the spaces between the detached photosynthetic biofilm and the microstromatolitic crust surface becomes temporarily controlled by microbial metabolic activity. This activity induces physicochemical conditions that promote the rapid growth of carbonate and subsequent cementation, favouring the development of mesoscale biofilms (Dupraz & Visscher, 2005; Riding, 2006; Westall et al., 2011). This mode of carbonate precipitation is consistent with the formation of filamentous casts within a cyanobacterial sheath (Petrash et al., 2012).

The filamentous structures preserved in the Lake Abhe microstromatolitic crusts are interpreted as cyanobacterial sheaths (Figs 7, 8) due to their unbranched filamentous morphology, nearly straight or flexuous morphology, and uniform diameters (Schopf, 2012; Cellamare et al., 2018) reaching up to 2.85 μm along the entire length. Many cyanobacteria are able to form mucilaginous sheaths, a distinct type of extracellular carbohydrate composed of a network of polysaccharide fibrils oriented variably relative to the cell surface (Hoiczyk, 1998; Cellamare et al., 2018). Among the morphological components of cyanobacteria, their extracellular sheath and envelopes, initially composed largely of carbohydrates and relatively resistant to degradation, are most frequently preserved in the fossil record (Schopf, 2012).

Fossilised sheaths are predominantly vertically oriented relative to the lamination of the columnar fabric (Fig. 7), suggesting that they reflect the life position of the microbes (Berelson et al., 2011). This spatial configuration is most consistent with photosynthetic growth (Noffke & Awramik, 2013; Hickman-Lewis et al., 2019) and in some instances forms a palisade texture (Fig. 7c-f) (e.g., Franchi & Frisia, 2020). The biogenic palisade texture indicates more stable physicochemical conditions; it is associated with the growth of filamentous and sheathed cyanobacteria, forming a predominantly phototrophic ecosystem, given the shallow depositional depths (Campbell et al., 2015; Álvaro et al., 2021; Hickman-Lewis et al., 2023). Calcification of cyanobacteria appears to result from alkalinity gradients within mucilaginous sheaths, associated with photosynthetic absorption of CO_2 and/or absorption of HCO_3, which increases alkalinity (Riding, 2000).

Although stromatolite-forming ecosystems are comprised of diverse phyla, cyanobacteria play a major role in the lithification process through oxygenic photosynthesis and producing copious quantities of extracellular polymeric substances (EPS) (Dupraz et al., 2009; Nguyen et al., 2022). The carbon-rich amorphous structures observed at Lake Abhe are interpreted as EPS secreted by cyanobacteria (Figs 8-9, 11). EPS plays a central role in the formation of microbial carbonates, accumulating outside cells to form a protective, adhesive matrix that anchors microbes to substrates and provides physical and chemical protection for the biofilm community (Nguyen et al., 2022).

The process of permineralisation within stromatolites occurs due to the encrustation of cyanobacterial filaments and micritisation associated with the decomposition of the extracellular organic matrix (Dupraz et al., 2009). The presence of EPS creates nucleation sites for mineral precipitation, both absorbing essential elements used by cyanobacteria (Dupraz et al., 2009) and chelating metals that may pose toxic stresses to organisms (Hickman-Lewis et al., 2019).

3.5.3. Microbial preservation in Lake Abhe microstromatolitic crusts

In the Lake Abhe samples, the presence of different EPS networks may indicate the influence of varying environmental conditions on EPS degradation and carbonate precipitation (Arp et al., 2003; Calça et al., 2016). In an experiment using freshwater biofilms, Pedley (2014) found a granular EPS network similar to that described in this study (Fig. 11b) and suggested that this EPS texture, formed by amorphous calcium carbonate nanospheres, represents the initial phase of precipitation of carbonate within a biofilm. The subsequent coalescence of

nanospheres and progressive occlusion of EPS resulted in the development of multilayered nanosphere aggregates, which neomorphically mature into well-ordered microsparite crystal fabrics (Manzo et al., 2012; Pedley, 2014).

Granular EPS in the microstromatolitic crusts of Lake Abhe exhibits an elemental trace composition of Al, Si, Na, Mg, Cl and K (Fig. 11b), suggesting the presence of aluminous phyllosilicates, such as kaolinite. Fiore et al. (2011) experimentally proposed that the formation of Al-rich silicate phases occurs through the precipitation of an aluminosilicate gel within the EPS; and the crystallisation of kaolinite takes place as a consequence of changes in the microenvironment induced by metabolic activity, suggesting localised syndepositional mineralisation and carbonate–silica interplay within granular EPS in the Lake Abhe microstromatolitic crusts.

In addition to the granular EPS, an alveolar network of EPS was also observed (Fig. 11c). Dupraz et al. (2004) proposed that alveolar EPS may form due to the initial precipitation of Mg-rich calcite and the activity of sulphate-reducing bacteria. This occurs because the acidic macromolecules in microbial biofilms can reorganise into a structured pattern to provide nucleation sites for carbonate, potentially influenced by decaying EPS, as suggested by Trichet et al. (2001) and Calça et al. (2016).

The alveolar EPS in Lake Abhe microstromatolitic crusts contains Mg, Si and O (Fig. 11c), interpreted as Mg-silicate. Burne et al. (2014) proposed that Mg-silicate forms within and around cyanobacterial sheaths and in the EPS alveolar network, driven by high silica activity and reduced C and Ca in the EPS due to biological processes. In Lake Abhe, cyanobacterial sheath molds filled with Mg- and Si-rich material (Fig. 12b-c) support this model, indicating the potential accumulation of Mg-silicate minerals as syndepositional clay within laminated sediments (DeMott et al., 2021).

The authigenic microbial precipitation of Mg-bearing phyllosilicates, such as stevensite, has been reported in alkaline lakes as a syngenetic phase often associated with carbonates. In Lake Clifton, Australia, Burne et al. (2014) described Mg-Si phases forming within and around cyanobacterial sheaths, similar to the filled molds in Lake Abhe samples (Fig. 12b-c). Burne et al. (2014) demonstrated that stevensite permineralised the walls of the filamentous sheaths and nucleated on the surface of the microbial filaments in thrombolites. This led to massive stevensite formation, followed by carbonate replacement of cyanobacterial remnants. Carbonates initially form radiating rhombic microcrystals that coalesce into dense aggregates, obscuring the original fabric, as demonstrated experimentally by Manzo et al. (2012).

Mg-bearing silicates play a crucial role in preserving filaments and their molds, as well as EPS, in volcanically influenced alkaline lacustrine systems (e.g., Mologni et al., 2021). Lincoln et al. (2022) studied Mg-silicates and aragonite in Great Salt Lake ooid cortices, concluding that microbial mediation is likely responsible for their formation. Raman analysis of Lake Abhe microstromatolitic crusts found a high concentration of presumably microbially derived CM in the concentric laminations of the carbonate-coated grains, supporting a similarly biomediated mechanism of formation. Pace et al. (2016) also documented amorphous Mg-silicates in modern microbialites from the Great Salt Lake, suggesting microbially mediated precipitation due to localised pH increases. The Mg-Si phase, a precursor to stevensite in the Great Salt Lake, was precipitated within the organic matrix by incorporating Mg^{2+} and SiO_2 from the lake water. The microbial metabolism lowers the kinetic barrier for Mg-Si phase nucleation and induces the precipitation of this poorly crystalline phase. According to Tosca et al. (2011), the formation of poorly crystalline Mg-silicate indicates that the lake waters were highly alkaline (pH > 8.7). Lake Abhe, characterised by pH 9.9 and a high content of dissolved SiO_2 (~ 416 mg/L^{-1}, Gasse, 1977), presents an ideal environment for Mg-silicate formation. In the chimney samples, the absence of significant diagenetic alteration features, such as dissolution, dolomitisation and cementation associated with pore occlusion, also suggests that the presence of magnesium-bearing clay minerals is neither a product of secondary minerals filling the pores, nor a result of early calcite alteration, consistent with the findings of DeMott et al. (2021).

3.6. Conclusions

This chapter reported the microstromatolitic encrustations from Lake Abhe. Their formation is influenced by cyanobacteria-dominated communities. Microcolumnar stromatolitic fabrics are dominated by filamentous structures; however, filamentous structures were also found to be preserved in crystalline fabrics and in association with carbonate-coated grains.

The Lake Abhe microstromatolitic crusts demonstrate good fossilisation potential. The biogenic components appear to be preserved in association with specific combinations of Mg-bearing silicate and carbonate phases. Such depositional and diagenetic conditions are beneficial for the formation of organic–mineral associations that promote the preservation of filamentous microfossils in highly alkaline, basalt-hosted lacustrine environments.

Chapter IV – Microbial Influence and Formation Processes of Stromatolites in the Carri Laufquen Lake System, Northern Patagonia, Argentina

The data presented in this chapter correspond to the following manuscript:

Dorneles, V.A.C., Hickman-Lewis, K., Millan, M., Najorka, J., Broderick, C., Šket, P. & Cavalazzi, B. Biosignatures in Stromatolites from Carri Laufquen Lakes System, Patagonia: Implications for Martian paleolacustrine environments. In preparation for *Earth and Planetary Science Letters*.

4.1. Introduction

In the high-altitude areas of the subtropical and tropical Andes in southernmost South America, there is a significant lack of in-depth research on lacustrine stromatolites (Pacton et al., 2015). Nevertheless, previous studies in the Patagonia and Andean plateau region known as the Puna, have demonstrated the stromatolites are often distributed along paleolake shorelines (e.g. Galloway et al., 1988; Ariztegui et al., 2001), which make them valuable indicators of hydrological variations in ancient lakes, thereby enhancing our understanding of historical continental climate patterns (e.g., Bradbury et al., 2001; Tatur et al., 2002). Despite the fact that in the Argentinean Patagonia region was documented sites with fossil occurrences of stromatolites build-ups (i.e. Alonso-Zarza et al., 2020); it is notable the modern active systems of stromatolite growing in the Andes lakes (e.g. Gomez et al., 2014; Buongiorno et al., 2019; Boidi et al., 2020; Muller et al., 2022).

In this chapter, we present a detailed study of sub-fossil stromatolites occurrences in the Carri Laufquen Lake system, in the northern Patagonia, Argentina (Fig. 1). A multi-analytical approach was used to describe the stromatolites and their microbial components. The stromatolites occurrences documented here present related characteristics with those mentioned in the Patagonia and Puna region, since the conditions of high altitude and alkalinity are similar.

We aim to characterise the microfacies of stromatolitic structures, seeking to investigate their formation processes and the influence of microorganisms in their micromorphologies and microstructures. In addition, to discuss the potential of microbial preservation in this extreme alkaline lacustrine system.

4.2. Geological setting

Laguna Carri Laufquen is a closed endorheic basin situated in the northern part of Argentine Patagonia, within the province of Río Negro (41°80 47″ S, 69°270 37″ W, Fig. 1). Presently, it constitutes a lacustrine system housing two primary lakes, Carri Laufquen Grande (CLG) and Carri Laufquen Chica (CLC), formerly connected by the ephemeral freshwater Maquinchao River (Pacton et al., 2015). The area is typified by an average annual temperature of 10°C, ranging from 16.1°C to 1.7°C during the Austral summer and winter seasons, with an

average annual precipitation of 200 mm (Agosta et al., 2015; Pacton et al., 2015). CLG sits at 825 m a.s.l., covering 18.2 km^2, with an average water depth of 8-10 m and a pH of 8.8; CLC is at 786 m a.s.l., encompassing 5.5 km^2, with an average depth of up to 10 m and a pH of 8.7. Both lakes exhibit variations in size and depth, including periods of complete dryness (Alvarez et al., 2022). During our studies in March 2023 the lakes were dry, and unconnected by the Maquinchao river, different from the reports in Pacton et al. (2015) and Eymard et al. (2021), as well as CLC showed the entire lakebed covered by grasses (Fig. 1).

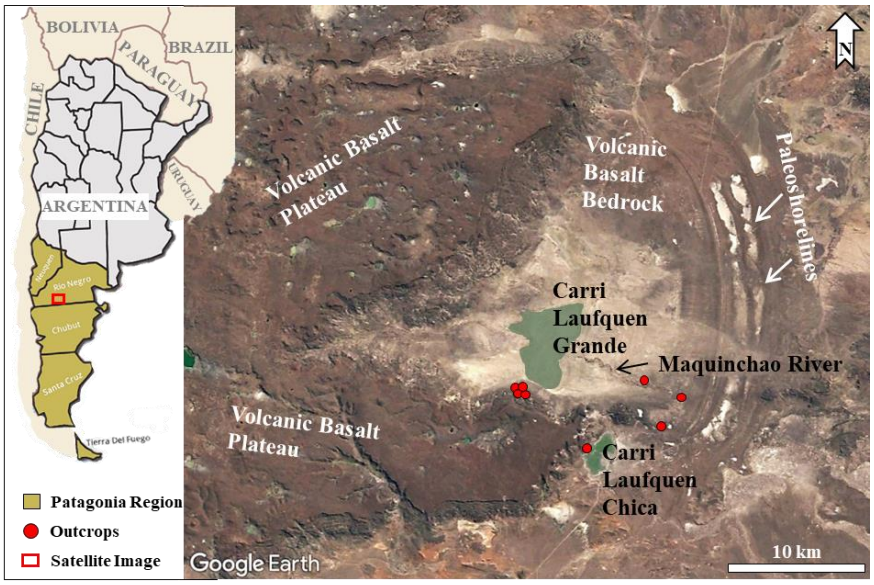

Fig. 1. Location map of the study area showing the outcrops studied in the Carri Laufquen Lake system, associated to the volcanic basalt plateau in the Rio Negro region, Patagonia, Argentina. The pale blue dashed line shows the current shore of Carri Laufquen Grande, which was completely dry during our field campaign in March 2023, while the green color in Carri Laufquen Chica corresponds to grass that covers the entire surface area of the lake. The image was obtained in 2024 from the Landsat Copernicus satellite.

The Maquinchao Basin evolved over a series of Mesozoic volcanic deposits, clays, calcareous sandstones, and conglomerates sequences, along with Miocene volcanic deposits (Whatley & Cusminsky, 1999). The Pleistocene sequence is characterised by fluvial and lacustrine deposits. The region constitutes a tectonic depression situated at an altitude of 800 m a.s.l., surrounded by Mesozoic to Tertiary basalt plateaus on the western and eastern flanks of the basin (Fig. 1), surpassing 1000 m of altitude (Alvarez et al., 2022; Aguilera et al., 2018; Pacton et al., 2015). The CLG and CLC lakes were positioned among the plateau basalts known as the Cari Laufquen "meseta" (Late Oligocene-Early Miocene), comprising sequences of dark basalts abundant in olivine, formed with lesser differentiation, generated by peridotite fusion in the upper mantle and a rapid, later ascent, devoid of advanced fractionation phenomena (Aguilera et al., 2018).

The formation of the Maquinchao Basin was hindered during the last glaciation of the Andes Cordillera (Ariztegui et al., 2008; Tatur et al., 2002). Satellite data reveals significant fluctuations in water levels of the CLG and CLC lakes over the past dozen years (Alvarez et al., 2022; Eymard et al., 2019). Clear paleoshorelines are observable on the eastern side of the CLG (Fig. 1), previously dated to around 19 ka (Galloway et al., 1988) and between 14 ka and 10–8 ka bp (Bradbury et al., 2001), indicating the existence of a large high-altitude palaeolake resulting from the merging with the CLC at the end of the Pleistocene, covering an area exceeding 1,500 km2 (Pacton et al., 2015; Ariztegui et al., 2008; Galloway et al., 1988). Numerous prior paleoclimate investigations employing various proxies suggest elevated lake levels during the late Pleistocene (Ariztegui et al., 2008; Galloway et al., 1988; Tatur et al., 2002; Whatley & Cusminsky, 1999). Additionally, fine-grained lacustrine deposits underlying the two upper shorelines contain abundant diatoms and ostracods, indicating deposition in a deeper, saline, and alkaline lake (Cusminsky and Whatley, 1996).

Previous studies have documented the occurrence of carbonate accumulations associated with lake deposits (Eymard et al., 2021; 2020; 2019; Pacton et al., 2015; Ariztegui et al., 2008), and described as tufas by Cartwright et al. (2011). These carbonate accumulations have typically been described as structures with globular morphologies, ranging from medium-sized, open flower-like to large, open, flower-like formations. Laminated globular carbonate structures generally surround basaltic cores and exhibit no preferential axis of growth or other indications of hydrodynamic conditions. Furthermore, Pacton et al. (2015) investigated modern microbialites growing in certain sectors of the Maquinchao River, exhibiting morphologies similar to some fossil examples.

4.3. Material and Methods

The field campaign for collecting stromatolites samples was carried out in March 2023 in the Laguna Carri Laufquen region. Sample preparation took place at the Università di Bologna, Italy, followed by investigation using routine and advanced analytical techniques. Nineteen samples were embedded in epoxy resin to produce 24 uncovered petrographic thin sections (~30 µm thickness and 60x90 mm dimension).

Microfacies and microbial textures were described under optical microscope. Elemental, mineralogical am biomolecular composition of selected regions of interests were

analyzed using Scanning Electron Microscopy and Energy Dispersive X-ray Spectroscopy (SEM-EDX), from six representative thin sections and eight freshly fractured pieces of the same six samples used to prepare the thin sections. The six thin sections metalized for SEM-EDX and TESCAN Integrated Mineral Analyzer (TIMA) analyses were duplicated to keep their respective samples free from contamination to be used in other techniques, such as Raman microspectroscopy, Micro X-ray Driffraction (μXRD) and Fourier-Transform Infrared microspectroscopy (FTIR). Raman was performed in four representative thin sections. μXRD measurements were conducted in five thin sections. For NMR, ten bulk samples were examined. For FTIR, representative spectral maps of four thin sections were obtained. Solid state 13C Nuclear Magnetic Resonance (NMR) spectroscopy was performed in order to investigate the mineralogical composition and molecular organic components of ten bulk samples.

4.4. Results

4.4.1. Field and outcrop observations

The choice of outcrops studied was based on previous work by Eymard et al. (2019) and Pacton et al. (2015), whose coordinates were essential for locating and identifying the outcrops of the CLG, CLC and Maquinchao River. The outcrops of Carri Laufquen Grande are located at several points between the south-southwest margin of the lake and the base of the basalt plateaus (Fig. 2A), and constitute deposits of carbonate buildups that extend laterally for a few tens of meters at altitudes varying from 823 to 851 m (Fig. 2B). Carri Laufquen Chica deposits include thin carbonate crusts coatings on pebbles that are deposited along the eastern margins of the lake, extending laterally for up to one hundred meters (Fig. 2C-D), at an altitude of 849 m. In addition, the outcrops of the Maquinchao River occur on both shores of the current dry river (Fig. 2E-F), at altitudes 810 to 837 m.

Outcrops in general are composed of dispersed rounded basalt pebbles of different sizes in cm to dm-scale, reaching up to one meter in diameter in CLG and Maquinchao River outcrops. The vertical extension of the layers containing the pebbles in the CLG outcrops does not exceed four meters (Fig. 2A). The pebbles are surrounded by carbonate crust, described as stromatolites, which vary in thickness on a mm to cm-scale and grow from the basaltic substrate in different directions, partially or completely surrounding the pebble, presenting distinctive

internal structure (Fig.s 2B, 2D and 2F). Stromatolites are often well preserved as an entire structure surrounding a basalt pebble; and may also be partially eroded and fragmented, as parts of the stromatolites are detached from the basalt blocks. In rare cases, we observed the growth of stromatolites without the presence of the basaltic nucleus (Fig. 2F).

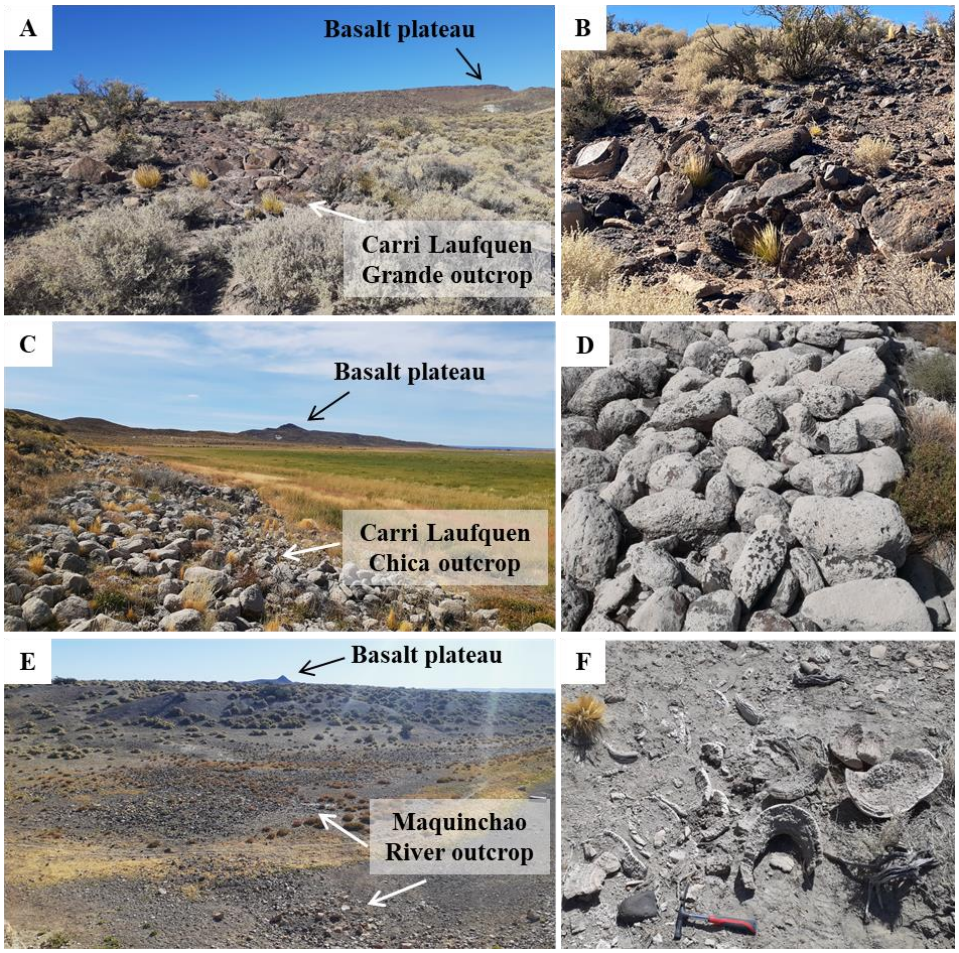

Fig. 2. Overview of the studied outcrops and samples. A) Outcrop of Carri Laufquen Grande at the base of the basalt plateaus. B) Close-up of the outcrop showing a layer composed of dm-scale pebbles surrounded by carbonate crusts identified as stromatolites. C) Outcrop of Carri Laufquen Chica on the shores of the lake. D) Close-up of the cm-scaled pebbles coated by the mm-scale carbonate crust. E) Outcrop on the shores of the Maquinchao River. F) Close-up of the fragmented stromatolites heads in the Maquinchao River outcrop showing a layered internal structure.

Five different morphological types were distinguished in the stromatolites of the studied outcrops, which represent five distinct stromatolitic facies (Fig. 3). Different morphologies possibly represent different stages of formation of stromatolitic crusts, since we observed an association between the stromatolite facies, varying between the base and the top of the structure. The stromatolite facies will be described below:

Dendrolite crust: presenting a very well-defined laminated structure composed of dendrite-like structures layers (Fig. 3A). Dendrite structures correspond to branches of dendrite crystals, displaying a tree-like structure (as described by Jones & Renaut, 1995; Jones et al., 2000b; Jones & Renaut, 2008). Each layer is less than 1.0 cm thick, so the internal dendrite-like structures are mm-scale and may be continuous from bottom to top of each layer (Fig. 3B). The external surface of the stromatolite shows a flat and smooth texture. This is the most common morphology found in outcrops, and they also have the greatest thickness, from the minimal 5 cm and reaching approximately 50 cm.

Globular crust: characterized by the lateral junction of globular and cerebroid columns (sensu Pacton et al., 2015) whose heights vary from 1 to 3 cm and diameter reaching 5 cm (Fig. 3C). The globular columns are not interconnected and do not have branches, which gives greater porosity due to the voids formed among the columns (Fig. 3D). Each column features a slight upward convex internal lamination of mm scale. The tops of the columns are reflected in the outer surface of the stromatolite suggesting a globular texture.

Laminated crust: refers to a very laminated carbonate crust, composed of millimetric flat, smooth and continuous laminae (Fig. 3E-F). The thickness of the crusts varies from a few millimeters to approximately 6 cm, and the external surface also presents a flat and smooth texture. It corresponds to the rarest morphology in the outcrops.

Lumpy crust: characterized by lumpy and irregular carbonate precipitations (e.g., Winsborough et al., 1994) (Fig. 3G). Includes the thinnest crusts in the outcrops, not exceeding 1 cm in thickness. Basaltic pebbles completely covered by lumpy crusts were not described, but only partially covered (Fig. 3H). In addition, lumpy crust occurs solely in contact with the basalt and sometimes grades into the next facies, usually columns.

Massive crust: corresponds to the coating of pebbles with a very thin layer of friable and massive carbonate, not exceeding 1 mm (Fig. 3I). The pebbles range in size from cm to dm and are usually continuously coated. In vesicular basalt pebbles the massive carbonate fills the vesicles (Fig. 3J).

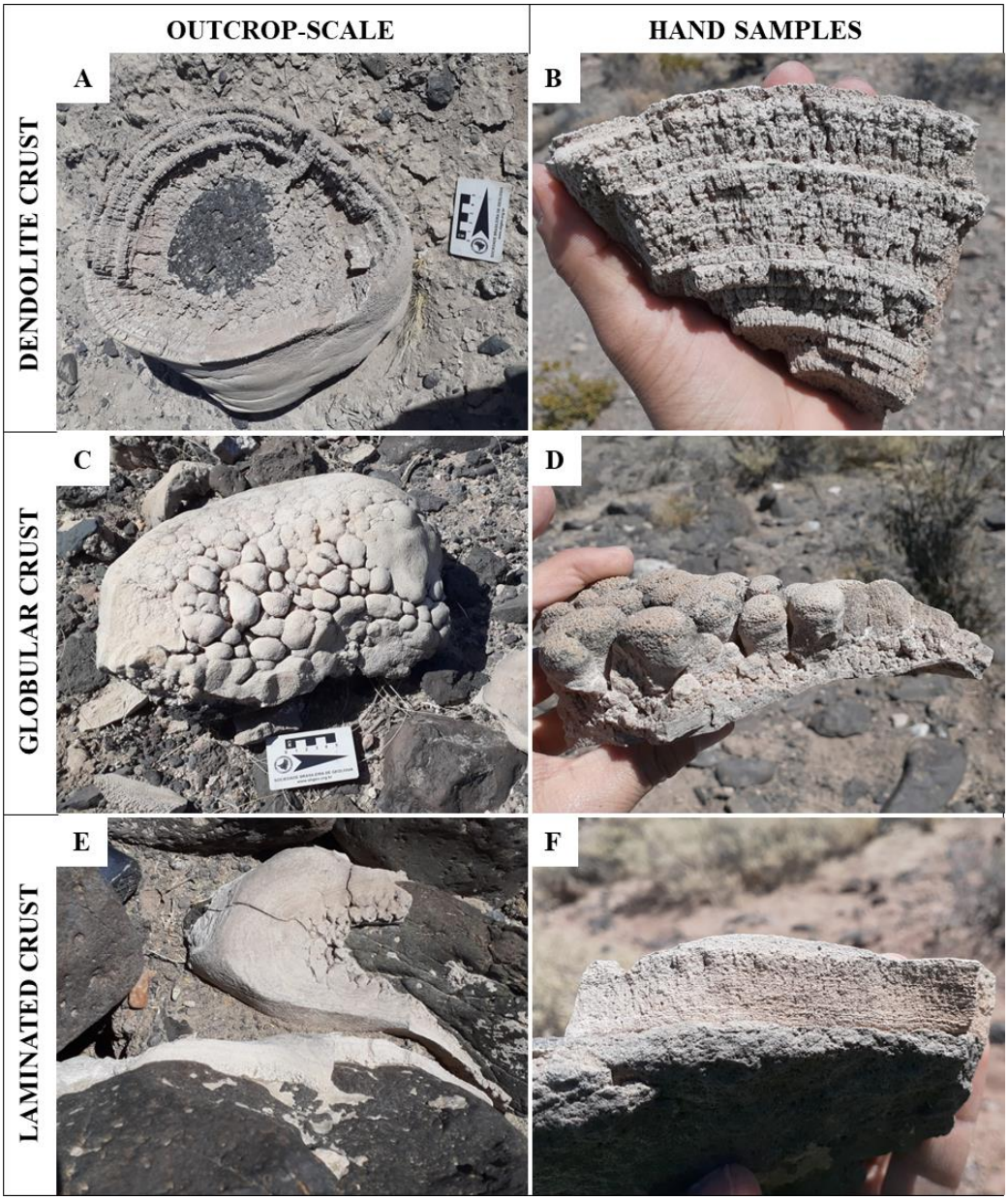

Fig. 3. Stromatolite field photographs, morphologies and samples. A-B) Dendrolite crust, composed of layers of shrub-like microcolumn structures. C-D) Globular crust, composed of globular and cerebroid columns. E-F) Laminated crust, including very flat and smooth laminated crust. G-H) Lumpy crust, characterized by lumpy and irregular carbonate precipitations. I-J) Massive crust, corresponding to the very thin and friable carbonate layers that completely coat the basalt pebbles.

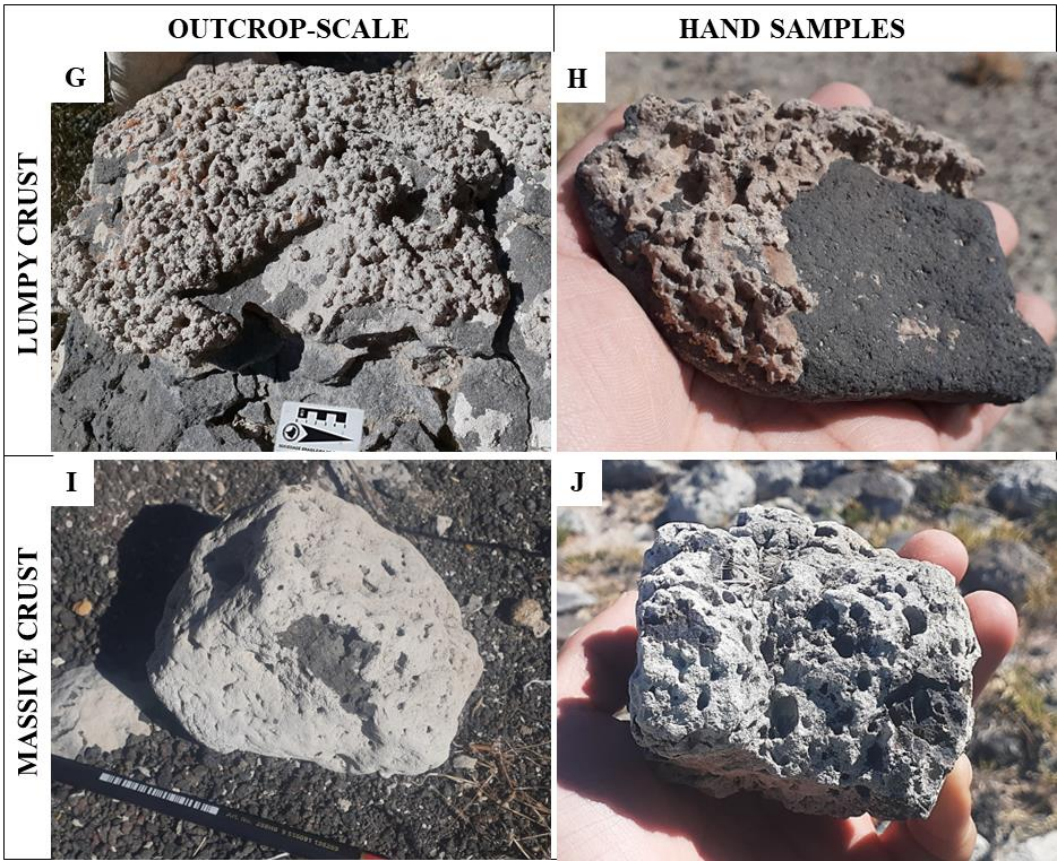

Fig. 3. (Continued)

4.4.2. Petrographical, mineralogical and chemical composition of stromatolites

Despite the description of five distinct macro morphologies, under optical microscopy only three microfacies were observed for the Carri Laufquen stromatolites. Microfacies are commonly repeated among the outcrop facies, so that the same sample contains a microfacies dominating the base, in contact with the basalt, and another microfacies predominating at the top of the sample.

The *laminated microsparitic microfacies* is composed of alternating layers of thicker radial-fibrous microsparite Mg-calcite, and thinner and darker layers of micrite (Fig. 4A). The layers vary from parallel and wavy, or form coalescing microcolumns whose internal lamination is convex upwards (Fig. 4B). The microfacies is dominated by microsparite, which provides a very low porosity and only few filaments have been identified.

The *micritic columnar microfacies* is characterized by a coalescence of dendritic columns composed of micrite, without an internal lamination (Fig. 4C). The columns contain many preserved filaments arranged mainly vertically following the orientation of the columns (Fig. 4D). The microfacies is predominantly micritic and the porosity is greater than in the

previous microfacies. We observed some samples filled with clay minerals and few diatom microfossils were observed in the sections.

The *botryoidal microfacies* is characterized by the intercalation of laminae of microsparite and micrite that form around a nucleus composed of rounded grains of Mg-calcite and grow in different directions (Fig. 4E), forming a botryoidal coalescence (e.g., Ge et al., 2021) (Fig. 4F). In the micritic portions, the presence of filaments is more notable, in contrast to the microsparite portions. We employed the non-interpretative term botryoidal to describe fans of fibrous crystals with non-spherical spatial organization growing from a nucleus with no preferential direction.

Exclusively in the massive crust samples observed under optical microscopy, we identified the presence of trapped diatom frustules associated with the filaments. In addition, other components were observed on a petrographic scale in several samples regardless of facies and microfacies, such as detrital grains of siliciclastic minerals, such as quartz, plagioclase, pyroxenes and clay minerals, generally trapped in the interstices of the microstructures.

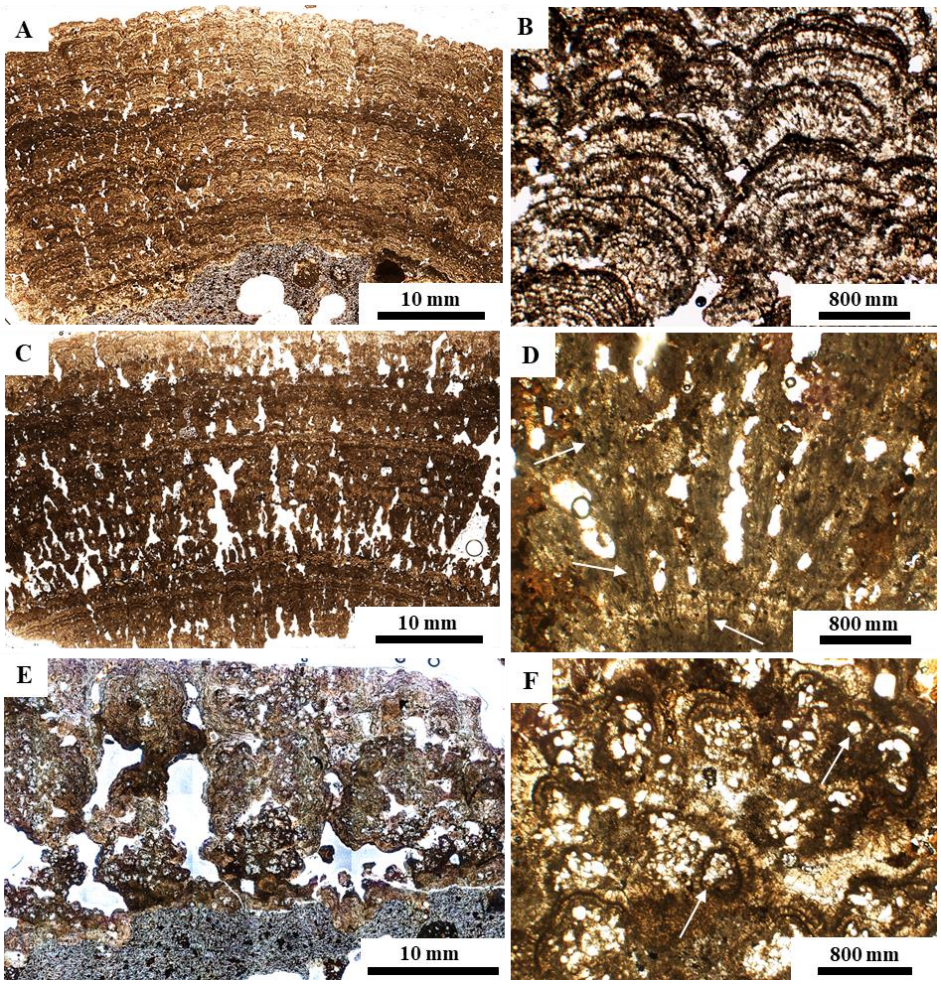

Fig. 4. Microphotographs of the Carri Laufquen stromatolite microfacies. A) Overview of the laminated microsparite microfacies. B) Detail of evident lamination in laminated microsparite microfacies coalescing to form microcolumns with internal convex lamination. C) Overview of the laminated microsparite microfacies. D) Detail of the microcolumns in the micritic columnar microfacies showing the presence of filaments (white arrows) associated with the micritic composition. E) Overview of the botryoidal microfacies. F) Detail of the irregular structures formed by the coalescence of pustules in the botryoidal microfacies, showing the presence of nuclei composed of calcitic grains (white arrows).

Micro-XRD and TIMA analysis confirmed the presence of Mg-calcite as the main mineral phase that construct the Carri Laufquen stromatolites. From the TIMA analysis, we observed a variation of the magnesium (Mg) throughout the stromatolite sample expressed in the paragenesis of calcite containing more or less magnesium, and can be distinguished into two phases, Mg-calcite and High Mg-calcite. This mineralogical variation is clearly expressed in the lamination of the stromatolites (Fig. 5A-B-C), represented in the colour of the laminae, as previously observed under the optical microscope, so that the dark laminae are composed of High Mg-calcite and the bright laminae by Mg-calcite (Fig. 5D). The spectra and boxplot graph obtained by micro-XRD analysis show the real variation of Mg in the mineral phases with respect to MgO% (Fig. 5E-F-G). The bright laminae, represented by Mg-calcite, contain 3 to 6% MgO, and average of 2.4%; while dark laminae, represented by High Mg-calcite, have a MgO variation of 3 to 10%, and average of 3.8%.

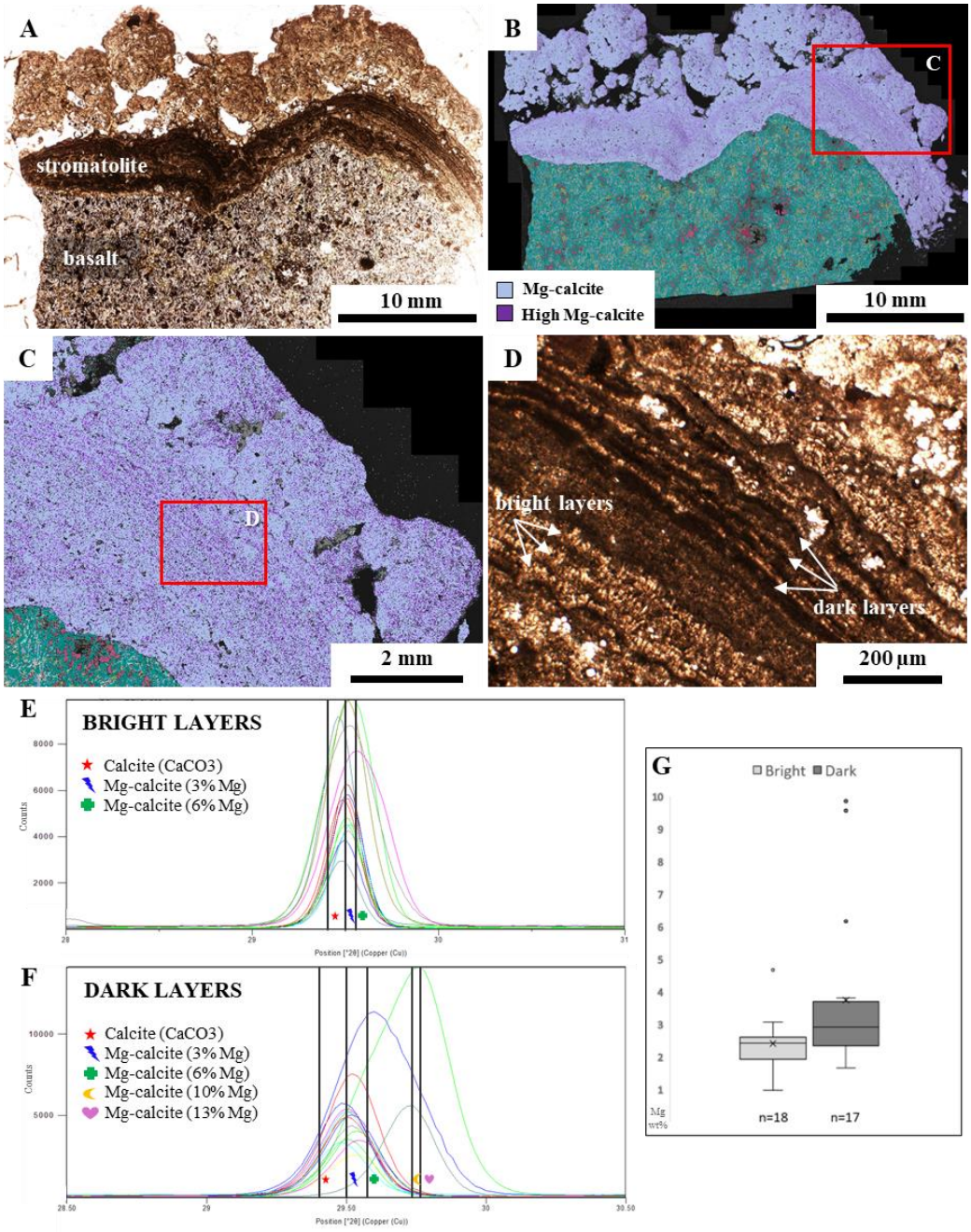

Fig. 5. Mineralogical composition of the Carri Laufquen stromatolites. A) Optical photomicrography showing an association between the botryoidal microfacies in contact with the basalt pebbles, showing a very defined lamination, and laminated microsparitic microfacies on the superior portion of the sample. B) TESCAN TIMA image showing the mineralogical variety of the sample, in which each color represents a mineral phase. C) Close-up of the mineral phases map in B showing an intercalation of Mg-calcite and High Mg-calcite phases in the stromatolite. D) Optical microscope image of the region of interest highlighted in C, showing that the variation in phases of calcite with more or less MgO content, is expressed in the color variation of the stromatolite laminae. E-F-G) Mineral patterns obtained by micro-XRD analysis and boxplot diagram show that the percentage of MgO in the different mineral phases varies from 3 to 6% of MgO for Mg-calcite, represented by the bright layers, and from 3 to ~10% of MgO for High Mg-calcite, represented by the dark layers.

SEM-EDX mapping analyses showed an elemental composition of the matrix in which the filamentous structures are preserved, typified by Ca and Mg; and a composition of the filamentous represented by Si and Al (Fig. 6). When observed in longitudinal cut the filamentous structure shows an Al rich composition throughout the extension (Fig. 7A-F). However, when in a cross-section view of the filament the concentration of Al is restrict to the walls of the filamentous structure (Fig. 7-L).

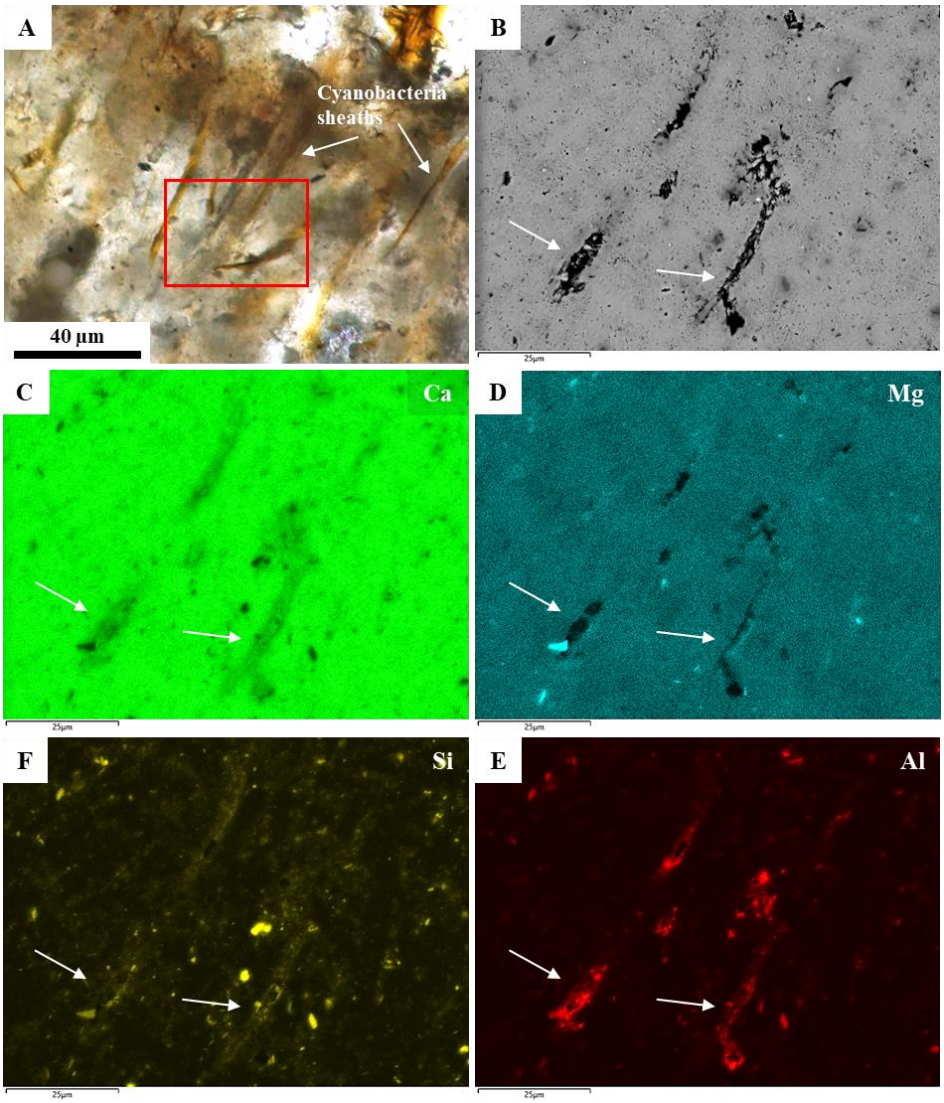

Fig. 6. Optical photomicrograph and EDX compositional maps. A) Optical photomicrograph showing filamentous structures filled with yellow-brown material (white arrows). B) SEM image of the area of interest corresponding to the following compositional maps of C) calcium, D) magnesium, E) silicon and E) aluminum.

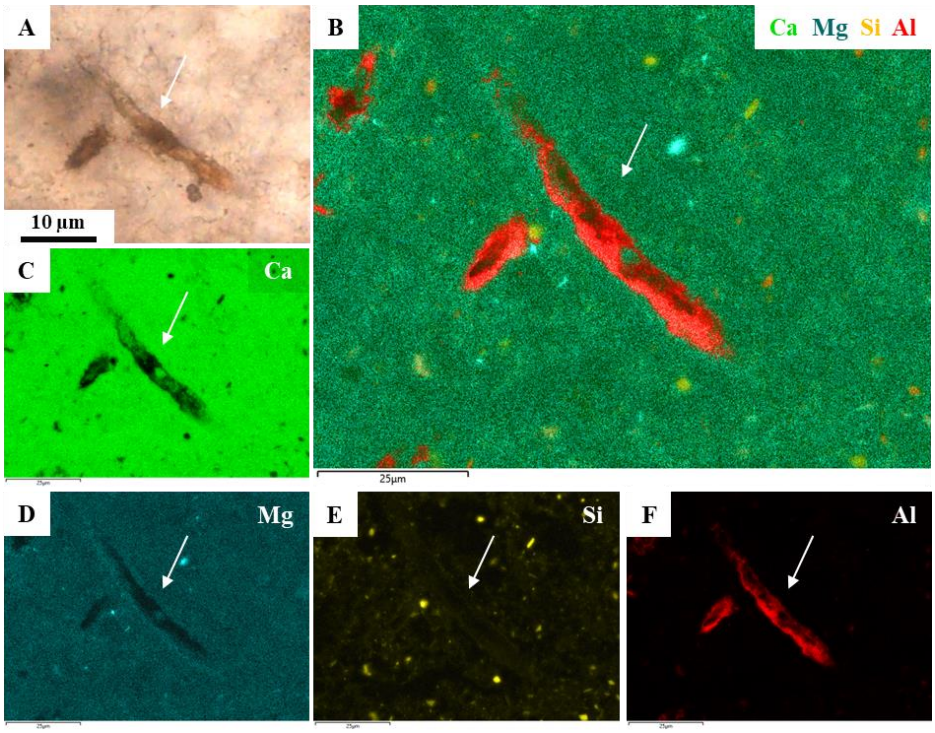

Fig. 7. Optical photomicrograph and EDX compositional maps of detailed areas. A) Optical photomicrograph showing a filamentous structure in sectional cut. B) Multicolor map of the filamentous structures showing an association of the elements. C-D-E-F) Single EDX elemental maps showing the respective distribution of calcium (Ca), magnesium (Mg), silicon (Si) and aluminum (Al). G) EDX image of the area of interest corresponding a transversal cut of the filamentous structure. H) Multicolor map showing the association of the following elemental maps I) Calcium, J) Magnesium, K) Silicon and L) Aluminum.

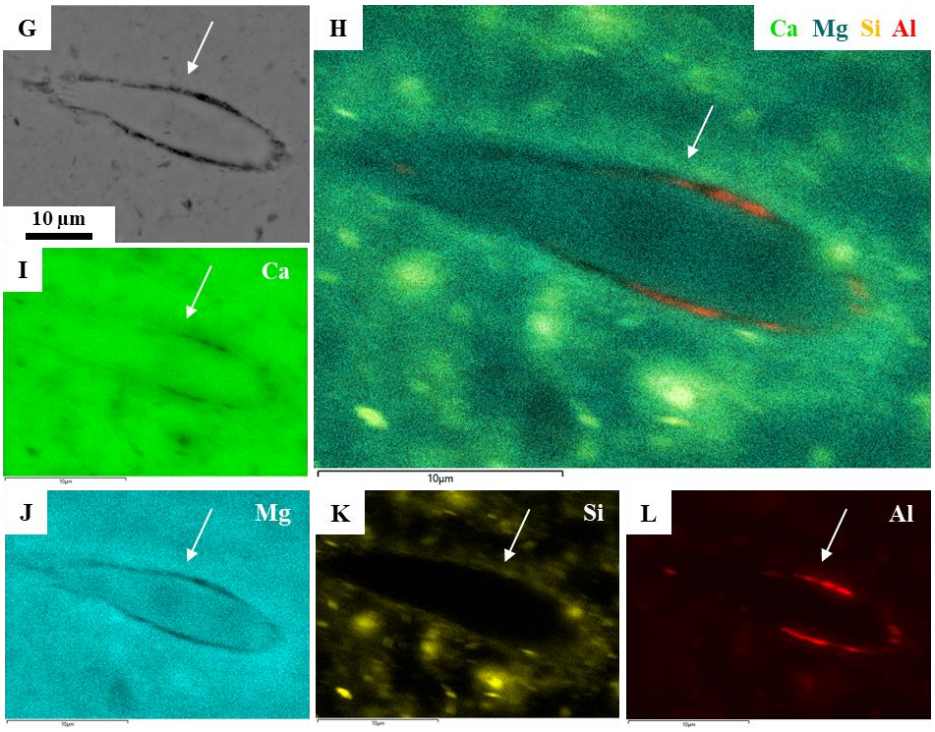

Fig. 7. (Continued)

Raman microspectroscopic mapping and spectral analysis display the filamentous structures containing carbonaceous materials (CM) concentrated in their walls (Fig. 8). CM was characterized by the D (1342 cm^{-1}; disordered carbon) and G (1590 cm^{-1}; graphite) bands in the Raman spectra; in addition to possible second order of carbonaceous matter (around 2800 – 3100 cm^{-1}). Mg-calcite (157, 284, 714 and 1088 cm^{-1}) composition for the matrix was also identified (Fig. 8D-E).

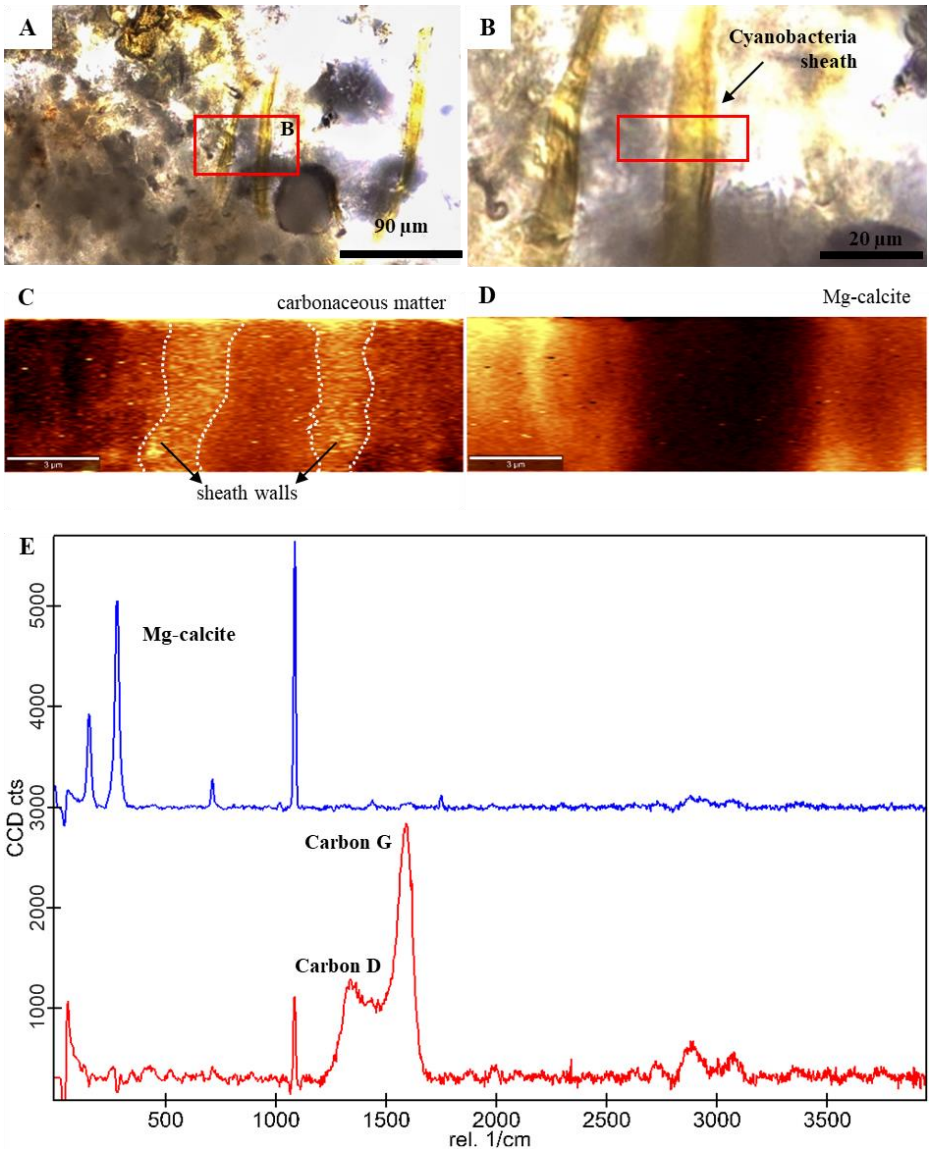

Fig. 8. Optical photomicrograph and Raman microspectroscopic maps. A-B) Optical photomicrographs showing single filamentous structures. The red square in B represents the area of interest from which the microspectroscopic maps were created. C) Raman compositional map corresponding to the Mg-calcite content. D) Raman compositional map of the carbonaceous matter. E) Raman spectra representing in blue the Mg-calcite phase; and carbonaceous matter represented in red by the carbon D and G bands.

4.4.3. Microbial composition and preservation

Under optical microscopic observations the stromatolites from Carri Laufquen lakes exhibit a moderate preservation of filamentous structures described as filamentous cyanobacteria and sheaths (Fig. 9). Mostly associated to the microsparitic laminae the filamentous cyanobacteria were observed as nearly straight or flexuous, non-septate and unbranched structures. They present uniform diameters through the entire longitudinal cut, which vary from approximately 3 to 5 µm for the filaments and reaching up to 8.5 µm diameter for the cyanobacterial sheaths.

The filamentous cyanobacterial structures may occur as isolated or in clusters; in the last case they are oriented vertically and perpendicular to the stromatolite laminar growth (Fig. 9A); or dispersed in the matrix showing not preferential orientation (Fig. 9B). Filamentous sheaths were observed right in contact with basalt substrate (Fig. 9C), vertically oriented, perpendicular to the contact.

Filamentous sheaths occur as empty thicker molds (Fig. 9D) or filled with a brown translucent phase (Fig. 9E), probably corresponding to the Al-bearing silicate, as observed previously in the EDX maps (Fig. 6-7). The sheath walls may display an exceptionally very-well preservation (Fig. 9F).

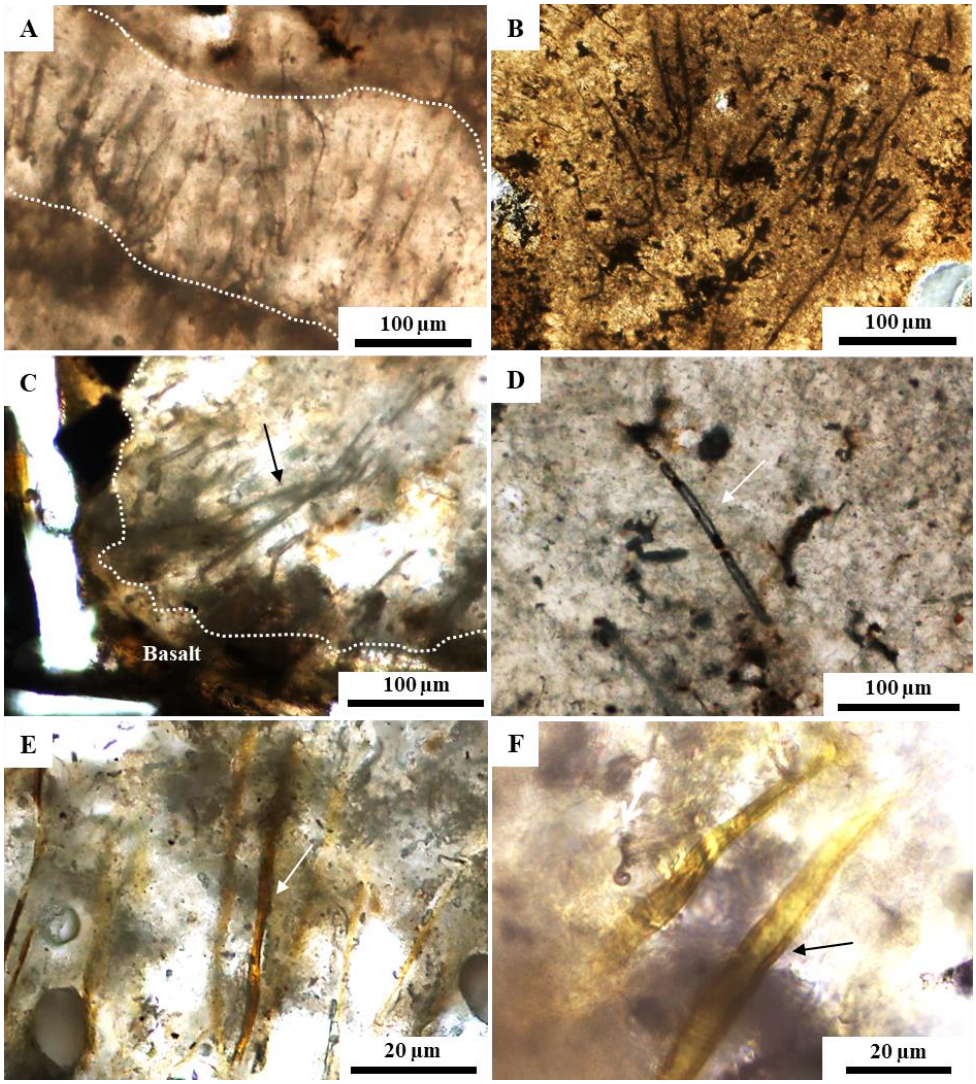

Fig. 9. Photomicrographs showing the several forms of filamentous cyanobacterial structures preserved within the Carri Laufquen stromatolites. A) Filamentous cyanobacteria oriented perpendicular to the layer and parallel to each other, associated to the microsparite (dashed white line) within the laminated microsparite microfacies. B) Filamentous cyanobacteria occurring as a cluster within the micritic columnar microfacies. C) Cluster of filamentous sheaths (arrowed) growing perpendicular to the basaltic substrate (dashed white line). D) Filamentous sheaths occurring as a single isolated and empty mold (arrowed). E) Filamentous structures may be filled with a yellow-brownish material (arrowed). F) Close-up a filamentous structure showing the sheath walls exceptionally well preserved (arrowed).

Under SEM observations the filamentous cyanobacteria structures and other microbial components were observed in the Carri Laufquen stromatolites. SEM imaging shows the preservation of extracellular polymeric substance – EPS, represented by amorphous mucus-like structures present in the matrix of stromatolites associated to the cyanobacteria filaments (Fig. 10A); as well as cyanobacterial sheaths clusters trapped in the matrix (Fig. 10B). In some rare cases filamentous molds were observed as empty tubes or filled with a poorly crystallized phase composed of Al-silicate (Fig. 10C).

Filamentous cyanobacteria may be preserved as a cluster of densely parallel vertically oriented filaments forming a palisade-like texture associated with microsparite laminae (Fig. 10D-E). Finally, frustules of diatoms trapped in the matrix, associated with EPS or not, were observed in localized regions. These diatom frustules may be fragmented (Fig. 10F) and partially dissolved.

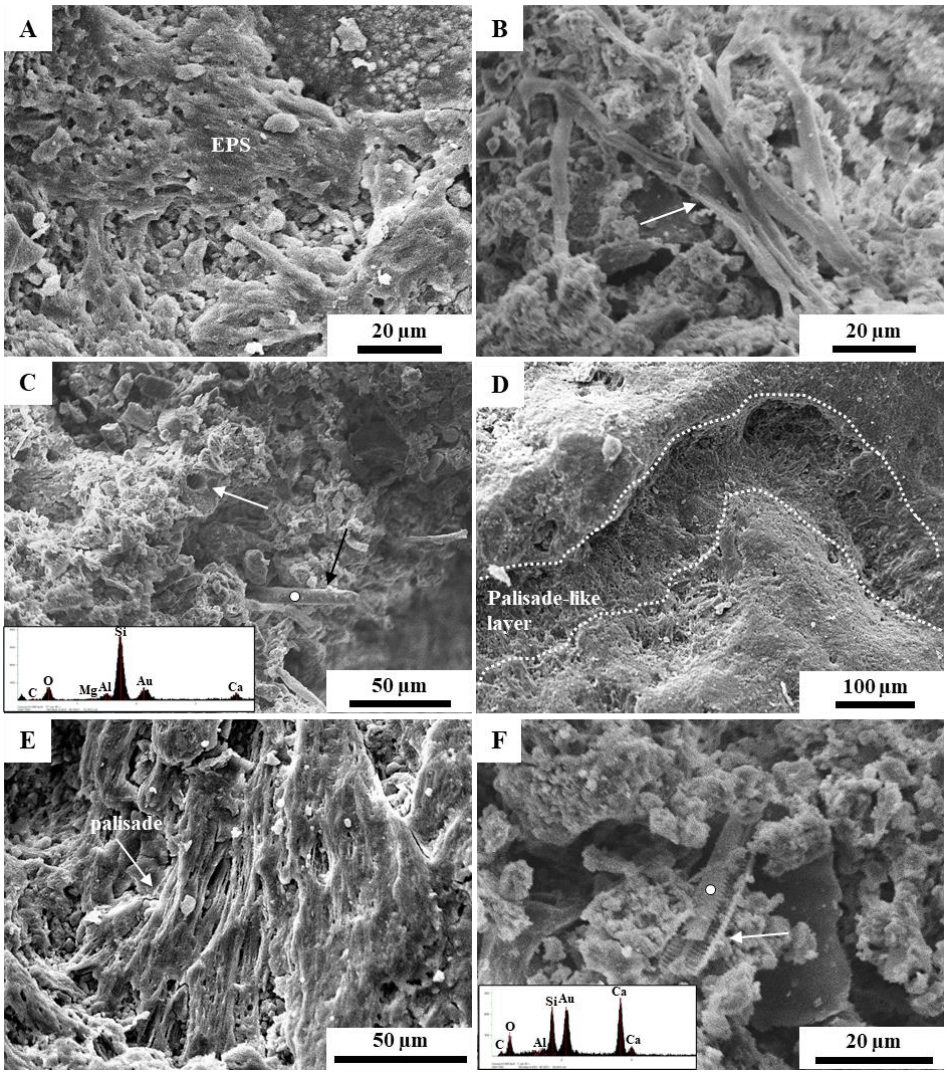

Fig. 10. SEM micrographs showing the micrometre-scale microbial components of the Carri Laufquen stromatolites. A) Amorphous mucus-like structures in the matrix, described as extracellular polymeric substances. B) Cluster of filamentous cyanobacterial sheaths (arrowed) showing diameters of approximately 3 to 5 µm. C) Empty mould of a possible filamentous structure highlighted by the white arrow and tubular structure protruding from one of the moulds (black arrow), whose composition rich in Si, O and Al is represented by the inset EDX spectrum. D) Palisade-like texture represented by a cluster of filamentous cyanobacteria structures vertically and perpendicular to the laminae between two micritic laminae. E) Close-up of the palisade-like texture evidencing the filamentous structures formed by the coalescence of filamentous structures vertically parallel to each other. F) Fragmented diatoms frustule trapped in the matrix.

The solid state ^{13}C NMR data exhibit the biomolecular components identified within the Carri Laufquen stromatolites. The spectra present strong signals ranging from 10 to 180 ppm, that corresponds to different organic bands. Representative spectra in Figure 11 demonstrate a composition dominated of broad bands of aliphatic carbon (CH) centered around 30 ppm (most intense signal); carbon-oxygenated (C–O) functionalities at ~75 ppm, unsaturated carbon (C=C) at 110 ppm, and carboxylic acid (CO_3^-) at ~175 ppm. Finally, ^{13}C NMR analysis display the composition of the carbonaceous material previously identified in Raman microspectroscopy (Fig. 8).

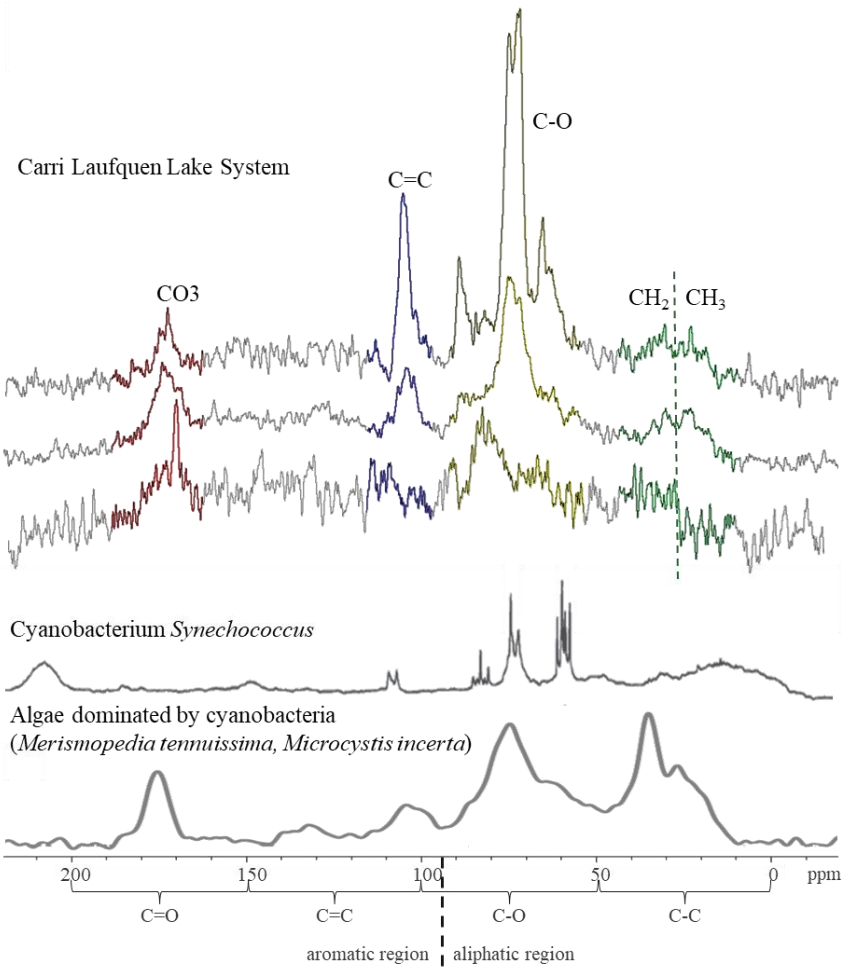

Fig. 11. Representative solid state 13C NMR spectra of Carri Laufquen stromatolites (blue spectra) showing the ranges of biomolecule bands recognized according to the 13C NMR intensity, such as aliphatic carbon (CH2, CH3), carbon-oxygen (C-O), unsaturated carbon (C=C) and carboxylic acid (CO3) moieties. For comparison proposal, the spectrum of cyanobacterium Synechococcus (adapted from Mackay and Norton, 1987) showing a correlation only in the C-O and C=C bands respect to this study; the following spectrum of an algae dominated by cyanobacteria (Merismopedia tennuissima, Microcystis incerta) collected from the Lake Smith, Virginia Beach, VA (adapted from Liu et al., 2009), correlates in all the main bands with Carri Laufquen spectra; and the extremely halophilic archaeon Natrinema ajinwuensis spectrum (adapted from Mahansaria et al., 2018), in which even though the bands may be correlated the peaks are not as broad as our data.

Complementary to the Raman and ^{13}C NMR data, the FTIR microspectroscopy maps suggest that filament-rich regions of the Carri Laufquen stromatolites correspond to more intense signals relative to the surrounding matrix (Fig. 12A-F), as well as the laminated structures (Fig. 12G-M); so, these regions of interest presented a concentration of carbonaceous matter. Intense signals in the hyperspectral FTIR mapping indicate a composition of aliphatic C–H stretching region (i.e. 3000–2800 cm^{-1}). The FTIR spectra obtained confirmed the detections of aliphatic carbon previously identified by ^{13}C NMR.

The absorption characteristics of filamentous structures show features consistent with the presence of CH_3 (the symmetrical stretch at ~2925 cm–1 and the asymmetrical stretch at ~2920 cm–1). While the laminae variation consists with the presence of CH_3 (the symmetrical stretch at ~2870 cm–1 and the asymmetrical stretch at ~2960 cm^{-1}), and CH_2 (the asymmetrical stretch at ~2925 cm–1).

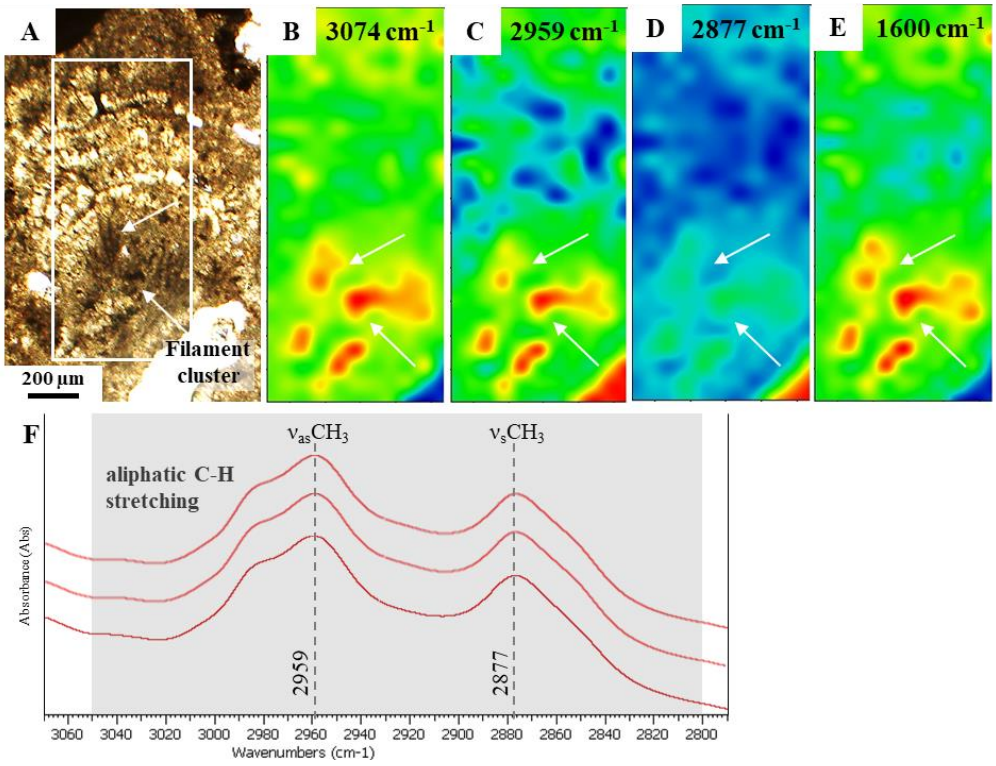

Fig. 12. FTIR microspectroscopy images for characterization of organic-rich samples. A) optical photomicrography presenting the region of interest dominated by filamentous structures and its representative FTIR spectra showing aliphatic C–H complexity in B-C-D-E), followed by the representative spectra in F). G) optical photomicrography showing the analysed region of interest composed of laminated structures represented by the white box and its following FTIR intensity mapping in H-I-J-K-L) of aliphatic C–H moieties (see text for details), and M) their correspondent spectra.

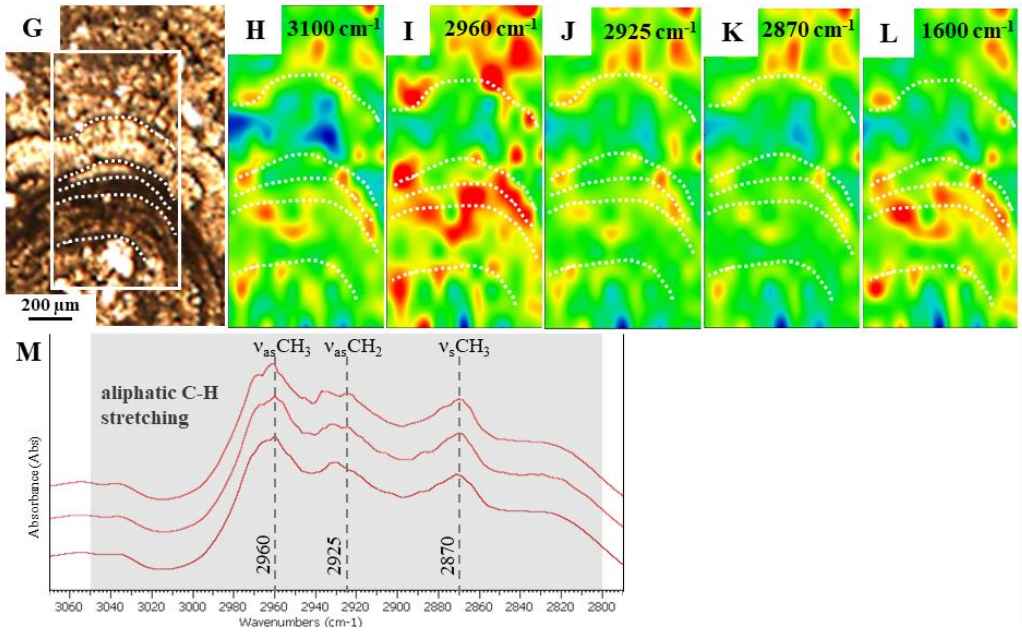

Fig. 12. (Continued)

4.5. Discussion

4.5.1. Growth and development of Carri Laufquen stromatolites

The stromatolites of Carri Laufquen Grande and Carri Laufquen Chica were collected in distinctive outcrops from both lakes, as well as on the shores of the Maquinchao river (Fig. 2); however, they were described as a single group of samples with their distinct morphologies (Fig. 3), since these morphologies were not restricted to a specific lake or outcrop. Therefore, in this section they will be discussed and treated generally as stromatolites from Carri Laufquen lakes system.

Occurrences of stromatolites grown surround basalt pebbles, such as those from Carri Laufquen lakes, have already been described for other lacustrine examples, i.e. in the East African Rift System (e.g. DeMott et al., 2021; Moussa et al., 2023; Dorneles et al., 2024). In the previous studies, the association with hydrothermal vents and weathering of basalt bedrock contributed to the formation of stromatolitic crusts, in specific geochemical conditions, forming mm- to cm-scale carbonate buildups. The stromatolites of Carri Laufquen lakes have larger sizes (Fig. 2-3), reaching meters in diameter, due to the more varied basaltic substrate from pebbles and cobbles to boulders (Eymard et al., 2019). Despite the fact that stromatolite morphologies are the result of a complex interplay of organism-sediment-environment

interactions (Pace et al., 2018), their macroscale structures are dominantly influenced by the environment with relatively little biological influence (Suosaari et al., 2019).

Eymard et al. (2019) also described the carbonate constructs of Carri Laufquen system and noticed that similar sized substrates produce different buildup morphologies, which in turn might be related to differences in water level. This assumption corroborates with our descriptions, in which the morphologies are independent of the size of the basaltic nucleus on which the stromatolitic crusts developed. Roche et al. (2019) demonstrated that despite the physicochemical and biological conditions were optimal for mineral precipitation, the potential of lithification depended on the presence of a suitable hard substrates. In stromatolite systems the microbial community needs a hard stable substrate to attack and develop, building morphologies such as columns (Ginsburg & Planavsky, 2008).

In case of Carri Laufquen system, lake-level fluctuations appear to influence the vertical extension of the carbonate buildups independently of the size of the basaltic material at each site (Eymard et a., 2019). The formation of carbonate buildups depends on the stability of the water level, given suitable extrinsic and intrinsic conditions (Dupraz et al., 2006; Eymard et al., 2019). Thus, stable, low-energy, and low-turbidity water conditions promote better development of stromatolites, while thinner stromatolitic crusts reflect water level instability, possibly indicating a brief high stand followed by regression.

In addition to the paleoshoreslines preserved in Carri Laufquen system (Fig. 1) indicating a lake-level variation, Ariztegui et al. (2001) documented several phases of lake-level changes associated with precipitation-evaporation patterns during the late Quaternary period in South America. These variations reflected in the morphology of the stromatolites. Dendrolite and globular morphologies (Fig. 3A-D) have been formed in a high lake-level conditions, while laminated, lumpy and massive crust (Fig. 3E-J) witnessed an evaporitic low-level phase.

The microfacies of stromatolites in the Carri Laufquen system (Fig. 4) are predominantly microcolumnar, displaying digitated laminated and micritic columnar types, as well as botryoidal non-columnar forms with a slightly laminated internal structure. Even within the micritic columnar microfacies, where distinct lamination is absent, variations between micritic and microsparitic portions are present. Lamination is thus the most prevalent microfabric in stromatolite deposits, with similar micritic and microsparitic laminations documented in numerous previous studies, from ancient Archean stromatolite fossils (e.g., Hickman-Lewis et al., 2019) to modern occurrences (e.g., Castro et al., 2014). This type of

lamination occurs consistently across both lacustrine (Frantz et al., 2014) and marine environments (Reid et al., 2024).

Laminated microfacies in Carri Laufquen stromatolites are irregular and not isopachous (Fig. 4B) suggesting microbially influenced growth, as observed by Awramik & Buchheim (2015) in giant stromatolites of the Eocene Green River Formation, USA. Laminated structures in stromatolites may be a byproduct of microbial metabolism (Reid et al., 2000; Dupraz et al., 2004), therefore, suggests their biological origin. Stromatolite lamination forms as cyanobacterial biofilms trap and bind sediment during high sedimentation rates, then lithify grains and create micritic laminae during low sedimentation, with laminae alternating to create the laminated structure (Frantz et al., 2015; Suosaari et al., 2016).

Pacton et al. (2015) indicated that the mineralogical composition of low-Mg-calcite in the Carri Laufquen lakes stromatolites remains consistent across different layers. However, our analysis using the TIMA technique revealed a distinction between Mg-calcite and high-Mg-calcite (Fig. 5), which correlates with the varying colours of the stromatolitic laminae, dark laminae predominantly composed of high-Mg-calcite and bright laminae of Mg-calcite. Typically, the darker laminations in stromatolites are associated with increased carbonaceous material within the micritic laminae (Dupraz et al., 2004; Brasier et al., 2015), a finding also supported by our FTIR analysis (Fig. 12G-M). Dupraz et al. (2004) studying microbialites from a hypersaline lake in Eleuthera Island, Bahamas, reported that EPS biofilm is calcified in micritic laminae, while microsparite may precipitate for physicochemical process from the alkaline water of the lake. FTIR results, coupled with TIMA data, suggest a fundamental relationship between magnesium concentration in Mg-carbonate minerals and the presence of microbial organic material. Zhang et al (2023) demonstrated experimentally that biomediated carbonates tend to enrich in $MgCO_3$ content by the EPS biofilm that provides nucleation sites, interacting with Mg^{2+}, adsorbing or incorporating mineral lattices, and inducing particle aggregation.

4.5.2. Biomediation on carbonate precipitation

Observations under optical microscope allowed the identification of cyanobacteria filaments and filamentous sheaths preserved as clusters or single isolated filaments (Fig. 6-7-8-9) in Carri Laufquen stromatolites. Under SEM analyses, other microbial components such as EPS biofilm and diatoms frustules were recognized (Fig. 10). Pacton et al. (2015) have previously described similar microfossils in freshwater stromatolites from Maquinchao river.

Later, Eymard et al. (2020) also identified such components in samples of stromatolitic crusts from the Maquinchao Basin, described as dense, tubular pores as remnants of former filamentous microorganisms in a micritic matrix. These authors attributed to microbial metabolism the role of carbonate organomineralization, through biologically induced mineralization. Cyanobacteria are widely regarded as the primary microorganisms driving the formation of modern stromatolites, significantly contributing to carbonate biomediation precipitation due to their abundant production of EPS (Riding, 2000; Dupraz et al., 2009; Schopf, 2012).

Clusters of cyanobacterial filaments densely packaged vertically oriented forming a palisade-like texture were identified in SEM images (Fig. 10D-E). The excellent preservation of cyanobacteria filaments and sheaths oriented vertically within the laminated layers of the microfacies (Fig. 9A, 10D-E) highlighting a substantial biogenic role in their development suggesting they were preserved in their original living positions (Castro-Contreras et al., 2014; Noffke & Awramik, 2013; Hickman-Lewis et al., 2019). Such an arrangement aligns with the growth patterns of photosynthetic microorganisms, as these microbial colonies would have oriented themselves toward sunlight to sustain their lamina-forming activity.

Photosynthesis is a vital metabolic process that contributes to the mineral precipitation in lacustrine environments. The process of permineralization in stromatolites arises from the encrustation of cyanobacterial filaments and the micritization that results from the breakdown of the EPS (Dupraz et al., 2009). By absorbing CO_2 molecules, photosynthesis processes raise the pH of the system and enhances the concentration of carbonate anions (CO_3^{2-}), leading to greater alkalinity (Dupraz et al., 2009; Petrash et al., 2012; Castro-Contreras et al., 2014). EPS macromolecules are rich in hydroxyl and carboxyl groups, which strongly bind with Ca^{2+} and Mg^{2+} cations, leading to the formation of $(Ca,Mg)CO_3$ crystals (Dupraz & Visscher, 2005).

4.5.3. Microbial preservation within Carri Laufquen stromatolites

In addition to the preservation of cyanobacterial filaments and EPS, the Carri Laufquen stromatolites also exhibit molds of filamentous sheaths. These molds are found in smaller quantities and can be either empty or filled with a poorly crystallized phase of Al-bearing silicate (Fig. 10C). Pacton et al. (2015) documented amorphous Mg-silicate phases closely associated with carbonate crystals and EPS, proposing microbial mediation in their precipitation. The minimal silicon amount detected in their study was likely attributed to diatom dissolution, with no aluminium identified. In contrast, our analysis not only revealed

fragmented diatom frustules (Fig. 10F) but also detected Al via EDX, with localized amorphous Al-silicate phases observed filling cyanobacterial filamentous molds (Fig. 6-7, 10C). Gomez et al (2018) reported the diatom impact in the preservation of microbialites textures and fabrics in the hypersaline lake Laguna Negra, Catamarca, Argentina. The authors demonstrated that the abundance of diatoms in the Laguna Negra microbial mats may play a fundamental role in EPS production.

Our Raman data (Fig. 8) revealed the concentration of organic matter within the sheath walls, precisely in the same region where the EDX maps (Fig. 7G–L) indicate a concentration of Si and Al., suggesting an association of the Al-rich silicates with carbonaceous matter. Poorly crystallized Al-Mg-bearing silicate deposits in alkaline environments have been linked to microbial activity in previous studies (Arp et al., 2003, in Satonda Crater Lake, Indonesia; Souza-Egipsy et al., 2005, in Mono Lake, USA). Fiore et al. (2011) suggested that Al-rich silicate phases form from the precipitation of an aluminosilicate gel promoted by EPS, with subsequent crystallization occurring due to changes in the microenvironment caused by metabolic activity. In addition, the concentration of Si-Al in the sheath walls (Fig. 7) demonstrated to favour an exceptional well preservation of these structure, as observed in optical microscope (Fig 8-9). The microbial remnants associated with silica, possibly from weathering volcanic bedrock or diatom dissolution (Muller et al., 2023), indicate syndepositional mineralization of cyanobacterial filaments at the Carri Laufquen site and highlight a carbonate-silica interplay.

Eymard et al. (2020) also described Al-silicates in Maquinchao Basin stromatolites and suggested that the Al-bearing silicate are usually associated with detrital phases. While the potentially authigenesis of clay mineral phases in microbial lacustrine systems remains poorly understood, our Raman data coupled with EDX maps represented another example that silicification may enhance the preservation of microbial structures and morphologies (e.g. Kremer et al., 2012, Burne et al., 2014; Moore et al., 2020).

Raman data revealed the presence of organic matter, indicated by the D and G bands in the spectrum (Fig. 8) and the ^{13}C NMR technique enables qualitative identification of this organic matter. The NMR spectra from the Carri Laufquen stromatolites exhibit broad bands representing unsaturated carbon, aliphatic carbon, and oxygenated carbon (Fig. 11), corresponding to organic matter in the form of kerogen (Mackay & Norton, 1987; Nguyen et al., 2003; Skrzypczak et al., 2005; Marshall et al., 2007; Delarue et al., 2016). Cyanobacterial group is a key precursor of kerogen due to its lipid membrane structure, consisting of bilayers of fatty acid lipid esters linked to glycerol-3-phosphate, which possess kerogen-forming

potential (Summons et al., 2022). NMR spectra from Carri Laufquen were compared with the spectrum of the cyanobacterium *Synechococcus*, as reported by Mackay and Norton (1987) (Fig. 11), and showed a strong correlation with the cyanobacteria-dominated algal spectrum from Liu et al. (2009). This correlation confirms that cyanobacteria are the predominant microorganisms involved in the construction of the Carri Laufquen stromatolites.

Cyanobacteria contain algaenan in their cell walls, which correspond to an aliphatic-rich biomacromolecule that is resistant to diagenetic degradation, thereby enhancing sediment preservation for kerogen formation (Biller et al., 2015; Vandenbroucke and Largeau, 2007). FTIR hyperspectral measurements demonstrated significant aliphatic C–H complexity, indicating a remarkable degree of organic preservation in the Carri Laufquen stromatolites (Fig. 12). The presence of symmetric and asymmetric absorption bands from CH_3 moieties, along with asymmetric bands from CH_2 groups, suggests that diagenetic influences on the original biochemistry were minimal. This supports a composition dominated by fatty acids, indicating that a bacteria-rich community primarily constructed these stromatolites (Igisu et al., 2012; Hickman-Lewis et al., 2020), further validating the NMR findings.

4.6. Conclusions

This chapter described the distinct morphologies Carri Laufquen stromatolites, such as dendrolite, globular, laminated, lumpy and massive crust, that may reach significant sizes due to a diverse basaltic clastic substrate. The variable morphology results from complex interactions among organisms, sediments, and the environment, with lake-level fluctuations influencing vertical carbonate buildup. While the microfacies displayed predominant internal laminated structures are an indicative of microbial growth.

Our main findings provide further evidence that silicification may enhance the preservation of microbial structures and biomolecular components in lacustrine environments, highlighting a potential association between Al-rich silicates and organic matter within cyanobacterial sheath walls.

Chapter V – Crystallization Pathways and Potential Mars-Analogue Lacustrine Environments in the East African Rift System and Patagonia

5.1. Introduction

In the previous chapters we documented the occurrence of stromatolitic structures according to their morphologies and microstructures at each site separately: Lake Ashenge, Ethiopia; Lake Abhe, Djibout; and Carri Laufquen lakes, Argentina. These study areas have similar geological settings, since they are highly alkaline, basalt-hosted lakes, and their occurrences correspond to generally layered stromatolitic structures growing on top of basaltic bedrock and surrounding basalt pebbles. They present distinctive morphological characteristics in macroscale, however, in microscale the dominant microfabrics in the three systems are laminated microcolumnar, although other laminated microfabrics were observed in a lesser extent. The mineral paragenesis from all the studied sites were dominated by Mg-calcite, whereas the organic matter was mostly associated with silicate mineral phases.

A multi-analytical approach was used to characterise the stromatolitic structures and their microbial components. Table 1 displays an overview of the main characteristics of each study area. Here we present a comparative study of the samples from Ethiopia, Djibouti and Argentina in a micro- and nanoscale, considering the same group of analytical techniques applied in the three sets of samples, i.e. optical microscopy, scanning electron microscopy (SEM-EDX), Raman microspectroscopy and ^{13}C nuclear magnetic resonance (NRM).

We aim to characterize similar microstructures in order to propose a model of the mineralization mechanisms involved in the formation of stromatolitic structures of the three studied sites. In addition, we seek to determine the processes of microbial preservation as biosignatures in alkaline lacustrine environments. These ecosystems may have formed in analogous environmental conditions to Jezero Crater on Mars, and may therefore inform us about potential Martian microbial ecosystems and their fossilisation processes.

Table 1. Comparison of the general characteristics of stromatolitic structures from the three studies sites from outcrop to microscale.

	Lake Ashenge	**Lake Abhe**	**Carri Laufquen Lakes**
Geological setting	basalt-hosted lake; pH 8.8; 2440 m alt;	basalt-hosted lake; hydrothermal systems associated; pH 9.9; 240 m alt;	basalt-hosted lakes; pH ~7.2–9.9; strong winds influence (100km/h); 825 m alt;
Hand-samples (macroscale)	domal stromatolites; columnar stromatolites;	domic and tabular microstromatolitic crust;	dendrolite crust; globular crust; laminated crust; lumpy crust; massive crust;
Microfabrics (microscale)	microcolumnar; bulbous;	microcolumnar; laminated crystalline; coated grains;	microcolumnar; microdigitated; botryoidal;
Mineral paragenesis	micrite and microsparite Mg-calcite;	micrite and microsparite Mg-calcite;	microsparite Mg-calcite (<4.7% MgO); micrite high Mg-calcite (<9.9% MgO);
Microbial components remain	EPS; filamentous cyanobacteria and sheaths; diatoms;	EPS; filamentous cyanobacteria and sheaths;	EPS; filamentous cyanobacteria and sheaths; diatoms;
Biomolecular components (FTIR/NMR)	Aliphatic (C-O, CH_2-CH_3); aromatic (C=C); = kerogen/algaenan	Aliphatic-rich moieties (C-O, CH_2-CH_3); = algaenan	aromatic (C=C); aliphatic moieties (C-O, CH_3); = kerogen
Filamentous structures preservation (optical)	shrub-like clusters; vertically parallel cluster (palisade-like texture);	vertically parallel cluster (palisade-like texture); single isolated filaments;	vertically parallel cluster (palisade-like texture); single isolated filaments;
Cyanobacterial sheaths preservation (SEM)	filled with stevensite; partially filled with EPS remains; empty molds;	filled with Mg-silicate; empty molds;	filled with Al-silicate; empty molds;
CM preservation (Raman)	Intrinsic to the filaments;	Concentrated within the laminae;	Concentrated in the sheath walls;

5.2. Mineralization pathways

Stromatolitic structures in the study areas present different morphologies in meso- and macroscale, however, at microscopic observations, they display similar microfabrics and microstructures which allow us to interpret similar processes of mineralization and preservation in the different lakes. Distinguishing the underlying mechanisms that lead to a particular microfabric is relevant, both in terms of environmental and diagenetic investigations. Thus, we proposed two mechanisms of mineralisation: 1) primary precipitation via nanocrystal aggregation; and 2) early diagenetic replacement.

The first mechanism was observed in the three sites associated to the formation of laminated microfabrics, in which micrite mineralized into microsparite within the EPS. Figure 1 correspond to the Lake Ashenge samples.

Primary precipitation via nanocrystal aggregation corresponds to the following stages:

A) nanospheroidal crystals of Mg-calcite initially precipitated in association with EPS biofilms, that serves as organic matrix for nucleation, to form the micrite laminae (Fig. 1A);

B) subsequently neoformed nanocrystals associated to EPS coalescing to form triangular crystals of Mg-calcite (Fig. 1B) and larger crystals of elongate polyhedrons (Fig. 1C);

C) then tetrahedral crystals of Mg-calcite formed by the aggregation of polyhedrons create pinnacles (Fig. 1D);

D) resulting in a microsparite laminae colonized by the cyanobacterial biofilm (Fig. 1E-F).

Manzo et al (2012) experimentally demonstrated that in such a process all stages occur if there is enough EPS as organic matrix. Pedley et al. (2009) described similar occurrences of triangular crystals formed by the coalescence of nanospheroids for fresh water microbial carbonates. The Mg-calcite nanospheres are the least complex initial product of nucleation within EPS and the larger microsparite crystals are the final stage in which almost all EPS is consumed (Dupraz et al., 2009; Perri et al., 2012; Willmer & Rasser, 2022). Depending on the parameters of pH, temperature, EPS production by microbial biofilm, the evolutionary process of growth is interrupted, in this case they are preserved as triangular nanocrystals or elongated polyhedrons, without forming larger pinnacles (Pedley et al., 2009; Manzo et al., 2012; Perri et al., 2012). This claim associated with the supplying of Ca^{2+} influences the formation of more or less thick micrite laminae in the microcolumns (Petryshyn et al., 2012). Similar processes were documented in Middle Miocene freshwater microbialites from the North Alpine Foreland

Basin of Mörsingen, Germany (Willmer & Rasser, 2022), in which continuing nucleation and precipitation of $CaCO_3$ caused a shape-retentive mineralization of the cyanobacterial sheaths.

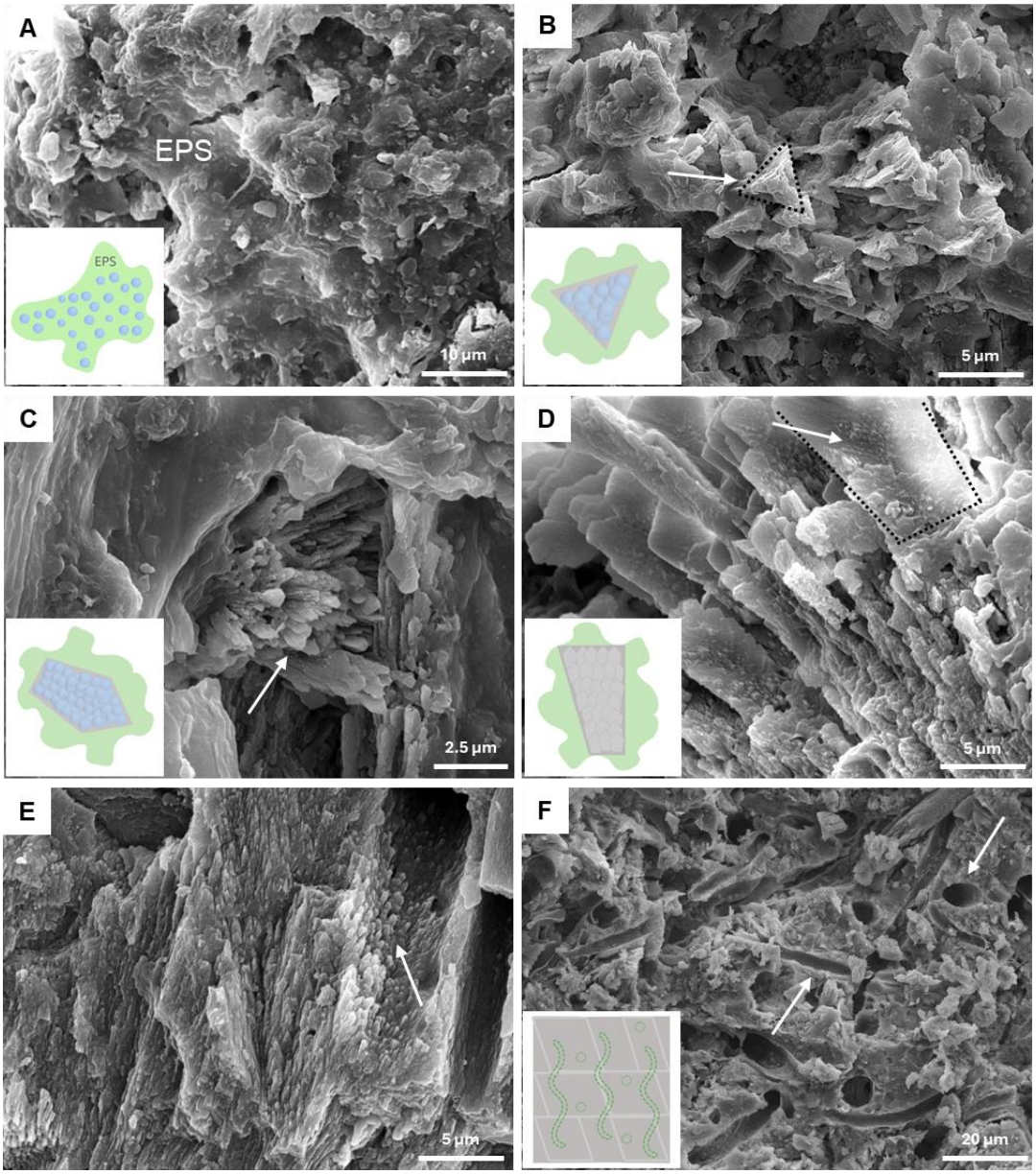

Fig. 1. Stages of primary precipitation via nanocrystal aggregation in Lake Ashenge stromatolites. A) nanospheroids crystals of Mg-calcite nucleating in the EPS matrix to form the micrite laminae. B) triangular (arrowed) and C) elongate polyhedrons (arrowed) of Mg-calcite formed by the coalescence of neoformed nanocrystals. D) pinnacles structures (arrowed) created by the aggregation of the polyhedrons. E) close-up of pinnacles structures showing the aggregation of the polyhedrons (arrowed). F) the resulted microsparite matrix formed by the larger tetrahedral crystals colonized by filamentous cyanobacterial, as observed in the preserved molds of filamentous structures (arrowed). The schematic images are not scaled.

The second mechanism was observed exclusively in Lake Abhe and Carri Laufquen samples (Fig. 2), and it is associated to the formation of the fabrics of laminated crystalline in Lake Abhe and botryoidal in Carri Laufquen lakes.

The early diagenetic replacement mechanism is represented by the following stages:

A) starts with the micritization of the former grains by endolithic microorganisms that lead to the destruction of the original fabric (Fig. 2A-C), disintegrating the crystals into rods enveloped by the EPS biofilm (Fig. 2D);

B) subsequently, due to the decomposition of the organic matrix by microbial processes, the neoformed rods are recrystallized into spheroidal nanocrystals of peloids (Fig. 2E);

C) for then to grow into subhedral crystals of Mg-calcite, such as fibrous fans or fibrous radial sparitic crystals (Fig. 2F);

D) and the resulted microstructures correspond to a micritized nucleus surrounded by microsparitic fibrous crystals (Fig. 2G).

Ge et al. (2021) demonstrated the same process for intertidal microbial bioherms from Abu Dhabi and the Great Salt Lake, USA. According to the authors, the evolutionary steps from nanocrystals and rods forming clotted peloidal micrite to fibrous and radial larger crystals via replacement and aggregation is related to increased alkalinity due to microbial activity associated with organic degradation in oxygen-limited environments. Similar features were also described for spring microbial carbonates from the Great Artesian Basin, Australia (Franchi and Frisia, 2020).

Despite the fact that abiotic $CaCO_3$ precipitation is also of importance in stromatolites consortia, since repeated abiotic dissolution and precipitation of Ca-carbonates can also lead to a micritized microfabric (Willmer & Rasser, 2022), EPS played a role in both mechanisms of mineralization presented here. Pedley (2014) experimentally demonstrated that the structure, function, and composition of natural and laboratory biofilms are remarkably similar, suggesting a unifying principle in the organization of these aquatic microbial ecosystems. In all cases, the primary function of biofilms is to capture and stabilize ions from the environment, which benefits the microbial community as a whole.

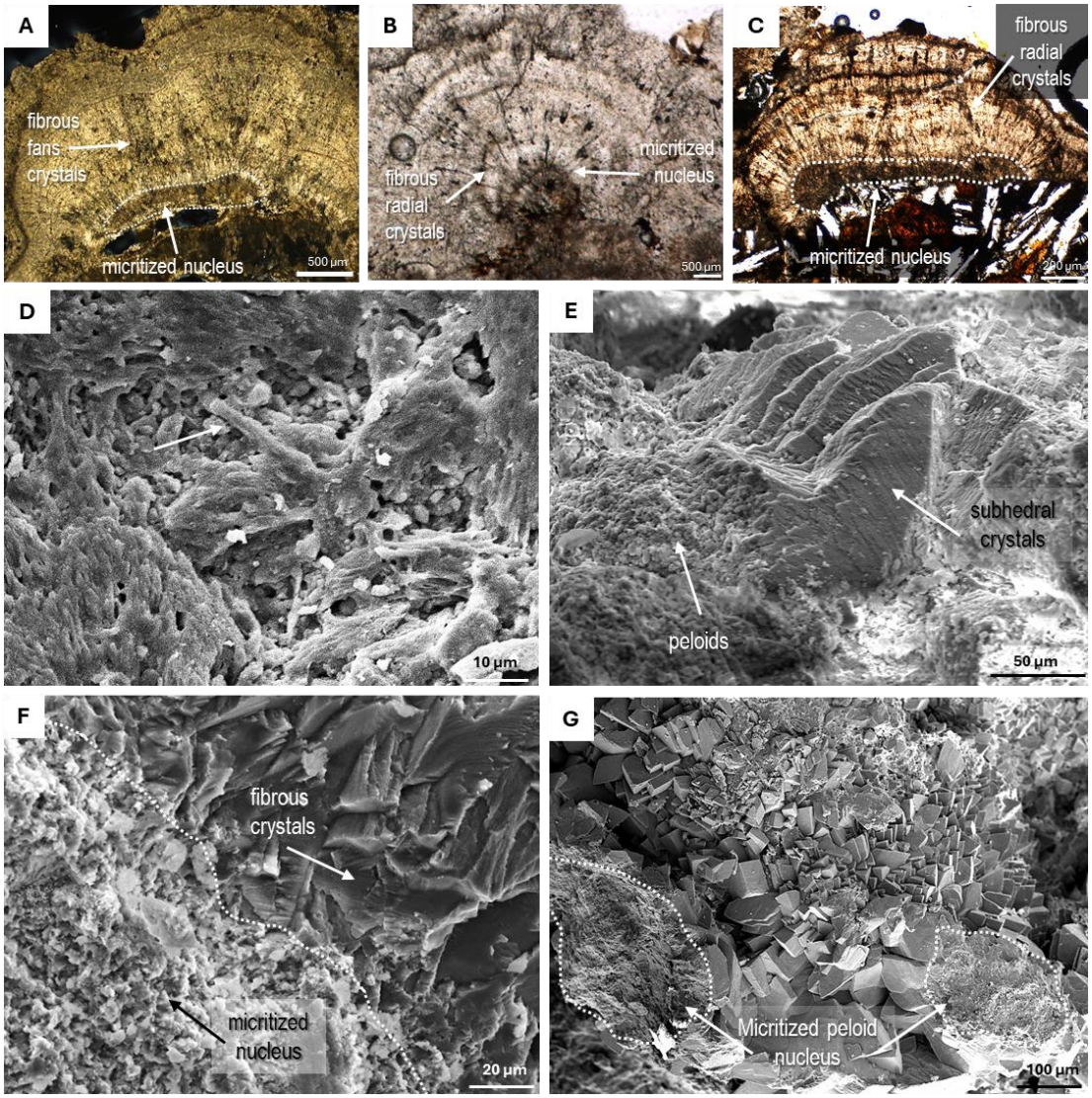

Fig. 2. Stages of the early diagenetic replacement mechanism. A) representative optical photomicrography of laminated crystalline microfacies sample in Lake Abhe. B) representative optical photomicrography of botryoidal microfacies sample in Carri Laufquen Grande. C) representative optical photomicrography of massive crust sample in Carri Laufquen Chica. D) example of disintegration of former crystals into rods (arrowed) within EPS biofilm. E) example of former rods and needles recrystallized into peloids. F) contact showing the growing of larger subhedral fibrous crystals from micritized nucleus. G) resulted microfabric composed of peloids nucleus surrounded by microsparite crystals of Mg-calcite.

5.3. Microbial preservation as biosignatures

Biomineralized biomass remnants (Fig. 3), which include extracellular polymeric substances – EPS and filamentous cyanobacteria and sheaths, were preserved in all study areas, in addition to diatoms described in Lake Ashenge and Carri Laufquen lakes samples; however, the modes of preservation of the microbial components were slightly different.

Biomolecular biosignatures in the studied stromatolitic structures are composed mainly of aliphatic and aromatic carbon moieties (Fig. 4). Broad signals of aromatic and aliphatic carbons from NMR spectra correspond to the preservation of organic matter as kerogen in Lake Ashenge and Carri Laufquen system. Lake Abhe spectra present strong bands of aliphatic carbon group, which may correspond to algaenan. In this way, in the three sites NMR data confirm cyanobacteria as the dominant microbial community responsible in the stromatolitic structures formation.

As cyanobacteria photosynthesize, they increase the pH of their immediate environment, promoting the precipitation of carbonate minerals (Petryshyn et al., 2012), such as Mg-calcite, within and around the sheath molds (Fig. 3D). In this case, the precipitation of carbonate might even obliterate the original filamentous molds (e.g. Kremer et al., 2012). The EPS within the sheath molds may undergo decomposition, releasing organic acids and causing a slight decrease in pH, which may influence the solubility of silicate minerals (Arp et al., 2003). Assuming that the lake water contains dissolved magnesium and silicate ions, the decrease in pH may create favourable conditions for the precipitation of Mg-silicate minerals (Pace et al., 2016). Clay minerals, such as authigenic stevensite, as identified in Lake Ashenge, may fill the empty sheath molds left behind after the decomposition of the EPS (Fig. 3E). Arp et al. (2003) already discussed the occurrence of similar Mg-silicate amorphous phases in microbialites of the Satonda crater Lake, Indonesia. Burne et al. (2014) reported authigenic stevensite as a syngenetic phase associated to carbonates in the alkaline Lake Clifton, Australia.

In some cases, remnants of organic matter, including EPS, may be preserved on the sheath walls (Fig. 3F). This preservation likely occurs when the rate of silicate precipitation is relatively slow, allowing for the organic material to be entombed before complete decomposition. The timing of Mg- silicate precipitation may vary depending on the rate of EPS decomposition and the availability of silicate ions in the lake water (Fiore et al., 2011). This assumption suggests that no significant replacement of organic tissues by silicate or carbonate occurred in the studied lakes; the silicate phases were observed only as molds filling, indicating a passive mineralisation of percolated siliceous fluids during deposition.

The source of this silica may be associated mainly with the weathering of basement rocks of the lakes and their composition. For example, peridotite xenoliths and basalts from the Ethiopian Plateau, and olivine-rich basalt of the Afar Formation, Djibouti, for the African examples; whereas andesites and basalts of the Maquinchao Basin and Carri Laufquen Plateau, for the Carri Laufquen occurrences. Another possible source of silica, even if not so efficient compared to the weathering of the basement, are the siliceous frustules of diatoms. Fragments

and partially dissolved diatoms were observed in the samples from Lake Ashenge and Carri Laufquen lakes. Arp et al. (2003) demonstrated that diatoms can be dissolved at high pH of 8.5-9.0, corresponding to the measured pH values in our studied lakes.

Wacey et al. (2017) reported that Mg-silicate-containing filaments likely represent an early permineralization stage primarily due to diagenetic processes. Initially, a nanocrystalline or amorphous Mg-silicate phase precipitates eventually filling any void spaces. This process creates a preservation bias, favouring the retention of primary morphology and organic components of cyanobacteria sheaths that promote significant authigenic Mg-silicate precipitation. This model provided a potential explanation for the occurrence of Mg-silicate minerals within stromatolites from lacustrine environments. It highlights the complex interplay between biological processes (cyanobacterial growth and EPS production), geochemical factors (carbonate precipitation and silicate solubility), and diagenetic processes (EPS decomposition and mineral precipitation). Further refining of this model and incorporating additional data from detailed petrographic and geochemical analyses of the stromatolitic structures may be necessary to gain a deeper understanding of the formation and preservation of Mg-bearing silicate stromatolites in lacustrine environments.

Regarding the preservation potential of the study areas, our studies demonstrated that microbial preservation is inversely correlated with syndepositional processes of early diagenesis in stromatolitic structures from alkaline environments (Fig. 4). A dominant preservation of the filamentous cyanobacteria and sheaths, as well as EPS remains in the matrix and within the sheaths molds (Fig. 3D) indicated that Lake Ashenge presents greater efficiency in preserving either morphological and biomolecular biosignatures comparing to Lake Abhe and Carri Laufquen. In addition, features of initial diagenesis, such as micritization, were not observed in Lake Ashenge. Carri Laufquen system preserved filamentous cyanobacterial sheaths more efficient than Lake Abhe, in which the carbonaceous material is preserved mainly as EPS dispersed in the matrix (Fig. 3A). The filamentous structures in Lake Abhe are restricted to empty and filled sheath molds, while in Carri Laufquen, both filaments and sheaths of cyanobacteria were identified (Fig. 3B). In Lake Abhe samples, early digenetic features, such as micritization, are more pervasive than Carri Laufquen stromatolitic crusts.

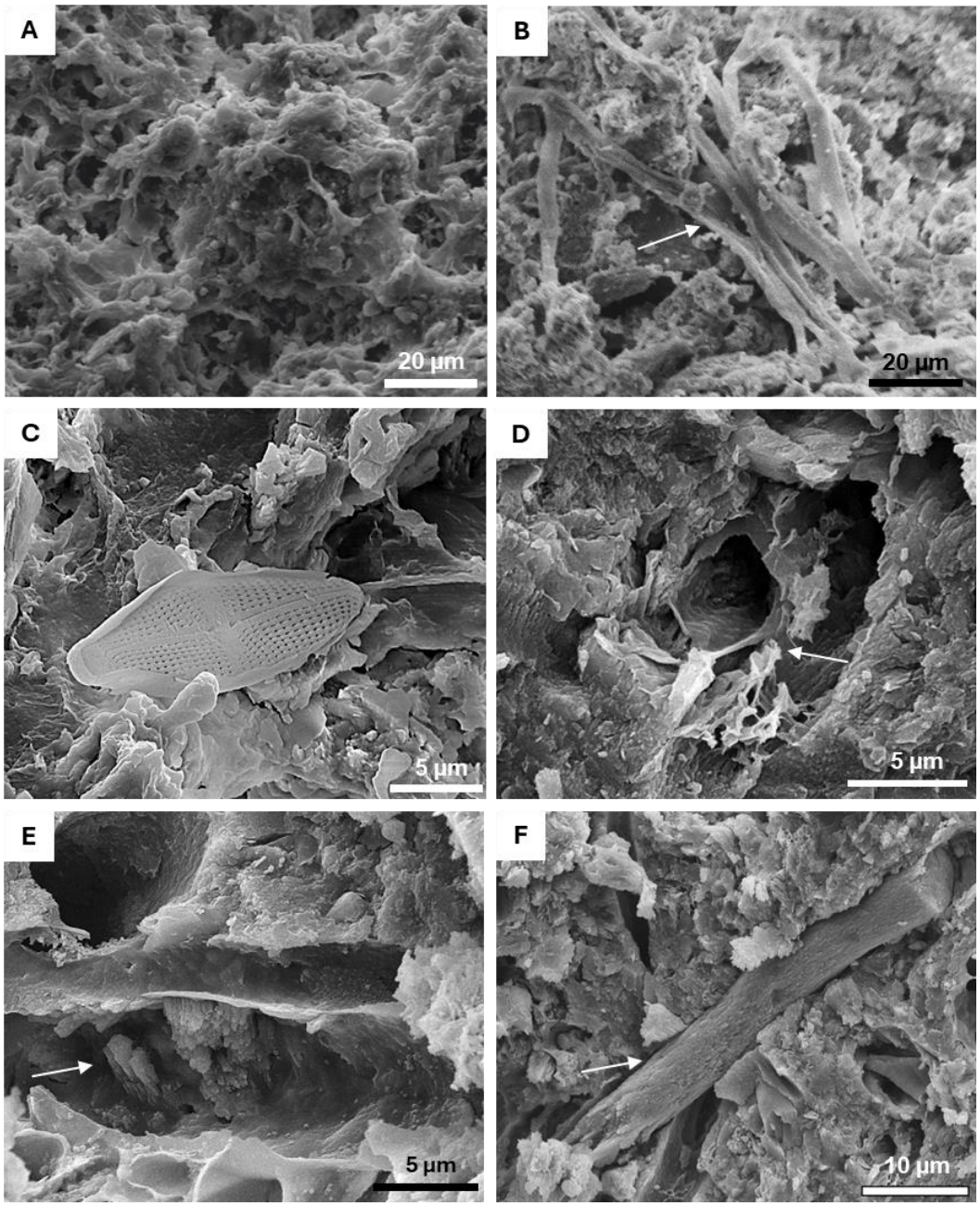

Fig. 3. Different modes of preservation of the microbial components in our study areas. A) representative extracellular polymeric substance preserved in samples from Lake Abhe. B) example of filamentous cyanobacteria sheaths from Carri Laufquen lakes. C) diatom valve preserved in Lake Ashenge stromatolites. D) cyanobacterial sheath mold preserved with EPS remains on the walls in Lake Ashenge. E) empty cyanobacterial sheath molds with nanocrystals of Mg-calcite growing on the sheath walls of Lake Ashenge samples. F) cyanobacterial molds completely filled with poorly crystallized Mg-bearing silicate in Lake Ashenge.

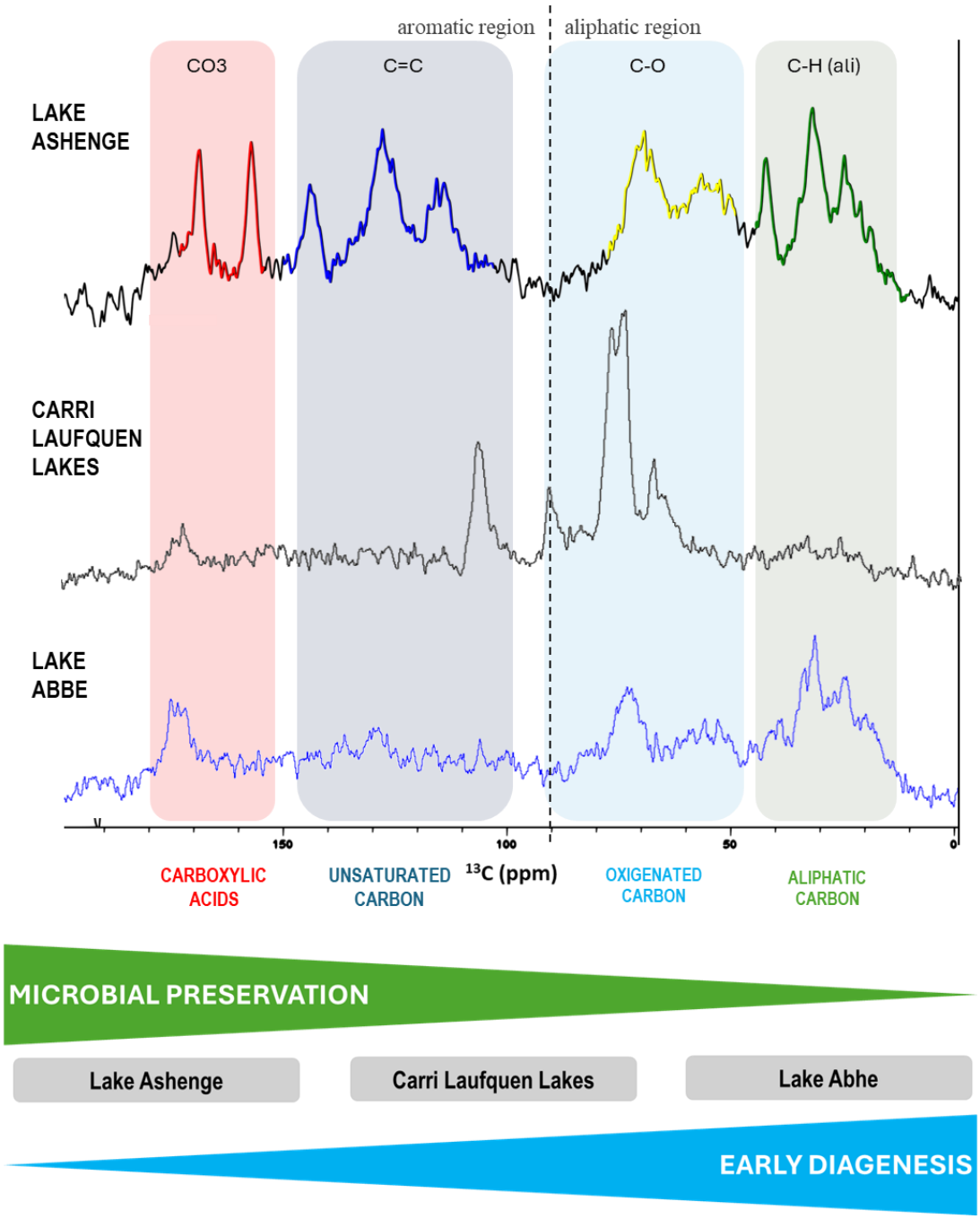

Fig. 4. Representative 13C NMR spectra and schematic diagram for a comparison of the studied lakes. 13C NMR spectra show the preservation of biomolecular compounds, in which the strong signals of carboxylic acid indicate carbonate mineral phases.

5.4. Potential planetary field analogues for Mars

Stromatolites, as detailed records, can provide valuable insights into microbial communities and their interactions with sediments over billions of years (Hickman-Lewis et al., 2019). They also serve as geochemical archives, offering information on the evolution of

microbial life and potential planetary studies (Hohl, 2021). These studies collectively highlight how stromatolites can hold key astrobiological insights that offer valuable context for interpreting early life evolution.

Early Earth and Mars exhibited comparable geodynamics, environments, and habitability until their evolutionary paths diverged around 4–3.5 Ga (Fairén et al., 2010; Ehlmann et al., 2016). The most relevant comparison between the two lies in their early history—spanning the Hadean to Palaeoarchaean on Earth and the Noachian to Early Hesperian on Mars—when both were habitable, at least at a microbial level (Tan et al., 2018).

Approximately 3.7 to 4.1 billion years ago during the Noachian period on Mars, habitable environments including alkaline lakes (Hays et al., 2017), similar to Lake Ashenge, Abhe and Carri Laufquen System were prevalent. Grotzinger et al (2014) and Boatwright & Head (2021) present evidence of ancient fluvio-lacustrine environments and proglacial paleolakes, suggesting their potential to support life. Martian paleolakes share characteristics with terrestrial lacustrine systems, suggesting the presence of habitable environments (Hurowitz et al., 2023). Consequently, lakes, particularly those with elevated carbonate alkalinity on the ancient Martian surface, could be regarded as conducive environments for the development of chemical conditions favorable to prebiotic synthesis (Grotzinger et al., 2015; Hurowitz et al., 2023).

The early prokaryotic biomass, encompassing anaerobic, photosynthetic, and chemosynthetic organisms, represents a form of life that could possibly have existed within the habitability constraints of early Mars (Westall et al., 2015). The habitats of these microorganisms, inferred from the geological record or identified in modern Mars-analogue environments, along with their preservation mechanisms, provide key insights into how microbial life on Mars might have been retained (Hays et al., 2017; Cavalazzi et al., 2019; Hickman-Lewis et al., 2022).

Habitability on the Noachian–Hesperian Mars may have been restricted to localised short- and long-lived environments, including diverse hydrothermal (Westall et al., 2015; Cavalazzi et al., 2019), lacustrine (Hurowitz et al., 2023) and endolithic (Onstott et al., 2019) settings. Modern analogues of such environments provide us with a basis for understanding the nature and distribution of life in such settings, and may be used to explore the depositional and diagenetic mechanisms by which traces of past life becomes preserved over geological timescales.

Extreme terrestrial environments may serve as planetary field analog, aiding in the study of biosignature preservation through geological, geomorphological, and mineral

characteristics (Martins et al., 2017). These analogs help identify potential spring deposits on Mars and develop remote sensing techniques for their detection (Cavalazzi et al., 2019). Additionally, studying Earth's extreme environments provides insights into microbial adaptation to Mars-like conditions, making hypersaline systems promising targets for exploring Martian habitability (e.g., Barbieri, 2013).

Recent investigations have detected the existence of marginal carbonates deposits along the proposed boundaries of Lake Jezero, today Jezero Crater (~3.5 Ga, Early Hesperian), a palaeolacustrine system on Mars (Fig. 5-6) (Tarnas et al., 2021; Horgan et al., 2020). These carbonates are particularly promising for preserving evidence of ancient life. Jezero's geological setting is a closed-basin displaying mafic and ultramafic spectral signatures and magnesium carbonate-bearing deposits along its lake margins. The diverse carbonate lithologies in Jezero indicate multiple periods of formation under varying conditions in a fluvio-lacustrine environment (Tarnas et al., 2021; Zastrow & Glotch, 2021). The research on Martian carbonates will be improved by a detailed comparison with the processes of preservation of biosignatures in terrestrial carbonates (Burnie et al., 2023).

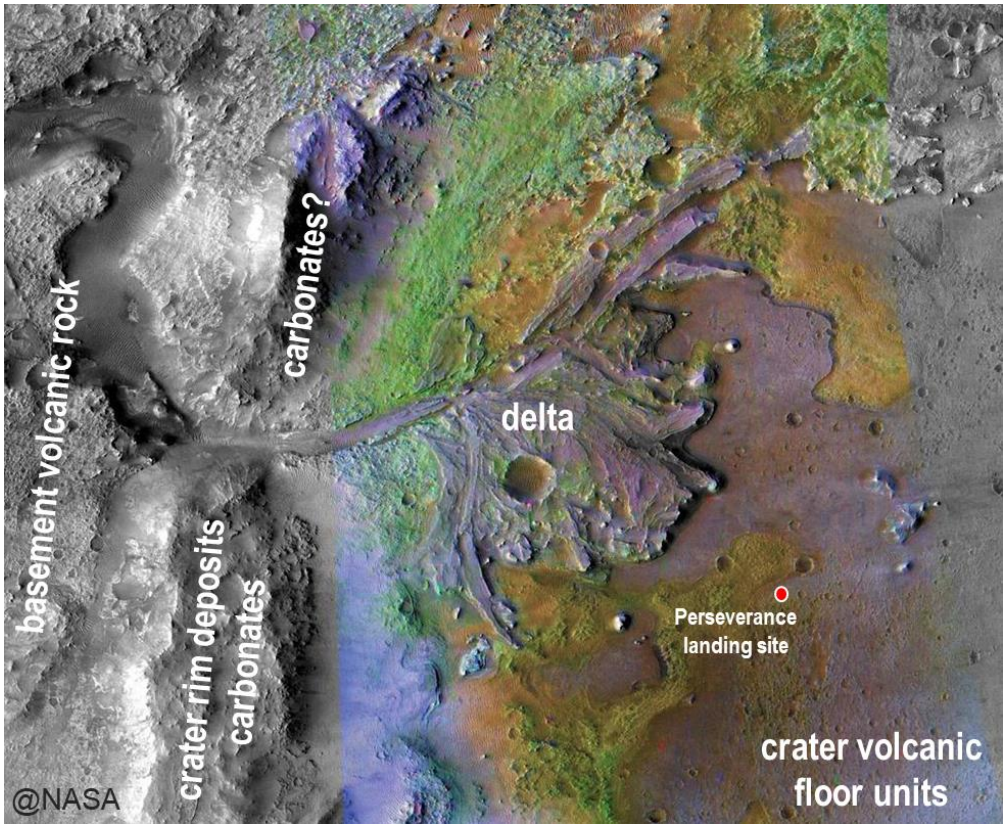

Fig. 5. Geological composition of Jezero crater, acquired from Perseverance rover, highlighting carbonate deposits along the shores of the crater, and the volcanic units as basement (Image source: NASA/JPL/JHUAPL/MSSS/Brown University).

Ancient Martian lakes show signs of authigenic minerals likely formed within lake water (Michalski et al., 2022). Outcrops of Martian lake deltas frequently contain olivine and pyroxene sediments from mafic volcanic crust, along with Fe-rich and Mg-bearing dioctahedral clays, which are the primary alteration phases in the Noachian crust, as well as minor amounts of Al-rich dioctahedral clays. While delta deposits generally mirror the mineral composition of their source regions, a substantial portion (~70%) may also include hydrated amorphous silica.

Our study described a mineral paragenesis closely resembling that found on Mars. In addition, the three sites in this work are situated on the basaltic terrains, which enhances the Mars analogy, as both Martin and terrestrial systems share a volcanic bedrock composition (Fig. 6). The preservation of stromatolite-building communities in Lake Ashenge, stromatolitic crusts in Lake Ahe and Carri Laufquen lakes despite fluctuations in lake levels and hydrological regimes, provides a positive indicator for the potential preservation of similar life traces on Mars. Therefore, our study areas served as a potential modern analogue for habitable environments on ancient Mars.

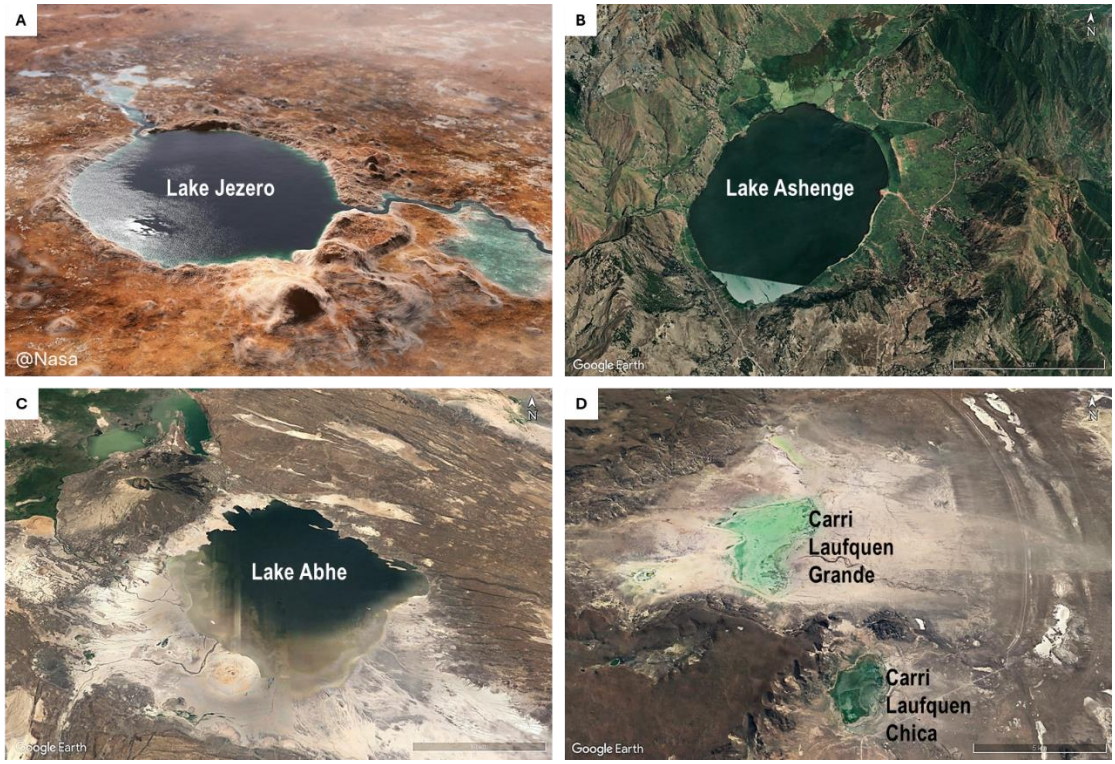

Fig. 6. Comparison of Lake Jezero on Mars (Image source: NASA/JPL-Caltech), and the three studied areas on Earth (Image source: Google Earth, 2024 imagery: CNES/Airbus-Landast; 2034 imagery: DigitalGlobe), regarding the geological setting, in which both Martian and terrestrial lacustrine lakes were situated on volcanic basaltic terrains.

Biosignatures similar to those presented in our African and Patagonian samples may be conserved within Martian carbonates, detectable either through rover exploration or subsequent analysis after Mars Sample Return mission (MSR). NASA Mars 2020 Perseverance rover is currently exploring Jezero crater, collecting geological samples — including carbonate-rich materials from crater margins — for the MSR. The techniques presented in this PhD thesis include those approximating rover capabilities, such as camera imaging, Raman microspectroscopy, infrared analysis, and mineralogical examination. Additionally, other techniques closely align with the datasets anticipated from MSR, including Raman and Infrared hyperspectral mapping, SEM-EDX mapping, and NMR.

Comprehensive, high-resolution observations are essential for comprehending the processes governing the growth and preservation of stromatolites. While some features may be observable in situ using rover instruments, a significant number will necessitate MSR for thorough examination (Farley et al., 2020). It is crucial to note that the exclusion of non-biological factors, such as hydrodynamic controls on stromatolite morphology, may also demand high-resolution observation (Farley et al., 2020).

The studied modern stromatolites from highly alkaline, basalt-hosted lacustrine environment demonstrated a good fossilization potential and suggested that the carbonaceous composition associated with Al-Mg-bearing silicate and carbonate phases, in addition to specific microstructures and micromorphologies, may be considered essentially relevant to training for the detection of biosignatures for modern and ancient records. The laboratory-based techniques developed in this work, although largely incompatible with the technological constraints of rover exploration, will likely form the basis of the analytical strategies applied to sedimentary rocks following MSR. In addition, to providing relevant material for comparison with samples from the MSR.

The challenge in Jezero Crater is to identify whether a structure was produced by life or formed abiotically (Chan et al., 2019). Our study showed that the formation of carbonates in lacustrine environments increases the chance of biotic origin, because these sites accumulate nutrients necessary for microbial survival. When selecting rock formations and outcrops for sample collection at the margins of Jezero crater, it is crucial to consider the significance of Mg-calcite, other calcium carbonates, and minor Mg-silicate phases in these systems (Farley et al., 2020). Regardless of whether the presence of microbial-induced carbonates is confirmed on Mars, studies of field analogues highlight the importance of understanding environmental conditions and processes that lead to the formation of authigenic carbonate minerals (Burnie et al., 2023).

5.5. Conclusions

This PhD thesis focused on the stromatolitic structures in three distinct basalt-hosted, alkaline lakes: Lake Ashenge in Ethiopia, Lake Abhe in Djibouti, and the Carri Laufquen lakes in Argentina. We have obtained an ensemble of evidence using microscopy and spectroscopy techniques arguing that exceptional biosignature preservation can be achieved in lacustrine carbonates from Mars-analogue environments.

Each location studied here shows unique, centimeter- to meter-scale stromatolite morphologies, yet they share similar microfabrics, suggesting common permineralization and preservation processes. We identified cyanobacterial filaments and sheaths and EPS remnants as preserved biosignatures within Mg-calcite and Mg-Al-silicate minerals in these lakes.

Two permineralization mechanisms were proposed: (1) primary precipitation, where Mg-calcite nanospheres form within EPS and grow into more complex crystals, and (2) early diagenetic replacement, involving initial structural degradation and recrystallization under low-oxygen, high-alkalinity conditions, resulting in fibrous and radial crystalline formations.

EPS biofilms play a key role in both mechanisms, stabilizing ions and fostering microbial communities, thereby supporting long-term biosignature preservation in lacustrine alkaline environments. Cyanobacteria-mediated pH shifts initially drive carbonate precipitation, while subsequent EPS decomposition and pH reduction favor silicate mineral formation, with clay minerals like stevensite filling microbial molds.

Early precipitation of Mg-rich clay minerals within the cyanobacterial filamentous molds and sheaths seems to be particularly beneficial for preserving their shape. Overall, the filamentous cyanobacteria and clay minerals within stromatolites have a symbiotic relationship. The cyanobacteria create the framework, and clay minerals contribute to the building materials and preservation process, leaving behind a testament to these ancient life forms. These conditions parallel the carbonate-rich, volcanic bedrock of Jezero Crater on Mars, suggesting that Martian paleolakes may similarly preserve microbial biosignatures.

Analytical techniques such as Raman microspectroscopy, FTIR mapping, and mineralogical assessments, employed in terrestrial analog studies, are well-suited for detecting potential biosignatures on Mars, aligning with the instrumentation of current and future Mars Samples Return missions.

Our studies demonstrated that Lake Ashenge, Lake Abhe and Carri Laufquen lakes as terrestrial planetary analogues of Martian palaeolake systems are valuable for an understanding of microbial ecosystems and their fossilisation models. The occurrence of microbial

biosignatures in these environments, coupled with the analytical requirements for their detection and characterisation, may be used as a framework for life detection in similar settings on Mars.

Acknowledgements

I would like to express my deepest gratitude to the University of Bologna for the opportunity to pursue a doctorate at such a prestigious and historic institution.

I extend my sincere thanks to my supervisors, Dr. Barbara Cavalazzi and Dr. Keyron Hickman-Lewis, for their patience, guidance, and for generously sharing their scientific expertise with me over the past three years.

I am also grateful to the Department of Biological, Geological and Environmental Sciences for providing the infrastructure that made this research possible; and to the laboratories and technical staff who assisted me numerous times in the preparation and execution of analyses.

I am deeply appreciative of the opportunity to work at The Natural History Museum in London, and I thank the museum laboratories, the technical team and my co-supervisor for their support during my time there.

My thanks also go to the Slovenian NMR Centre and its team for their hospitality and collaboration during the ^{13}C NMR analyses.

I gratefully acknowledge the Europlanet Society for the travel grants, including the Europlanet Expert Exchange Programme and Europlanet 2024 Research Infrastructure (TA1 – Planetary Field Analogues) 1st Fast Track Call RI TA. I also thank the CERIC-ERIC Consortium for providing experimental facilities and travel grants; as well as the Marco Polo Programme for the incentive and opportunity to develop international mobility.

I am also immensely grateful to my friends and family outside Italy, above all my mother Marli, who, despite being an ocean away, continuously believed and supported me on this journey. Special thanks go to my great friends Giovana, Wagner, Giovanni, Veleda, Maria, Camila, Mariane, Arthur, Nayane and Jam Studio folks whose encouragement and motivation were crucial in keeping me moving forward.

To other friends, colleagues and flatmates I met along the way in Italy, in the UK and across Europe, thank you for making this experience even more rewarding. I would also like to thank all the people who, in some way, directly or indirectly, contributed to the conclusion of this phase.

Finally, I extend my heartfelt thanks to the city of Bologna for welcoming me and providing countless unforgettable moments. It will forever be my second home!

References

Abbate E., Passerini P. & Zan L. (1995). Strike-slip faults in a rift area: a transect in the Afar Triangle, East Africa. *Tectonophysics*, 241: 67-97.

Agosta, E., Compagnucci, R. and Ariztegui, D., (2015). Precipitation linked to Atlantic moisture transport: clues to interpret Patagonian palaeoclimate. *Climate Research*, 62(3), pp.219-240.

Aguilera, E., Mazzoni, E. and Rabassa, J., (2018). Patagonian cenozoic magmatic activity. In *Volcanic Landscapes and Associated Wetlands of Lowland Patagonia*, pp.31-67.

Aitken, J. D. (1967). Classification and environmental significance of cryptalgal limestones and dolomites, with illustrations from the Cambrian and Ordovician of southwestern Alberta. *Journal of Sedimentary Research*, *37*(4), 1163-1178.

Allwood, A. C., Walter, M. R., Kamber, B. S., Marshall, C. P., & Burch, I. W. (2006). Stromatolite reef from the Early Archaean era of Australia. *Nature*, 441(7094), 714-718.

Alonso-Zarza, A. M., Cabaleri, N. G., Huerta, P., Armella, C., Rodríguez-Berriguete, Á., Monferran, M. D., ... & Nieto, D. S. (2020). Lacustrine microbialite pinnacles in the Palaeogene of Patagonia, Argentina: Facies and controls. *Sedimentary Geology*, *408*, 105742.

Alvarez, M. P., Carol, E., Eymard, I., Bilmes, A. and Ariztegui, D., (2022). Hydrochemistry, isotope studies and salt formation in saline lakes of arid regions: Extra-Andean Patagonia, Argentina. *Science of the Total Environment*, 816, p.151529.

Álvaro J.J., Sánchez-Román M., Nierop K.G. & Peterse F. (2021). Multiscale microbial preservation and biogeochemical signals in a modern hot-spring siliceous sinter rich in CO2 emissions, Krýsuvík geothermal field, Iceland. *Minerals*, 11: 263.

Ariztegui, D., Anselmetti, F. S., Kelts, K., Seltzer, G. O., & D'Agostino, K. (2001). Identifying paleoenvironmental change across South and North America using high-resolution seismic stratigraphy in lakes. In *Interhemispheric climate linkages* (pp. 227-240). Academic Press.

Ariztegui, D., Anselmetti, F.S., Gilli, A. and Waldmann, N., (2008). Late Pleistocene environmental change in Eastern Patagonia and Tierra del Fuego–A limnogeological approach. *Developments in Quaternary Sciences*, 11, pp.241-253.

Arp, G., Reimer, A., & Reitner, J. (2003). Microbialite formation in seawater of increased alkalinity, Satonda Crater Lake, Indonesia. *Journal of sedimentary research*, 73(1), 105-127.

Arrigo, K. (2022). Research in analog environments to enable studies of ocean world. *Oceanography*, *35*(1), 39-44.

Awaleh M.O., Hoch F.B., Boschetti T., Soubaneh Y.D., Egueh N.M., Elmi S.A., Mohamed J. & Khaireh M.A. (2015). The geothermal resources of the Republic of Djibouti—II: Geochemical study of the Lake Abhe geothermal field. *Journal of Geochemical Exploration*, 159: 129-147.

Awramik, S. M. (1992). The history and significance of stromatolites. In *Early organic evolution: implications for mineral and energy resources* (pp. 435-449). Berlin, Heidelberg: Springer Berlin Heidelberg.

Awramik, S. M., & Buchheim, H. P. (2015). Giant stromatolites of the Eocene Green River Formation (Colorado, USA). *Geology*, *43*(8), 691-694.

Awraniik, S.M. & Margulis, L. (1974). Strornatolitc *Newsletter* 2, 5.

Balci, N., Gunes, Y., Kaiser, J., On, S. A., Eris, K., Garczynski, B., & Horgan, B. H. (2020). Biotic and abiotic imprints on Mg-rich stromatolites: Lessons from lake Salda, SW Turkey. *Geomicrobiology Journal*, 37(5), 401-425.

Barbieri, R. (2013). The role of terrestrial analogs in the exploration of the habitability of martian evaporitic environments. In *Habitability of Other Planets and Satellites* (pp. 163-180). Dordrecht: Springer Netherlands.

Batchelor, M. T., Burne, R. V., Henry, B. I., & Jackson, M. J. (2004). A case for biotic morphogenesis of coniform stromatolites. Physica A: *Statistical Mechanics and its Applications*, 337(1-2), 319-326.

Berelson W.M., Corsetti F.A., Pepe-Ranney C., Hammond, D.E., Beaumont, W. & Spear, J.R. (2011). Hot spring siliceous stromatolites from Yellowstone National Park: assessing growth rate and laminae formation. *Geobiology*, 9: 411-424.

Biller, P., Ross, A. B., & Skill, S. C. (2015). Investigation of the presence of an aliphatic biopolymer in cyanobacteria: Implications for kerogen formation. *Organic Geochemistry*, 81, 64-69.

Bisse S.B., Ekoko B.E., Gerber J., Ekomane E., Franchi F. (2022). Influence of biotic vs abiotic processes on the genesis of non-marine carbonates along the Cameroon Volcanic Line (Cameroon) and palaeofluid provenance. *The Depositional Record*, 8: 102-26.

Bissett, A., Reimer, A., de Beer, D., Shiraishi, F., & Arp, G. (2008). Metabolic microenvironmental control by photosynthetic biofilms under changing macroenvironmental temperature and pH conditions. *Applied and Environmental Microbiology*, *74*(20), 6306-6312.

Bloszies, C., & Forman, S. L. (2015). Potential relation between equatorial sea surface temperatures and historic water level variability for Lake Turkana, Kenya. *Journal of Hydrology*, 520, 489-501.

Boatwright, B. D., & Head, J. W. (2021). A Noachian proglacial paleolake on Mars: fluvial activity and lake formation within a closed-source drainage basin crater and implications for early Mars climate. *The Planetary Science Journal*, 2(2), 52.

Boidi, F. J., Mlewski, E. C., Gomez, F. J., & Gérard, E. (2020). Characterization of microbialites and microbial mats of the Laguna Negra hypersaline lake (Puna of Catamarca, Argentina). In *Microbial ecosystems in Central Andes extreme environments: biofilms, microbial mats, microbialites and endoevaporites*, pp. 183-203.

Bontognali, T.R., Vasconcelos, C., Warthmann, R.J., Bernasconi, S.M., Dupraz, C., Strohmenger, C.J. & Mckenzie, J.A. (2010). Dolomite formation within microbial mats in the coastal sabkha of Abu Dhabi (United Arab Emirates). *Sedimentology*, 57(3), 824-844.

Bosak T., Knoll A.H. & Petroff A.P. (2013). The meaning of stromatolites. Annual *Review of Earth and Planetary Sciences*, 41: 21-44.

Boschetti T., Awaleh M. & Barbieri M. (2018). Waters from the Djiboutian Afar: A Review of Strontium Isotopic Composition and a Comparison with Ethiopian Waters and Red Sea Brines. *Water*, 10: 1700.

Bougeault C., Vennin E., Durlet C., Muller E., Mercuzot M., Chavez M., Gérard E., Ader M., Virgone A. & Gaucher E.C. (2019). Biotic–abiotic influences on modern Ca–Si-rich hydrothermal spring mounds of the Pastos Grandes volcanic caldera (Bolivia). *Minerals*, 9: 380.

Bradbury, J.P., Grosjean, M., Stine, S. and Sylvestre, F., (2001). Full and late glacial lake records along the PEP 1 transect: their role in developing interhemispheric paleoclimate interactions. In *Interhemispheric climate linkages* (pp. 265-291). Academic Press.

Brasier, A. T., Rogerson, M. R., Mercedes-Martin, R., Vonhof, H. B., & Reijmer, J. J. G. (2015). A test of the biogenicity criteria established for microfossils and stromatolites on Quaternary tufa and speleothem materials formed in the "Twilight Zone" at Caerwys, UK. *Astrobiology*, *15*(10), 883-900.

Brasier, A., Wacey, D., Rogerson, M., Guagliardo, P., Saunders, M., Kellner, S., Mercedes-Martin, R., Prior, T., Taylor, C., Matthews, A. & Reijmer, J. (2018). A microbial role in the construction of Mono Lake carbonate chimneys?. *Geobiology*, 16(5), 540-555.

Briones-Nagata, M. P., Martinez-Goss, M. R., & Hori, K. (2007). A comparison of the morpho-cytology and chemical composition of the two forms of the cyanobacterium, Nostoc commune Vauch., from the Philippines and Japan. *Journal of applied phycology*, 19, 675-683.

Buongiorno, J., Gomez, F. J., Fike, D. A., & Kah, L. C. (2019). Mineralized microbialites as archives of environmental evolution, Laguna Negra, Catamarca Province, Argentina. *Geobiology*, 17(2), 199-222.

Burne R.V. & Moore L.S. (1987). Microbialites: organosedimentary deposits of benthic microbial communities. *Palaios*, 1: 241-254.

Burne R.V., Moore L.S., Christy A.G., Troitzsch U., King P.L., Carnerup A.M. & Hamilton P.J. (2014). Stevensite in the modern thrombolites of Lake Clifton, Western Australia: a missing link in microbialite mineralization?. *Geology*, 42: 575-578.

Burnie, T. M., Power, I. M., Paulo, C., Alçiçek, H., Falcón, L. I., Lin, Y., & Wilson, S. (2023). Environmental and Mineralogical Controls on Biosignature Preservation in Magnesium Carbonate Systems Analogous to Jezero Crater, Mars. *Astrobiology*, 23(5), 513-535.

Burns, B. P., Goh, F., Allen, M., & Neilan, B. A. (2004). Microbial diversity of extant stromatolites in the hypersaline marine environment of Shark Bay, Australia. *Environmental microbiology*, *6*(10), 1096-1101.

Çağatay M.N., Damci E., Bayon G. & Sari M. (2024). Microbialites on the northern shelf of Lake Van, eastern Türkiye: Morphology, texture, stable isotope geochemistry and age. *Sedimentology*, 71: 850-870.

Calça C.P., Fairchild T.R., Cavalazzi B., Hachiro, J., Petri S., Huila M.F.G., Toma H.E. & Araki K. (2016). Dolomitized cells within chert of the Permian Assistência Formation, Paraná Basin, Brazil. *Sedimentary Geology*, 335: 120-135.

Caminiti A.M. (2000). *Le fossé d'Asal et le Lac Abhé: deux sites géologiques exceptionnels en République de Djibouti*. 132 pp. Edition Couleur Locale, Djibouti.

Campbell K.A., Lynne B.Y., Handley K.M., Jordan S., Farmer J.D., Guido D.M., Foucher F., Turner S. & Perry R.S. (2015). Tracing biosignature preservation of geothermally silicified microbial textures into the geological record. *Astrobiology*, 15: 858-882.

Cartwright, A., Quade, J., Stine, S., Adams, K.D., Broecker, W. and Cheng, H., (2011). Chronostratigraphy and lake-level changes of Laguna Cari-Laufquén, Río Negro, Argentina. *Quaternary Research*, 76(3), pp.430-440.

Casanova J. (1994). Stromatolites from the East African Rift: A synopsis. In Bertrand-Sarfati J. & Monty C. (eds) *Phanerozoic Stromatolites II*. Springer, Dordrecht: 193-226.

Casanova, J., & Hillaire-Marcel, C. (1992). Chronology and paleohydrology of Late Quaternary high lake levels in the Manyara Basin (Tanzania) from isotopic data (18O, 13C, 14C, Th/U) on fossil stromatolites. *Quaternary Research*, 38(2), 205-226.

Castro-Contreras S.I., Gingras M.K., Pecoits E., Aubet N.R., Petrash D., Castro-Contreras S.M., Dick G., Planavsky N. & Konhauser K.O. (2014). Textural and geochemical features of freshwater microbialites from Laguna Bacalar, Quintana Roo, Mexico. *Palaios*, 29: 192-209.

Cavalazzi B, Barbieri R., Cady S.L., George A.D., Gennaro S., Westall F., Lui A., Canteri R., Rossi A.P., Ori G.G. & Taj-Eddine K. (2012). Iron-framboids in the hydrocarbon-related Middle Devonian Hollard Mound of the Anti-Atlasmountain range in Morocco: Evidence of potential microbial biosignatures. *Sedimentary Geology*, 263-264: 183-193.

Cavalazzi, B., Barbieri, R., Gómez, F., Capaccioni, B., Olsson-Francis, K., Pondrelli, M., Rossi, A.P., Hickman-Lewis, K., Agangi, A., Gasparotto, G., Glamoclija, M., Ori, G. G.,

Rodriguez, N. & Hagos, M. (2019). The Dallol geothermal area, Northern Afar (Ethiopia)—An exceptional planetary field analog on Earth. *Astrobiology*, 19(4), 553-578.

Cavalazzi, B., Westall, F., Cady, S. L., Barbieri, R., & Foucher, F. (2011). Potential fossil endoliths in vesicular pillow basalt, Coral Patch Seamount, eastern North Atlantic Ocean. *Astrobiology*, 11(7), 619-632.

Cellamare M., Duval C., Drelin Y., Djediat C., Touibi N., Agogué H., Leboulanger C., Ader M. & Bernard C. (2018). Characterization of phototrophic microorganisms and description of new cyanobacteria isolated from the saline-alkaline crater-lake Dziani Dzaha (Mayotte, Indian Ocean). *FEMS Microbiology Ecology*, 94: 108.

Cerling, T. E. (1994). Chemistry of closed basin lake waters: a comparison between African Rift Valley and some central North American rivers and lakes. *The Global Geological Record of Lake Basins*, 1, 29-30.

Chafetz, H. S., & Guidry, S. A. (1999). Bacterial shrubs, crystal shrubs, and ray-crystal shrubs: bacterial vs. abiotic precipitation. *Sedimentary Geology*, 126(1-4), 57-74.

Chan, M. A., Hinman, N. W., Potter-McIntyre, S. L., Schubert, K. E., Gillams, R. J., Awramik, S. M., ... & Cleaves, H. J. (2019). Deciphering biosignatures in planetary contexts. *Astrobiology*, *19*(9), 1075-1102.

Cockell, C. S., Balme, M., Bridges, J. C., Davila, A., & Schwenzer, S. P. (2012). Uninhabited habitats on Mars. *Icarus*, *217*(1), 184-193.

Cockell, C. S., Bush, T., Bryce, C., Direito, S., Fox-Powell, M., Harrison, J. P., Lammer, H., Landenmark, H., Martin-Torres, J., Nicholson, N., Noack, L., O'Malley-James, J., Payler, S.J., Rushby, A., Samuels, T., Schwendner, P., Wadsworth, J. & Zorzano, M. P. (2016). Habitability: a review. *Astrobiology*, *16*(1), 89-117.

Cohen, A. S., Talbot, M. R., Awramik, S. M., Dettman, D. L., & Abell, P. (1997). Lake level and paleoenvironmental history of Lake Tanganyika, Africa, as inferred from late Holocene and modern stromatolites. *Geological Society of America Bulletin*, 109(4), 444-460.

Coman C., Chiriac C.M., Robeson M.S., Ionescu C., Dragos N., Barbu-Tudoran L., Andrei A.Ş., Banciu H.L., Sicora C. & Podar M. (2015). Structure, mineralogy, and microbial

diversity of geothermal spring microbialites associated with a deep oil drilling in Romania. *Frontiers in Microbiology*, 6: 253.

Corti, G. (2009). Continental rift evolution: from rift initiation to incipient break-up in the Main Ethiopian Rift, East Africa. *Earth-science reviews*, 96(1-2), 1-53.

Cusminsky, G.C. and Whatley, R.C., (1996). Quaternary non-marine ostracods from lake beds in northern Patagonia. *Spanish journal of palaeontology*, 11(2), pp.143-154.

Dekov V.M., Egueh N.M., Kamenov G.D., Bayon G., Lalonde S.V., Schmidt M., Liebetrau V., Munnik F., Fouquet Y., Tanimizu M. & Awaleh M.O. (2014). Hydrothermal carbonate chimneys from a continental rift (Afar Rift): Mineralogy, geochemistry, and mode of formation. *Chemical Geology*, 387: 87-100.

Dekov V.M., Gueguen B., Yamanaka T., Moussa N., Okumura T., Bayon G., Liebetrau V., Yoshimura T., Kamenov G., Araoka D. & Makita, H. (2021). When a mid-ocean ridge encroaches a continent: Seafloor-type hydrothermal activity in Lake Asal (Afar Rift). *Chemical Geology*, 568: 120126.

Delarue, F., Rouzaud, J. N., Derenne, S., Bourbin, M., Westall, F., Kremer, B., Sugitani, K., Deldicque, D. & Robert, F. (2016). The Raman-derived carbonization continuum: a tool to select the best preserved molecular structures in Archean kerogens. *Astrobiology*, 16(6), 407-417.

Demange J., Di Paola G.M., Lavigne J.J., Lopoukhine M. & Stieltjes L. (1971). Etude géothermique du Territoire Français des Afars et des Issas. *Rapport de Recherches Géologiques et Minières*, 71: 262.

DeMott L.M., Scholz C.A. & Awaleh M.O., (2021). Lacustrine carbonate towers of Lake Abhe, Djibouti: Interplay of hydrologic and microbial processes. *Sedimentary Geology*, 424: 105983.

Deocampo, D. M., & Renaut, R. W. (2016). Geochemistry of African soda lakes. In *Soda Lakes of East Africa*, 77-93.

Des Marais, D. J., Nuth III, J. A., Allamandola, L. J., Boss, A. P., Farmer, J. D., Hoehler, T. M., Jakosky, B.M., Meadows, V.S., Pohorille, A., Runnegar, B. & Spormann, A. M. (2008). The NASA astrobiology roadmap. *Astrobiology*, *8*(4), 715-730.

Dorneles, V. A. C., Hickman-Lewis, K., Barbieri, R., Caminiti, A. M., & Cavalazzi, B. (2024). Microbe-mineral interactions in the microstromatolitic crusts of the lacustrine chimneys and volcanic bedrock of Lake Abhe, Republic of Djibouti. *Bollettino della Società Paleontologica Italiana*, 63(3), 229-244.

Dupraz C. & Visscher P.T. (2005). Microbial lithification in marine stromatolites and hypersaline mats. *Trends in microbiology*, 13: 429-438.

Dupraz C., Reid R.P., Braissant O., Decho A.W., Norman R.S. & Visscher P.T. (2009). Processes of carbonate precipitation in modern microbial mats. *Earth-Science Reviews*, 96:141-162.

Dupraz C., Visscher P.T., Baumgartner L.K. & Reid R.P. (2004). Microbe–mineral interactions: early carbonate precipitation in a hypersaline lake (Eleuthera Island, Bahamas). *Sedimentology*, 51: 745-765.

Dupraz, C., & Visscher, P. T. (2005). Microbial lithification in marine stromatolites and hypersaline mats. *Trends in microbiology*, 13(9), 429-438.

Dupraz, C., Pattisina, R., & Verrecchia, E. P. (2006). Translation of energy into morphology: simulation of stromatolite morphospace using a stochastic model. *Sedimentary Geology*, 185(3-4), 185-203.

Ebinger, C. J. (1989). Tectonic development of the western branch of the East African rift system. *Geological Society of America Bulletin*, 101(7), 885-903.

Ehlmann, B., Stevenson, D., Stack, K., Lunine, J., Kinch, K., Mahaffy, P., Werner, S., Herd, C., Elkins-Tanton, L., Kerber, L., Horgan, B., Fraeman, A., Anderson, F., Fassett, C., Kasting, J., Edwards, C., Hamilton, V., Golombek, M., Niles, P., … Zahnle, K. (2016). The sustainability of habitability on terrestrial planets: Insights, questions, and needed measurements from Mars for understanding the evolution of Earth-like worlds. Journal of Geophysical Research: Planets, 121(10), 1927–1961.

Eme, L., Spang, A., Lombard, J., Stairs, C. W., & Ettema, T. J. (2017). Archaea and the origin of eukaryotes. *Nature Reviews Microbiology*, *15*(12), 711-723.

Eymard, I., Alvarez, M.D.P., Bilmes, A., Vasconcelos, C. and Ariztegui, D., (2020). Tracking organomineralization processes from living microbial mats to fossil microbialites. *Minerals*, 10(7), p.605.

Eymard, I., Álvarez, M.D.P., Bilmes, A., Vasconcelos, C., Thomas, C. and Ariztegui, D., (2021). Evolving controls on mineralization in Patagonian microbial mats as inferred by water chemistry, microscopy and DNA signatures. *Latin American journal of sedimentology and basin analysis*, 28(2), pp.133-151.

Eymard, I., Bilmes, A., Alvarez, M.D.P., Feo, R., Hunger, G., Vasconcelos, C. and Ariztegui, D., (2019). Growth morphologies and plausible stressors ruling the formation of Late Pleistocene lacustrine carbonate buildups in the Maquinchao Basin (Argentina). *The Depositional Record*, 5(3), pp.498-514.

Fairén, A. G., Bonaccorsi, R., Lim, D., Uceda, E. R., Stoker, C., Zavaleta, J., Davila, A. F., Amils, R., Andersen, D., Bramall, N., Dohm, J. M., Wierzchos, J., & Mckay, C. P. (2010). Astrobiology through the Ages of Mars: The Study of Terrestrial Analogues to Understand the Habitability of Mars. Astrobiology, 10(8), 821–843.

Farías M.E., Rascovan N., Toneatti D.M., Albarracín V.H., Flores M.R., Poiré D.G., Collavino M.M., Aguilar O.M., Vazquez M.P. & Polerecky L. (2013). The discovery of stromatolites developing at 3570 m above sea level in a high-altitude volcanic lake Socompa, Argentinean Andes. *PLOS ONE*, 8: e53497.

Farías, M. E., Rascovan, N., Toneatti, D. M., Albarracín, V. H., Flores, M. R., Poiré, D. G., ... & Polerecky, L. (2013). The discovery of stromatolites developing at 3570 m above sea level in a high-altitude volcanic lake Socompa, Argentinean Andes. *PloS one*, *8*(1), e53497.

Farley, K. A., Williford, K. H., Stack, K. M., Bhartia, R., Chen, A., de la Torre, M., Hand, K., Goreva, Y., Herd, C.D., Hueso, R. and Liu, Y., Maki, J. N., Martinez, G., Moeller, R. C., Nelessen, A., Newman, C. E., Nunes, D., Ponce, A., Spanovich, N., Willis, P. A., Beegle, L. W., Bell III, J. F., Brown, A. J., Hamran, S., Hurowitz, J. A., Maurice, S., Paige, D. A., Rodriguez-Manfredi, J. A., Schulte, M. & Wiens, R. C. (2020). Mars 2020 mission overview. *Space Science Reviews*, 216, 1-41.

Fiore S., Dumontet S., Huertas F.J. & Pasquale, V. (2011). Bacteria-induced crystallization of kaolinite. *Applied Clay Science*, 53: 5566-571.

Foerster, V., Junginger, A., Langkamp, O., Gebru, T., Asrat, A., Umer, M., Lamb, H. F., Wennrich, V., Rethemeyer, J., Nowaczyk, N., Trauth, M. H. & Schaebitz, F. (2012).

Climatic change recorded in the sediments of the Chew Bahir basin, southern Ethiopia, during the last 45,000 years. *Quaternary International*, 274, 25-37.

Fontes J.C. & Pouchan P. (1975). Les cheminées du Lac Abbé (TFAI): *Stations hydroclimatiques de l'Holocéne. Comptes Rendus de l'Académie des Sciences Paris*, 280: 383-385.

Foster J.S., Green S.J., Ahrendt S.R., Golubic S., Reid R.P., Hetherington K.L. & Bebout L. (2009). Molecular and morphological characterization of cyanobacterial diversity in the stromatolites of Highborne Cay, Bahamas. *The ISME Journal - Multidisciplinary Journal of Microbial Ecology*, 3: 573-587.

Foster, J. S., Babilonia, J., Parke-Suosaari, E., & Reid, R. P. (2020). Stromatolites, Biosignatures, and Astrobiological Implications. In *Astrobiology and Cuatro Ciénegas Basin as an Analog of Early Earth*, 89-105.

Foucher, F., Hickman-Lewis, K., Hutzler, A., Joy, K. H., Folco, L., Bridges, J. C., Wozniakiewicz, P., Martínez-Frías, J., Debaille, V., Zolensky, M., Yano, H., Bost, N., Ferrière, L., Lee, M., Michalski, J., Schroeven-Deceuninck, H., Kminek, G., Viso, M., Russell, S., Smith, C., Zipfel, J. & Westall, F. (2021). Definition and use of functional analogues in planetary exploration. *Planetary and Space Science*, *197*, 105162.

Franchi F. & Frisia S. (2020). Crystallization pathways in the Great Artesian Basin (Australia) spring mound carbonates: implications for life signatures on Earth and beyond. *Sedimentology*, 67: 2561-2595.

Frantz C.M., Petryshyn V.A., Marenco P.J., Tripati A., Berelson W.M. & Corsetti F.A. (2014). Dramatic local environmental change during the Early Eocene Climatic Optimum detected using high resolution chemical analyses of Green River Formation stromatolites. *Palaeogeography, Palaeoclimatology, Palaeoecology*, 405: 1-15.

Frantz, C. M., Petryshyn, V. A., & Corsetti, F. A. (2015). Grain trapping by filamentous cyanobacterial and algal mats: implications for stromatolite microfabrics through time. *Geobiology*, *13*(5), 409-423.

Frezzotti M.L., Tecce F. & Casagli A. (2011). Raman spectroscopy for fluid inclusion analysis. *Journal of Geochemical Exploration*, 112: 1-20.

Galloway, R.W., Markgraf, V. and Bradbury, J.P., (1988). Dating shorelines of lakes in Patagonia, Argentina. *Journal of South American Earth Sciences*, 1(2), pp.195-198.

Gasse E. & Street F.A. (1978). Late Quaternary lake-level fluctuations and environments of the northern Rift Valley and Afar region (Ethiopia and Djibouti). *Palaeogeography, Palaeoclimatology, Palaeoecology*, 24: 279-325.

Gasse F. & Fontes J.C. (1989). Palaeoenvironments and palaeohydrology of a tropical closed lake (Lake Asal, Djibouti) since 10,000 yr BP. *Palaeogeography, Palaeoclimatology, Palaeoecology*, 69: 67-102.

Gasse F. (1977). Evolution of Lake Abhé (Ethiopia and TFAI), from 70,000 bp. *Nature*, 265: 42-45.

Gasse F. (2000). Hydrological changes in the African tropics since the Last Glacial Maximum. *Quaternary Science Reviews*, 19: 189-211.

Gasse F., Fontes J.C. & Rognon P., (1974). Variations hydrologiques et extension des lacs holocènes du desert Danakil. *Palaeogeography, Palaeoclimatology, Palaeoecology*, 15: 109-148.

Ge, Y., Della Porta, G., Pederson, C. L., Lokier, S. W., Hoffmann, R., & Immenhauser, A. (2021). Botryoidal and spherulitic aragonite in carbonates associated with microbial mats: precipitation or diagenetic replacement product?. *Frontiers in Earth Science*, *9*, 698952.

Gerdes, G., Claes, M., Dunajtschik-Piewak, K., Riege, H., Krumbein, W. E., & Reineck, H. E. (1993). Contribution of microbial mats to sedimentary surface structures. *Facies*, *29*, 61-74.

Ghinassi, M., D'Oriano, F., Benvenuti, M., Awramik, S., Bartolini, C., Fedi, M., Ferrari, G., Papini, M., Sagri, M. & Talbot, M. (2012). Shoreline fluctuations of Lake Hayk (northern Ethiopia) during the last 3500 years: geomorphological, sedimentary, and isotope records. *Palaeogeography, Palaeoclimatology, Palaeoecology*, 365, 209-226.

Ginsburg, R. N., & Planavsky, N. J. (2008). Diversity of Bahamian microbialite substrates. In *Links Between Geological Processes, Microbial Activities&Evolution of Life: Microbes and Geology* (pp. 177-195). Dordrecht: Springer Netherlands.

Gomez, F. J., Kah, L. C., Bartley, J. K., & Astini, R. A. (2014). Microbialites in a high-altitude Andean lake: multiple controls on carbonate precipitation and lamina accretion. *Palaios*, *29*(6), 233-249.

Gomez, F. J., Mlewski, C., Boidi, F. J., Farías, M. E., & Gérard, E. (2018). Calcium carbonate precipitation in diatom-rich microbial mats: the Laguna Negra hypersaline lake, Catamarca, Argentina. *Journal of Sedimentary Research*, *88*(6), 727-742.

Grotzinger J.P. & Knoll A.H. (1999). Stromatolites in Precambrian carbonates: evolutionary mileposts or environmental dipsticks?. *Annual Review of Earth and Planetary Sciences*, 27: 313-358.

Grotzinger, J. P., Gupta, S., Malin, M. C., Rubin, D. M., Schieber, J., Siebach, K., Sumner, D. Y., Stack, K. M., Vasavada, A. R., Arvidson, R. E., Calef III, F., Edgar, L., Fischer, W. F., Grant, J. A., Griffes, J., Kah, L. C., Lamb, M. P., Lewis, K. W., Mangold, N., Minitti, M. E., Palucis, M., Rice, M., Williams, R. M. E., Yingst, R. A., Blake, D., Blaney, D., Conrad, P., Crisp, J., Dietrich, W. E., Dromart, G., Edgett, K. S., Ewing, R. C., Gellert, R., Hurowitz, J. A., Kocurek, G., Mahaffy, P., McBride, M. J., McLennan, S. M., Mischna, M., Ming, D., Milliken, R., Newsom, H., Oehler, D., Parker, T. J., Vaniman, D., Wiens, R. C. & Wilson, S. A. (2015). Deposition, exhumation, and paleoclimate of an ancient lake deposit, Gale crater, Mars. *Science*, 350(6257), aac7575.

Grotzinger, J. P., Sumner, D. Y., Kah, L. C., Stack, K., Gupta, S., Edgar, L., Rubin, D., Lewis, K., Schieber, J., Mangold, N. and Milliken, R., Conrad, P. G., DesMarais, D., Farmer, J., Siebach, K., Calef III, F., Hurowitz, J., McLennan, S. M., Ming, D., Vaniman, D., Crisp, J., Vasavada, A. R., Edgett, K. S., MSL Science Team. & Sirven, J. B. (2014). A habitable fluvio-lacustrine environment at Yellowknife Bay, Gale Crater, Mars. *Science*, 343(6169), 1242777.

Grotzinger, J., & Jordan, T. (2013). *Para Entender a Terra-6*. Bookman Editora.

Gupta, G. N., Srivastava, S., Khare, S. K., & Prakash, V. (2014). Extremophiles: an overview of microorganism from extreme environment. *International Journal of Agriculture, Environment and Biotechnology*, *7*(2), 371-380.

Gutherz X., Lesur J., Cauliez J., Charpentier V., Diaz A., Ismaël M.O., Pène J.M., Sordoillet D. & Zazzo A. (2015). New insights on the first Neolithic societies in the Horn of Africa: The site of Wakrita, Djibouti. *Journal of Field Archaeology*, 40: 55-68.

Hays, L. E., Graham, H. V., Des Marais, D. J., Hausrath, E. M., Horgan, B., McCollom, T. M., Parenteau, M.N., Potter-McIntyre, S.L., Williams, A.J. & Lynch, K. L. (2017). Biosignature preservation and detection in Mars analog environments. *Astrobiology*, *17*(4), 363-400.

Hickman-Lewis, K., Cavalazzi, B., Giannoukos, K., D'Amico, L., Vrbaski, S., Saccomano, G., Dreossi, D., Tromba, G., Foucher, F., Brownscombe, W., Smith, C.L. & Westall, F. (2023). Advanced two-and three-dimensional insights into Earth's oldest stromatolites (ca. 3.5 Ga): Prospects for the search for life on Mars. *Geology*, 51(1), 33-38.

Hickman-Lewis, K., Cavalazzi, B., Giannoukos, K., d'Amico, L., Vrbaski, S., Saccomano, G., Dreossi, D., Tromba, G., Foucher, F., Brownscombe, W., Smith, C.L. & Westall, F. (2023). Advanced two-and three-dimensional insights into Earth's oldest stromatolites (ca. 3.5 Ga): Prospects for the search for life on Mars. *Geology*, *51*(1), 33-38.

Hickman-Lewis, K., Cavalazzi, B., Sorieul, S., Gautret, P., Foucher, F., Whitehouse, M. J., Jeon, H., Georgelin, T., Cockell, C. S. & Westall, F. (2020). Metallomics in deep time and the influence of ocean chemistry on the metabolic landscapes of Earth's earliest ecosystems. *Scientific Reports*, 10(1), 4965.

Hickman-Lewis, K., Gautret, P., Arbaret, L., Sorieul, S., De Wit, R., Foucher, F., Cavalazzi, B. & Westall, F. (2019). Mechanistic morphogenesis of organo-sedimentary structures growing under geochemically stressed conditions: keystone to proving the biogenicity of some Archaean stromatolites?. *Geosciences*, 9(8), 359.

Hillaire-Marcel, C., Carro, O., & Casanova, J. (1986). 14C and Th/U dating of Pleistocene and Holocene stromatolites from East African paleolakes. *Quaternary Research*, 25(3), 312-239.

Hofmann, H. J. (1969). Stromatolites from the Proterozoic Animikie and Sibley Groups, Ontario. *(No Title)*, 77.

Hofmann, H. J. (1973). Stromatolites: characteristics and utility. *Earth-Science Reviews*, 9(4), 339-373.

Hohl, S. V., & Viehmann, S. (2021). Stromatolites as geochemical archives to reconstruct microbial habitats through deep time: Potential and pitfalls of novel radiogenic and stable isotope systems. Earth-Science Reviews, 218, 103683.

Hoiczyk, E. (1998). Structural and biochemical analysis of the sheath of Phormidium uncinatum. *Journal of bacteriology*, 180(15), 3923-3932.

Horgan, B. H., Anderson, R. B., Dromart, G., Amador, E. S., & Rice, M. S. (2020). The mineral diversity of Jezero crater: Evidence for possible lacustrine carbonates on Mars. *Icarus*, 339, 113526.

Houssein B., Chandrasekharam D., Chandrasekhar V. & Jalludin M. (2014). Geochemistry of thermal springs around Lake Abhe, Western Djibouti. *International Journal of Sustainable Energy*, 33: 1090-1102.

Hrstka, T., Gottlieb, P., Skala, R., Breiter, K., & Motl, D. (2018). Automated mineralogy and petrology-applications of TESCAN Integrated Mineral Analyzer (TIMA). *Journal of Geosciences*, *63*(1), 47-63.

Hurowitz, J. A., Catling, D. C., & Fischer, W. W. (2023). High carbonate alkalinity lakes on Mars and their potential role in an origin of life beyond Earth. *Elements*, 19(1), 37-44.

Igisu, M., Takai, K., Ueno, Y., Nishizawa, M., Nunoura, T., Hirai, M., Kaneko, M., Naraoka, H., Shimojima, M., Hori, K., Nakashima, S., Ohta, H., Maruyama, S. & Isozaki, Y. (2012). Domain-level identification and quantification of relative prokaryotic cell abundance in microbial communities by micro-FTIR spectroscopy. *Environmental Microbiology Reports*, 4(1), 42-49.

Ingalls, M., Fetrow, A. C., Snell, K. E., Frantz, C. M., & Trower, E. J. (2022). Lake level controls the recurrence of giant stromatolite facies. *Sedimentology*, 69(4), 1649-1674.

Jahnert R.J. & Collins L.B. (2012). Characteristics, distribution and morphogenesis of subtidal microbial systems in Shark Bay, Australia. *Marine Geology*, 303: 115-136.

Jahnert, R. J., & Collins, L. B. (2011). Significance of subtidal microbial deposits in Shark Bay, Australia. *Marine Geology*, 286(1-4), 106-111.

Jones B. (2017). Review of aragonite and calcite crystal morphogenesis in thermal spring systems. *Sedimentary Geology*, 354: 9-23.

Jones, B., & Renaut, R. W. (1995). Noncrystallographic calcite dendrites from hot-spring deposits at Lake Bogoria, Kenya. *Journal of Sedimentary Research*, *65*(1a), 154-169.

Jones, B., & Renaut, R. W. (2008). Cyclic development of large, complex, calcite dendrite crystals in the Clinton travertine, Interior British Columbia, Canada. Sedimentary Geology, 203(1-2), 17-35.

Jones, B., Renaut, R. W., & Rosen, M. R. (2000a). Stromatolites forming in acidic hot-spring waters, North Island, New Zealand. *Palaios*, *15*(5), 450-475.

Jones, B., Renaut, R. W., & Rosen, M. R. (2000b). Trigonal dendritic calcite crystals forming from hot spring waters at Waikite, North Island, New Zealand. *Journal of Sedimentary Research*, *70*(3), 586-603.

Kalkowsky, E. (1908). Oolith und stromatolith in Norddeutschen Buntsandstein. *Deutsch Geologisches Gesellschaft zeitschrift*, *60*, 68-125.

Kaźmierczak J., Kempe S., Kremer B., López-García P., Moreira D. & Tavera R. (2011). Hydrochemistry and microbialites of the alkaline crater lake Alchichica, Mexico. *Facies*, 57: 543-570.

Kempe, S., Kazmierczak, J., Landmann, G., Konuk, T., Reimer, A., & Lipp, A. (1991). Largest known microbialites discovered in Lake Van, Turkey. *Nature*, 349(6310), 605-608.

Kremer, B., Kazmierczak, J., Łukomska-Kowalczyk, M., & Kempe, S. (2012). Calcification and silicification: fossilization potential of cyanobacteria from stromatolites of Niuafo ‘ou's Caldera Lakes (Tonga) and implications for the early fossil record. *Astrobiology*, 12(6), 535-548.

Laetsch T.A. & Downs R.T. (2006). Software for identification and refinement of cell parameters from powder diffraction data of minerals using the RRUFF Project and American Mineralogist Crystal Structure Databases. *Program and Abstracts of the 19th General Meeting of the International Mineralogical Association in Kobe*, Japan, 2006: 08-25.

Lanckriet, S., Rucina, S., Frankl, A., Ritler, A., Gelorini, V., & Nyssen, J. (2015). Nonlinear vegetation cover changes in the North Ethiopian Highlands: evidence from the Lake Ashenge closed basin. *Science of the Total Environment*, 536, 996-1006.

Le Gall B., Jalludin M., Maury R., Gasse F., Daoud M. A., Gutherz X., Doubre C., Caminiti A.M., Moussa N., Rolet J. (2018). *Notice de la carte géologique au 1/200000*

Legesse, D., Gasse, F., Radakovitch, O., Vallet-Coulomb, C., Bonnefille, R., Verschuren, D., ... & Barker, P. (2002). Environmental changes in a tropical lake (Lake Abiyata, Ethiopia) during recent centuries. *Palaeogeography, Palaeoclimatology, Palaeoecology*, 187(3-4), 233-258.

Lincoln T.A., Webb S.M., Present T.M., Magyar J.S. & Trower E.J. (2022). Microbial activity and neomorphism influence the composition and microfabric of ooids from Great Salt Lake, UT. *The Sedimentary Record*, 20: 1-10.

Logan, B. W., Rezak, R., & Ginsburg, R. N. (1964). Classification and environmental significance of algal stromatolites. *The Journal of Geology*, 72(1), 68-83.

Mackay, M. A., & Norton, R. S. (1987). 13C nuclear magnetic resonance study of biosynthesis of glucosylglycerol by a cyanobacterium under osmotic stress. *Journal of general microbiology*, 133(6), 1535-1542.

Manzo E., Perri E. & Tucker M.E. (2012). Carbonate deposition in a fluvial tufa system: processes and products (Corvino Valley–southern Italy). *Sedimentology*, 59: 553-577.

Marcus, H. G. (1975). The life and times of Menelik II: Ethiopia, (*No Title*). 1844-1913.

Marshall, C. P., & Coyle, C. M. (2006). *Why choose Raman spectroscopy for the exploration of Mars?*. Institute of Metals and Materials Australasia Limited.

Marshall, C. P., Love, G. D., Snape, C. E., Hill, A. C., Allwood, A. C., Walter, M. R., ... & Summons, R. E. (2007). Structural characterization of kerogen in 3.4 Ga Archaean cherts from the Pilbara Craton, Western Australia. *Precambrian Research*, 155(1-2), 1-23.

Marshall, M. H., Lamb, H. F., Davies, S. J., Leng, M. J., Kubsa, Z., Umer, M., & Bryant, C. (2009). Climatic change in northern Ethiopia during the past 17,000 years: a diatom and stable isotope record from Lake Ashenge. *Palaeogeography, Palaeoclimatology, Palaeoecology*, 279(1-2), 114-127.

Marshall, M. H., Lamb, H. F., Huws, D., Davies, S. J., Bates, R., Bloemendal, J., Boyle, J., Leng, M.J., Umer, M. & Bryant, C. (2011). Late Pleistocene and Holocene drought events at Lake Tana, the source of the Blue Nile. *Global and Planetary Change*, 78(3-4), 147-161.

Martínez-Espinosa, R. M. (2020). Microorganisms and their metabolic capabilities in the context of the biogeochemical nitrogen cycle at extreme environments. *International journal of molecular sciences*, *21*(12), 4228.

Martins, Z., Cottin, H., Kotler, J. M., Carrasco, N., Cockell, C. S., de la Torre Noetzel, R., Demets, R., de Vera, J.P., d'Hendecourt, L., Ehrenfreund, P., Elsaesser, A., Foing, B., Onofri, S., Quinn, R., Rabbow, E., Rettberg, P., Ricco, A.J., Slenzka, K., Stalport, F., ten Kate, I.L., van Loon, J.J.W.A. & Westall, F. (2017). Earth as a tool for astrobiology—a European perspective. *Space Science Reviews*, *209*, 43-81.

McCall J. (2010). Lake Bogoria, Kenya: Hot and warm springs, geysers and Holocene stromatolites. *Earth-Science Reviews*, 103: 71-79.

McNair, H. M., Brzezinski, M. A., Till, C. P., & Krause, J. W. (2018). Taxon-specific contributions to silica production in natural diatom assemblages. *Limnology and oceanography*, 63(3), 1056-1075.

McNamara, K. J., & Awramik, S. M. (1992). Stromatolites: a key to understanding the early evolution of life. *Science Progress (1933-)*, 345-364.

Michalski, J. R., Dobrea, E. Z. N., Niles, P. B., & Cuadros, J. (2017). Ancient hydrothermal seafloor deposits in Eridania basin on Mars. *Nature communications*, *8*(1), 15978.

Michalski, J. R., Goudge, T. A., Crowe, S. A., Cuadros, J., Mustard, J. F., & Johnson, S. S. (2022). Geological diversity and microbiological potential of lakes on Mars. *Nature Astronomy*, *6*(10), 1133-1141.

Michalski, J. R., Onstott, T. C., Mojzsis, S. J., Mustard, J., Chan, Q. H., Niles, P. B., & Johnson, S. S. (2018). The Martian subsurface as a potential window into the origin of life. *Nature Geoscience*, *11*(1), 21-26.

Mologni C., Bruxelles L., Schuster M., Davtian G., Ménard C., Orange F., Doubre C., Cauliez J., Taezaz H.B., Revel M. & Khalidi L. (2021). Holocene East African monsoonal variations recorded in wave-dominated clastic paleo-shorelines of Lake Abhe, Central Afar region (Ethiopia & Djibouti). *Geomorphology*, 391: 107896.

Moore, K. R., Pajusalu, M., Gong, J., Sojo, V., Matreux, T., Braun, D., & Bosak, T. (2020). Biologically mediated silicification of marine cyanobacteria and implications for the Proterozoic fossil record. *Geology*, *48*(9), 862-866.

Moussa, N., Bayon, G., Dekov, V., Yamanaka, T., Shinjo, R., Toki, T., Le Gall, B., Grassineau, N., Langlade, J.A., Awaleh, M.O. & Pelleter, E. (2023). Mixed carbonate-siliceous hydrothermal chimneys ahead of the Asal propagating rift (SE Afar Rift, Republic of Djibouti). *Journal of African Earth Sciences*, *197*, 104765.

Muller E., Ader M., Aloisi G., Bougeault C., Durlet C., Vennin E., Benzerara, K., Gaucher, E.C., Virgone, A., Chavez, M., Souquet, P. & Gérard E. (2022). Successive Modes of Carbonate Precipitation in Microbialites along the Hydrothermal Spring of La Salsa in Laguna Pastos Grandes (Bolivian Altiplano). *Geosciences*, 12: 88.

Newman, S. A., Mariotti, G., Pruss, S., & Bosak, T. (2016). Insights into cyanobacterial fossilization in Ediacaran siliciclastic environments. *Geology*, 44(7), 579-582.

Nguyen S.T., Vardeh D.P., Nelson T.M., Pearson L.A., Kinsela A.S. & Neilan B.A. (2022). Bacterial community structure and metabolic potential in microbialite-forming mats from South Australian saline lakes. *Geobiology*, 20: 546-559.

Nguyen, R. T., Harvey, H. R., Zang, X., van Heemst, J. D., Hetényi, M., & Hatcher, P. G. (2003). Preservation of algaenan and proteinaceous material during the oxic decay of Botryococcus braunii as revealed by pyrolysis-gas chromatography/mass spectrometry and 13C NMR spectroscopy. *Organic Geochemistry*, 34(4), 483-497.

Noffke, N., & Awramik, S. M. (2013). Stromatolites and MISS—differences between relatives. *Gsa Today*, 23(9).

Noffke, N., Gerdes, G., Klenke, T., & Krumbein, W. E. (1997). A microscopic sedimentary succession of graded sand and microbial mats in modern siliciclastic tidal flats. *Sedimentary Geology*, 110(1-2), 1-6.

Nutman A.P., Bennett V.C., Friend C.R., Van Kranendonk M.J. & Chivas A.R. (2016). Rapid emergence of life shown by discovery of 3,700-million-year-old microbial structures. *Nature*, 537: 535-538.

Onstott, T. C., Ehlmann, B. L., Sapers, H., Coleman, M., Ivarsson, M., Marlow, J. J. & Niles, P. (2019). Paleo-rock-hosted life on Earth and the search on Mars: a review and strategy for exploration. Astrobiology, 19(10), 1230-1262.

Pace, A., Bourillot, R., Bouton, A., Vennin, E., Braissant, O., Dupraz, C., Duteil, T., Bundeleva, I., Patrier, P., Galaup, S., Yokoyama, Y., Franceschi, M., Virgone, A. & Visscher, P. T. (2018). Formation of stromatolite lamina at the interface of oxygenic–anoxygenic photosynthesis. *Geobiology*, 16(4), 378-398.

Pace A., Bourillot R., Bouton A., Vennin E., Galaup S., Bundeleva I., Patrier P., Dupraz C., Thomazo C., Sansjofre P. & Yokoyama Y. (2016). Microbial and diagenetic steps leading to the mineralisation of Great Salt Lake microbialites. *Scientific Reports*, 6: 31495.

Pacton, M., Hunger, G., Martinuzzi, V., Cusminsky, G., Burdin, B., Barmettler, K., Vasconcelos, C. and Ariztegui, D., (2015). Organomineralization processes in freshwater stromatolites: a living example from eastern P atagonia. *The Depositional Record*, 1(2), pp.130-146.

Pamela Reid, R., James, N. P., Macintyre, I. G., Dupraz, C. P., & Burne, R. V. (2003). Shark Bay stromatolites: microfabrics and reinterpretation of origins. *Facies*, *49*, 299-324.

Papineau D., Walker J.J., Mojzsis S.J. & Pace N.R. (2005). Composition and structure of microbial communities from stromatolites of Hamelin Pool in Shark Bay, Western Australia. *Applied and Environmental Microbiology*, 71: 4822-4832.

Pedley M. (2014). The morphology and function of thrombolitic calcite precipitating biofilms: A universal model derived from freshwater mesocosm experiments. *Sedimentology*, 61: 22-40.

Pedley, M., Rogerson, M., & Middleton, R. (2009). Freshwater calcite precipitates from in vitro mesocosm flume experiments: a case for biomediation of tufas. *Sedimentology*, *56*(2), 511-527.

Perri, E., Tucker, M. E., & Spadafora, A. (2012). Carbonate organo-mineral micro-and ultrastructures in sub-fossil stromatolites: Marion lake, South Australia. *Geobiology*, 10(2), 105-117.

Petrash, D. A., Gingras, M. K., Lalonde, S. V., Orange, F., Pecoits, E., & Konhauser, K. O. (2012). Dynamic controls on accretion and lithification of modern gypsum-dominated thrombolites, Los Roques, Venezuela. *Sedimentary Geology*, 245, 29-47.

Petryshyn, V.A., Corsetti, F.A., Berelson, W.M., Beaumont, W. & Lund, S.P. (2012). Stromatolite lamination frequency, Walker Lake, Nevada: implications for stromatolites as biosignatures. *Geology*, 40(6), pp. 499-502.

Rampelotto, P. H. (2013). Extremophiles and extreme environments. *Life*, *3*(3), 482-485.

Reid, R. P., Suosaari, E. P., Oehlert, A. M., Pollier, C. G., & Dupraz, C. (2024). Microbialite accretion and growth: lessons from Shark Bay and the Bahamas. *Annual review of marine science*, *16*(1), 487-511.

Reid, R. P., Visscher, P. T., Decho, A. W., Stolz, J. F., Bebout, B. M., Dupraz, C., Macintyre, I. G., Paerl, H. W., Pinckney, J. L., Prufert-Bebout, L., Steppe, T. F. & DesMarais, D. J. (2000). The role of microbes in accretion, lamination and early lithification of modern marine stromatolites. *Nature*, 406(6799), 989-992.

Renaut, R. W., Owen, R. B., & Ego, J. K. (2017). Geothermal activity and hydrothermal mineral deposits at southern Lake Bogoria, Kenya Rift Valley: Impact of lake level changes. *Journal of African Earth Sciences*, 129, 623-646.

Riding R. (2000). Microbial carbonates: the geological record of calcified bacterial–algal mats and biofilms. *Sedimentology*, 47: 179-214.

Riding R. (2011). Microbialites, stromatolites, and thrombolites. In Reitner J. & Thiel V. (eds), *Encyclopedia of Geobiology.* Springer Science, Heidelberg: 635-654.

Riding, R. (1991). Classification of microbial carbonates. In *Calcareous algae and stromatolites*, pp. 21-51.

Riding, R. (1999). The term stromatolite: towards an essential definition. *Lethaia*, *32*(4), 321-330.

Riding, R. (2000). Microbial carbonates: the geological record of calcified bacterial–algal mats and biofilms. *Sedimentology*, *47*, 179-214.

Riding, R. (2006). Cyanobacterial calcification, carbon dioxide concentrating mechanisms, and Proterozoic–Cambrian changes in atmospheric composition. *Geobiology*, 4: 299-316.

Roche, A., Vennin, E., Bundeleva, I., Bouton, A., Payandi-Rolland, D., Amiotte-Suchet, P., Gaucher, E.C., Courvoisier, H. & Visscher, P. T. (2019). The role of the substrate on the mineralization potential of microbial mats in a modern freshwater river (Paris Basin, France). *Minerals*, *9*(6), 359.

Rogerson, M., Pedley, H. M., Greenway, G. M., & Wadhawan, J. D. (2022). Interaction of temperature, salinity and extracellular polymeric substances controls trace element incorporation into tufa calcite. *The Depositional Record*, 8(1), 210-219.

Sanz-Montero, M. E., Cabestrero, Ó., & Sánchez-Román, M. (2019). Microbial Mg-rich carbonates in an extreme alkaline lake (Las Eras, Central Spain). *Frontiers in Microbiology*, 10, 148.

Sarg, J. F., Suriamin, Tänavsuu-Milkeviciene, K., & Humphrey, J. D. (2013). Lithofacies, stable isotopic composition, and stratigraphic evolution of microbial and associated carbonates, Green River Formation (Eocene), Piceance Basin, Colorado. *AAPG bulletin*, 97(11), 1937-1966.

Schopf J.W. (2012). The fossil record of cyanobacteria. In Whitton B.A. & Potts M. (eds), *Ecology of Cyanobacteria II: Their Diversity in Space and Time*. Springer Science, Dordrecht: 15-36.

Schopf, J. W. (2006). Fossil evidence of Archaean life. *Philosophical Transactions of the Royal Society B: Biological Sciences*, 361(1470), 869-885.

Schopf, J. W., Kudryavtsev, A. B., Agresti, D. G., Czaja, A. D., & Wdowiak, T. J. (2005). Raman imagery: a new approach to assess the geochemical maturity and biogenicity of permineralized Precambrian fossils. *Astrobiology*, *5*(3), 333-371.

Schopf, J. W., Kudryavtsev, A. B., Czaja, A. D., & Tripathi, A. B. (2007). Evidence of Archean life: stromatolites and microfossils. *Precambrian Research*, 158(3-4), 141-155.

Shapiro, R. S. (2007). Stromatolites: A 3.5-billion-year ichnologic record. In *Trace Fossils* (pp. 382-390). Elsevier.

Shiraishi F, Hanzawa Y, Asada J, et al. (2022) Microbial influences on tufa deposition in a tropical climate. *Sediment Geology* 427:106045; doi: 10.1016/j.sedgeo.2021.106045

Shiraishi F, Hanzawa Y, Okumura T, et al. (2017) Cyanobacterial exopolymer properties differentiate microbial carbonate fabrics. *Scientific Reports* 7(1):11805; doi: 10.1038/s41598-017-12303-9

Shiraishi, F., Okumura, T., Takahashi, Y., & Kano, A. (2010). Influence of microbial photosynthesis on tufa stromatolite formation and ambient water chemistry, SW Japan. *Geochimica et Cosmochimica Acta*, 74(18), 5289-5304.

Shishaye, H. A., & Asfaw, A. T. (2020). Analysis and evaluation of the spatial and temporal variabilities of river water quality parameters. *Applied Water Science*, 10(6), 1-20.

Skrzypczak, A., Derenne, S., Binet, L., Gourier, D., & Robert, F. (2005). Characterization of a 3.5 Billion year old organic matter: Electron paramagnetic resonance and pyrolysis GC–MS, tools to assess syngeneity and biogenicity. *In Lunar and Planetary Science XXXVI, Abstract* (Vol. 1351).

Souza-Egipsy, V., Wierzchos, J., Ascaso, C., & Nealson, K. H. (2005). Mg–silica precipitation in fossilization mechanisms of sand tufa endolithic microbial community, Mono Lake (California). *Chemical Geology*, 217(1-2), 77-87.

Summons, R. E., Welander, P. V., & Gold, D. A. (2022). Lipid biomarkers: molecular tools for illuminating the history of microbial life. *Nature Reviews Microbiology*, 20(3), 174-185.

Suosaari, E. P., Reid, R. P., & Andres, M. S. (2019). Stromatolites, so what?! A tribute to Robert N. Ginsburg. *The Depositional Record*, *5*(3), 486-497.

Suosaari, E. P., Reid, R. P., Playford, P. E., Foster, J. S., Stolz, J. F., Casaburi, G., Hagan, P. D., Chirayath, V, Macintyre, I. G., Planavsky, N. J. & Eberli, G. P. (2016). New multi-scale perspectives on the stromatolites of Shark Bay, Western Australia. *Scientific reports*, *6*(1), 20557.

Tan, J., Sephton, M. A., & Lewis, J. M. T. (2018). The Fate of Lipid Biosignatures in a Mars-Analogue Sulfur Stream. Scientific Reports, 8(1).

Tarnas, J. D., Stack, K. M., Parente, M., Koeppel, A. H. D., Mustard, J. F., Moore, K. R., Horgan, B. H. N., Seelos, F. P., Cloutis, E. A., Kelemen, P. B. and Flannery, D., Brown,

A. J. Frizzell, K. R. & Pinet, P. (2021). Characteristics, origins, and biosignature preservation potential of carbonate-bearing rocks within and outside of Jezero Crater. *Journal of Geophysical Research: Planets*, 126(11), e2021JE006898.

Tatur, A., del Valle, R., Bianchi, M.M., Outes, V., Villarosa, G., Niegodzisz, J. and Debaene, G., (2002). Late Pleistocene palaeolakes in the Andean and Extra-Andean Patagonia at mid-latitudes of South America. *Quaternary International*, 89(1), pp.135-150.

Tesfaye S., Harding D.J. & Kusky T.M. (2003). Early continental breakup boundary and migration of the Afar triple junction, Ethiopia. *Geological Society of America Bulletin*, 115: 1053-1067.

Tiercelin, J. J. (1991). Natural resources in the lacustrine facies of the Cenozoic rift basins of East Africa. *Lacustrine Facies Analysis*, 1-37.

Tiercelin, J. J., Michaux, J., & Bandet, Y. (1979). Le Miocene superieur du sud de la depression de l'Afar, Ethiopie; sediments, faunes, ages isotopiques. *Bulletin de la Société géologique de France*, 7(3), 255-258.

Tosca N.J., Macdonald F.A., Strauss J.V., Johnston D.T. & Knoll A.H. (2011). Sedimentary talc in Neoproterozoic carbonate successions. *Earth and Planetary Science Letters*, 306: 11-22.

Trichet J., Défarge C., Tribble J., Tribble G. & Sansone F. (2001). Christmas Island lagoonal lakes, models for the deposition of carbonate–evaporite–organic laminated sediments. *Sedimentary Geology*, 140: 177-189.

Valdespino-Castillo, P. M., Alcántara-Hernández, R. J., Alcocer, J., Merino-Ibarra, M., Macek, M., & Falcón, L. I. (2014). Alkaline phosphatases in microbialites and bacterioplankton from Alchichica soda lake, Mexico. *FEMS Microbiology Ecology*, 90(2), 504-519.

Valette J.N. (1975). Le lac Abhé (T.F.A.I.): étude morphologique et géochimique. *Bulletin Bureau de Recherches Géologiques et Minières, deuxième série, Section II*, 2: 143-155.

Van Kranendonk, M. J. (2006). Volcanic degassing, hydrothermal circulation and the flourishing of early life on Earth: A review of the evidence from c. 3490-3240 Ma rocks of

the Pilbara Supergroup, Pilbara Craton, Western Australia. *Earth-Science Reviews*, 74(3-4), 197-240.

Vandenbroucke, M., & Largeau, C. (2007). Kerogen origin, evolution and structure. *Organic Geochemistry*, 38(5), 719-833.

Varet J. (2018). *Geology of Afar* (East Africa), 336 pp. Springer International Publishing.

Verburga, P., & Hecky, R. E. (2009). The physics of the warming of Lake Tanganyika by climate change. *Limnology and Oceanography*, 54(6part2), 2418-2430.

Wacey, D., Urosevic, L., Saunders, M., & George, A. D. (2018). Mineralisation of filamentous cyanobacteria in Lake Thetis stromatolites, Western Australia. *Geobiology*, *16*(2), 203-215.

Walter B., Géraud Y., Favier A., Chibati N. & Diraison M. (2023). Hydrothermal activity of the Lake Abhe geothermal field (Djibouti): Structural controls and paths for further exploration. *EGUsphere*, 2023: 1-24.

Walter, M. R., Buick, R., & Dunlop, J. S. R. (1980). Stromatolites 3,400–3,500 Myr old from the North pole area, Western Australia. *Nature*, 284(5755), 443-445.

Wang, X., Wu, M., Ma, S., Su, J., He, K., Wang, H., & Zhang, S. (2023). From cyanobacteria to kerogen: A model of organic carbon burial. *Precambrian Research*, 390, 107035.

Westall, F., Hickman-Lewis, K., Cavalazzi, B., Foucher, F., Clodoré, L., & Vago, J. L. (2021). On biosignatures for Mars. *International Journal of Astrobiology*, 20(6), 377-393.

Whatley, R.C. and Cusminsky, G.C., (1999). Lacustrine ostracoda and late Quaternary palaeoenvironments from the lake Cari-Laufquen region, Rio Negro province, Argentina. *Palaeogeography, Palaeoclimatology, Palaeoecology*, 151(1-3), pp.229-239.

Willmer, B. J., & Rasser, M. W. (2022). Calcification patterns of Rivularia-type cyanobacteria: examples from the Miocene of the North Alpine Foreland Basin. *Facies*, 68(4), 16.

Wilmeth, D. T., Myers, K. D., Lalonde, S. V., Mänd, K., Konhauser, K. O., Grandin, P., & van Zuilen, M. A. (2022). Evaporative silicification in floating microbial mats: patterns

of oxygen production and preservation potential in silica-undersaturated streams, El Tatio, Chile. *Geobiology*, 20(2), 310-330.

Wilmeth, D. T., Nabhan, S., Myers, K. D., Slagter, S., Lalonde, S. V., Sansjofre, P., Homann, M., Konhauser, K.O., Munoz-Saez, C. & Van Zuilen, M. A. (2020). Depositional evolution of an extinct sinter mound from source to outflow, El Tatio, Chile. *Sedimentary Geology*, 406, 105726.

Winsborough, B. M., Seeler, J. S., Golubic, S., Folk, R. L., & Maguire, B. (1994). Recent fresh-water lacustrine stromatolites, stromatolitic mats and oncoids from northeastern Mexico. In: Bertrand-Sarfati, J., Monty, C. (eds) *Phanerozoic Stromatolites II*. Springer, Dordrecht. (pp. 71-100).

Wright, V. P. (2012). Lacustrine carbonates in rift settings: the interaction of volcanic and microbial processes on carbonate deposition. *Geological Society, London, Special Publications*, 370(1), 39-47.

Yeşilova Ç., Gülyüz E., Huang C.R. & Shen C.C. (2019). Giant tufas of Lake Van record lake-level fluctuations and climatic changes in eastern Anatolia, Turkey. *Palaeogeography, Palaeoclimatology, Palaeoecology*, 533: 109226.

Zăinescu, F., Van der Vegt, H., Storms, J., Nutz, A., Bozetti, G., May, J. H., ... & Schuster, M. (2023). The role of wind-wave related processes in redistributing river-derived terrigenous sediments in Lake Turkana: A modelling study. *Journal of Great Lakes Research*, 49(2), 368-386.

Zastrow, A. M., & Glotch, T. D. (2021). Distinct carbonate lithologies in Jezero crater, Mars. *Geophysical Research Letters*, 48(9), e2020GL092365.

Zhang, C., Li, F., Lyu, J., & Yao, Y. (2023). Biomimetic mineralization of Ca-Mg carbonates: relevance to microbial cells and extracellular polymeric substances. *Microscopy and Microanalysis*, *29*(2), 665-674.